



**Pilkington Library**

Author/Filing Title . . . . . **MASTERS, B.J.** . . . . .

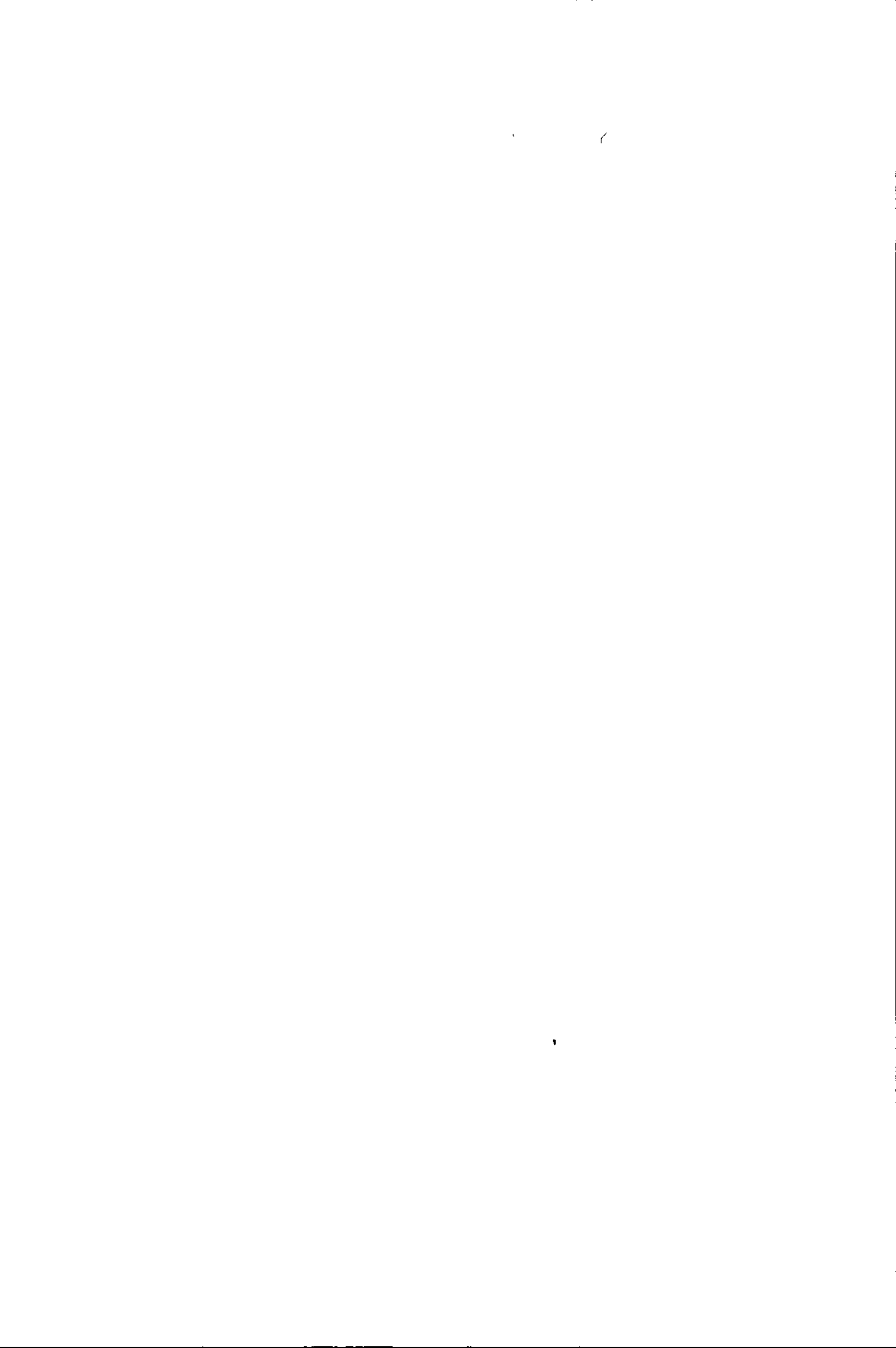
Accession/Copy No

Vol No. . . . .	Class Mark . . . . . <b>T</b> . . . . .
-----------------	---

<b>26 MAR 1999</b>	<b>LOAN COPY</b>
<b>29 APR [2000]</b>	
<b>13 MAY 2000</b>	
<b>-7 AUG 2000</b>	

0401659860





**A NOVEL CALIBRATION STRATEGY FOR  
LASER ABLATION ICP-MS**

by

**Barrie James Masters**


**A Doctoral Thesis**

**Submitted in partial fulfilment of the requirements  
for the award of**

**Doctor of Philosophy of Loughborough University**

**21<sup>st</sup> August 1997**

**© by Barrie James Masters 1997**

 Loughborough University P... ..brary
Date Aug 98
Class
Acc No. 040165986

K0628997

## Abstract

Sample introduction by laser ablation has many desirable features: reduction of the time involved in sample pre-analysis processing, avoiding the use of hazardous reagents and reducing the risk of contamination by reagent impurities. It is also possible to produce spatial analytical profiles across small sections of samples. Laser spots of  $<10\ \mu\text{m}$  in diameter are possible with the latest commercial instrumentation.

Additionally, for plasma spectrometry, the presence of molecular species derived from the plasma gases and the solvent vapour results in interferences, particularly for elements with an atomic mass of less than 80. Sampling with a laser removes the need for a solvent.

The type of laser used for sampling is an important consideration. Ultraviolet lasers give better coupling between the laser and sample with ablation being mainly photochemical in nature. With infrared lasers, coupling with some samples is inefficient and is generally thermal in nature leading to poor crater definition.

Calibration is one of the main difficulties associated with quantitative analysis by laser ablation. The majority of papers associated with the use of lasers for solid sampling give reference to the difficulty of reproducible calibration and in particular the lack of matrix matched standards. The most commonly used calibration method to date involves the use of the National Institute of Standards and Technology (NIST) standard reference materials, particularly the 600 series glass standards. The disadvantages associated with these standards are: the analyst has no control over the elemental make up of the standard, they are relatively expensive and most importantly the matrix is fixed and cannot be matched to the sample.

This thesis describes a calibration technique based on the ablation of aqueous standards. Water is transparent to the commonly used UV laser wavelengths, 193, 248 and 266 nm resulting in poor energy coupling between the laser and the aqueous standard. The addition of a photo-stable chromophore results in modification of the standards absorption coefficient and enables them to mimic the behaviour of solid samples. The benefit of such standards is that they are easy to produce in any analytical laboratory. The elemental and matrix composition can be controlled by the analyst. The standards also offer the advantage of a constantly renewable surface.

Initial work involved design and set-up of an optical system and laser to couple the laser with an ICP-MS. Poly(sodium 4-styrene-sulphonate) was identified as a suitable chromophore. The main criteria for the additive being that it absorbed at the excimer laser wavelengths and had an acceptable lifetime to allow adequate analytical data to be generated. Investigation into the characteristics of the chromophore including effect of concentration, laser energy and laser frequency were investigated.

Calibration and validation of the aqueous calibration technique was demonstrated by comparison with NIST standard reference materials. The absorption coefficient of the aqueous standard was matched with that of the NIST reference material. Both samples were then analysed by ICP-MS. The count rates observed were initially found to be similar for both samples, however the signal for the aqueous standard remained stable but the signal for the NIST glass decreased. This was thought to be due to the laser channelling into the solid sample causing loss of focus. The aqueous standard in effect provides a constantly renewable surface and no loss of focus. An internal standard was used to correct for the differing sensitivities obtained.

The final part of the work involved application of the calibration method to two biological matrices: Bone samples from patients with osteoporosis and porcine liver

samples. Elemental profiles across the samples are presented which are in general agreement with the expected and certified concentrations.

# Acknowledgements

I wish to express my thanks to Dr B.L. Sharp for all his help throughout my research and the odd games of golf we managed to play. I would also like to thank Alan Stevens and Simon Riggot for their help in keeping the instrument operational. Elaine and Bev for their help in the laboratory.

I am grateful to the British Geological Survey for the loan of the instrument used herein and V.G. Elemental for their assistance in maintenance and the provision of consumable items.

I would like to thank V.G Elemental and the Engineering and Physical Research Council for their financial support.

Finally I would like to thank Louise, my family and friends for their support throughout my research programme



# Table of Contents

Page

Abstract

Acknowledgements

## 1. Inductively Coupled Plasma Mass Spectrometry

1.1 Historical Development of ICP Spectrometry 1

1.2 ICP-MS Systems

1.2.1 ICP-MS Sample Excitation / Ionisation 2

1.2.2 Ion Extraction 4

1.2.3 Mass Analyser 4

1.2.4 Ion Detection 5

1.3 ICP-MS Calibration Modes

1.3.1 Mass Calibration 7

1.3.2 Semi-quantitative Calibration 7

1.3.3 Quantitative Analysis 7

1.4 Data Handling 9

## 2. Solid Sample Introduction

2.1 Introduction 11

2.2 Electrothermal Vaporisation 12

2.3 Direct Sample Insertion Devices 13

2.4 Arc Nebulisation 14

2.5 Slurry Nebulisation 14

2.6 Laser Ablation 15

2.6.1 Processes Occurring During the Ablation Event 16

2.6.2 Models of the Ablation Event 17

2.6.3 Effect of Laser Wavelength 23

2.6.4	Effect of Laser Parameters	26
2.6.5	Homogeneity and Sampling	27
2.6.6	Interferences	29
<b>3.</b>	<b>Instrumentation</b>	
3.1	ICP-MS	31
3.2	Excimer Lasers	33
3.2.1	Structure of Excimer Lasers	35
3.2.2	The Laser	36
3.3	Typical Run Sequence of the LA-ICP-MS System	39
<b>4.</b>	<b>Calibration for Laser Ablation ICP-MS</b>	
4.1	Review	40
4.2	Calibration Strategies Currently in Use	41
4.2.1	Solid Standard Calibration	41
4.2.2	Aqueous Standard Calibration	43
<b>5.</b>	<b>Analysis of Environmental / Biological Materials by LA-ICP-MS</b>	
5.1	Review	47
<b>6.</b>	<b>Fundamental Studies on the Production of Aqueous Standards with Modified Absorption Coefficients</b>	
6.1	Introduction	55
6.1.1	The Coupling of Laser Energy into Aqueous Solutions Containing an Absorbing Chromophore	56
6.2	Estimation of the Laser Power Density	56
6.3	Investigation of the Absorption Characteristics of Poly(sodium 4-styrene sulphonate) and Napthalene-2-sulphonic acid	58
6.4	Calculation of Absorption Coefficients	62
6.5	System Optimisation	66
6.6	Determination of System Stability	67

6.7	Effect of Laser Energy and Frequency on the Observed Count Rate	68
6.8	Production of a Calibration Graph	69
6.9	Effect of Polymer Additive Concentration on the Observed Count Rate	70
6.10	Investigation of Fractionation	70
6.11	Comparison of Wet and Dry Plasma Conditions	72
6.12	Determination of Oxide Ratios for Dry Plasma Conditions	74
6.13	Determination of Detection Limits	74
<b>7.</b>	<b>Results for the Analysis of Reference Materials and Biological Samples</b>	
	Introduction	77
7.1	Analysis of NIST 613 Using an Aqueous Calibration Procedure	78
7.2	Osteoporosis	81
7.3	Analysis of Biological Materials	86
7.4	Experimental	87
7.5	Analysis of Bone Samples	89
7.6	Analysis of Liver Samples	91
7.7	Experiments on a Commercial Laser Microprobe ICP-MS System	93
	7.7.1 Experimental	94
	7.7.2 Polymer Additive Concentration	94
	7.7.3 Detection Limits	95
	7.7.4 Calibration Graphs	97
	7.7.5 Analysis of Bone Samples	97
	7.7.6 Analysis of Liver Samples	99

<b>8.</b>	<b>Conclusions and Future Work</b>	
8.1	Initial Studies	101
8.2	Validation	102
8.3	Analysis of Biological Materials	104
8.4	Future Work	104
	References	107

# Chapter 1:

## Inductively Coupled Plasma Mass Spectrometry

### 1.1 Historical Development of ICP Spectrometry

The development of a new analytical technique rarely involves the development of a fundamentally new technology, it has tended to rely on the application and utilisation of an existing concept. Inductively coupled plasma (ICP) spectrometry is no exception to this rule. The ICP, operating at atmospheric pressure, was first described and used by Reed<sup>1</sup> as a technique for growing crystals under high temperature conditions, but later<sup>2</sup> as a spectral emission source. The analytical potential of the technique followed from the work of Greenfield *et al*<sup>3</sup> and Wendt and Fassel<sup>4</sup>. These early workers did much to establish the ICP as a spectroscopic source and it is the application and refinement of the ideas developed in their research which are now used as the basis of quantitative ICP source spectrometry.

A conventional ICP consists of a volume of partially ionised argon gas formed in a torch of the Fassel or Scott type<sup>5</sup>. The torch consists of three concentric quartz tubes surrounded at its upper end by a three turn water cooled copper induction coil that carries radio frequency (R.F.) power, conventionally oscillated at 27.12 MHz. The argon gas is introduced as three separate flows. The *outer flow* is introduced tangentially between the two outer tubes. This flow cools the outer tube and prevents the plasma fireball from coming into contact with it. The flow rate is typically between 10 and 20 litres per minute. The flow introduced between the two inner tubes is termed the *intermediate flow*, it essentially adds to the body of the fireball, pushing it higher in the load coil and keeping it away from the injector tube. Typical flow rates are between 0 and 3 l min<sup>-1</sup>. The third and final gas flow is, in terms of analytical performance, the

most important It conveys the aerosol from the sample introduction system and usually has a flow rate of the order of  $0.8 \text{ l min}^{-1}$ . This is sufficient in the small diameter of the injector tube to produce a high velocity jet of gas which punches a cooler hole through the centre of the plasma. This is termed the central channel.

## **1.2 ICP-MS Systems**

### **1.2.1 Sample Excitation / Ionisation**

A plasma is a gas in which atoms are present in an ionised state. For the plasma to be sustained by induction, a sufficiently large proportion of the atoms must be ionised to make the gas conducting. When a high frequency current flows in an induction coil it generates a rapidly varying magnetic field within the coil. If charged particles (particularly electrons) flow through the coil then ohmic heating follows. This interaction of the oscillating magnetic field with electrons in the flowing gas generates the ICP. To initiate electrical conductivity in the gas, as it flows through the coil, a Tesla spark is used to 'seed' the argon gas with electrons. Inductive heating of the flowing gas then maintains the plasma at temperatures of 6000-10000 K.

The great attraction of the ICP as a spectrometric source lies in the solution it offers to two basic problems encountered in the design of such sources: (i) the attainment of a sufficiently high temperature to produce a controlled and uncontaminated environment required for sample conditioning and excitation; (ii) the introduction of the sample to such an environment for a sufficient time for all the desired processes to occur.

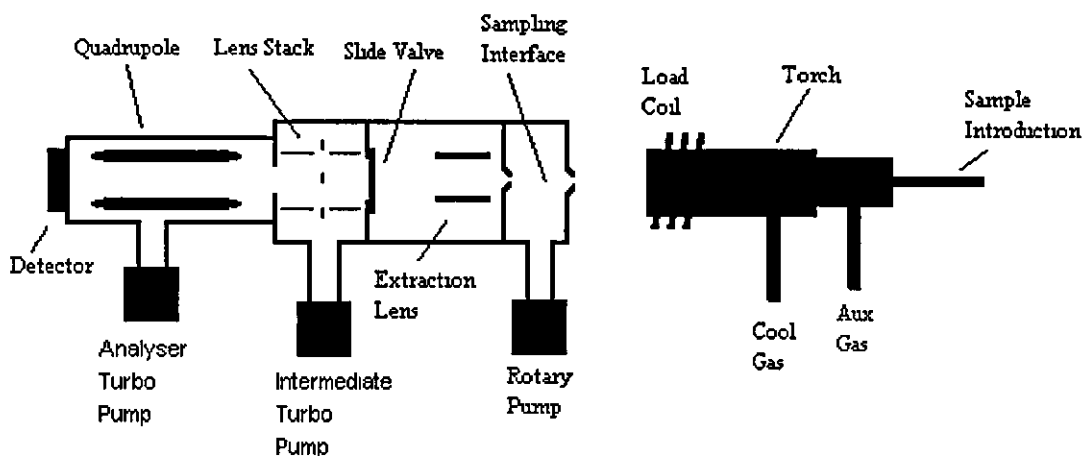
The typical 'doughnut' form of an ICP<sup>6</sup>, in which the R.F. energy is coupled to the outer annulus in the gas stream, provides a region from which energy is transferred by thermal conduction to the central channel. The central channel is usually about 3 mm in

diameter and the gas temperature rises from ambient, at the entrance, to about 8000 K by the time the gas has reached the mouth of the torch, a few milliseconds later.

During its transit through the central channel, the analyte goes through successive stages of desolvation, vaporisation, atomisation and ionisation. It emerges from the torch mouth as a mixture of atoms, ions, residual molecular fragments that may remain undissociated and some unvolatilised particles together with the large quantity of argon carrier gas. The central channel of the plasma remains distinct for a distance of about 10 mm above the load coil, beyond this the analyte progressively diffuses into the outer annulus<sup>7</sup>.

It is evident from the appearance of many intense ionic lines in the emission spectrum, that the ICP can be used as an effective ion source. The major problem arising when the ICP is coupled to a mass spectrometer (MS) is that of pressure difference. The ICP operates at atmospheric pressure, whereas the MS requires an operating pressure of  $<10^{-5}$  mbar for resolution and detection of ions. To overcome this problem it is necessary to use an interface between the source and analyser. Fig 1 shows a schematic of a typical ICP-MS system.

**Figure 1. ICP-MS Schematic**



### **1.2.2 Ion Extraction**

A portion of ions from the ICP are extracted via a circular orifice, usually 1.0 mm in diameter within a water cooled sampler cone made of nickel, into a differentially pumped region at approximately 1 mbar. The volume of plasma sampled is three orifice diameters wide and two deep. The gas expanding into this low pressure region reaches a velocity exceeding the speed of sound. The temperature drops rapidly and reactions which could change the composition of the extracted gas are halted. As the gas pressure and temperature drop, the kinetic energy is converted into directed flow along the axis and a free jet is formed. The central orifice of a conical skimmer cone is located 6.5 mm behind the sampler to transmit as much of the sampled beam as possible into a second vacuum chamber. The pressure in this second chamber is low enough and the mean free path long enough for an ion lens stack to collect, focus and transmit the ions to a mass analyser. Photon noise from the plasma is minimised by including a photon stop, located behind the skimmer, in the ion optics<sup>8</sup>.

### **1.2.3 Mass Analyser**

The axial beam of ions from the ion lenses is focused into the mass analyser, which is generally a quadrupole system for ICP-MS, having rods of 12-18 mm in diameter and 200 mm long. In order to maintain ion transmission out to high masses, it is important that ions travel along the axis of the rods relatively slowly so that they experience an adequate number of R.F. field cycles for good resolution. This requires that the ions enter the rod system with a low mean ion energy.

A quadrupole mass analyser operates as a filter along the axis of which a stable ion path exists for ions of only one mass/charge ratio. The transmitted mass is determined by the amplitude of the combined R.F. and D.C. potentials fed to the rods from the R.F. generator, and the resolution determined by their ratio. The mass resolution achievable



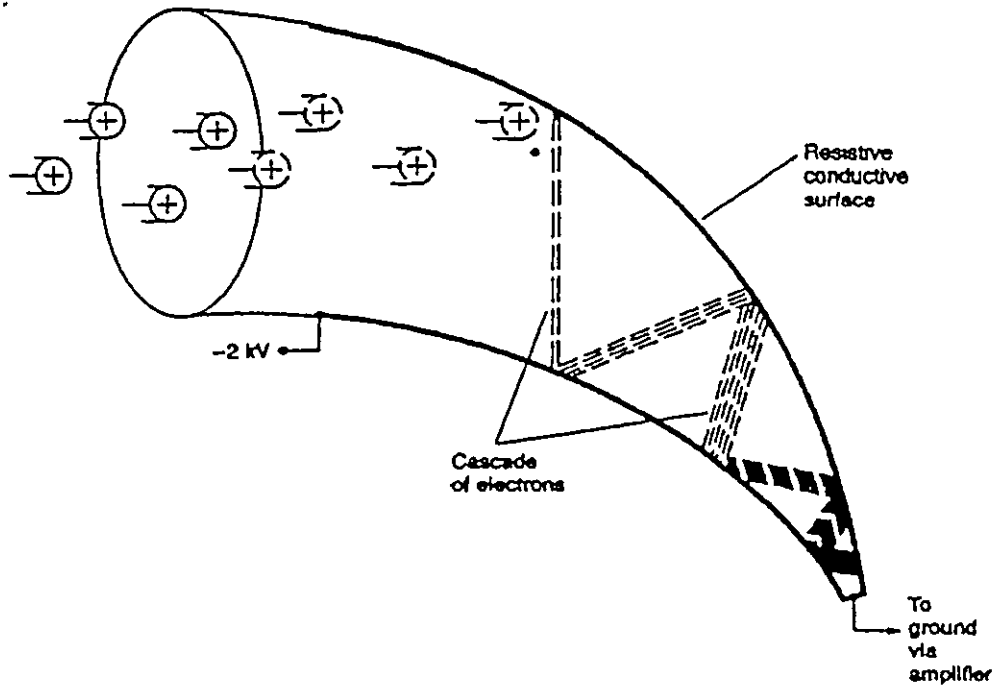
is usually sufficient to completely separate adjacent elemental peaks, but not sufficient enough to separate an oxide peak from an elemental peak with which it interferes.

In ICP-MS systems the ion densities are generally much lower than those found in organic work and therefore very little contamination is deposited on the analysing rods, which must be kept clean for optimum performance.

#### **1.2.4 Ion Detection**

The number of analyte ions in the beam entering the mass analyser in an ICP-MS is small, typically giving beam currents of less than  $1 \cdot 10^{-13}$  A. The instrumental background is also extremely low, only a few ions per second. The full capability and sensitivity of the technique, which is largely due to this very low background, can only be exploited by counting individual ions. Sufficient electrical gain and fast response can only be obtained by using electron multiplier detectors which are capable of counting pulses at rates above  $10^6$  counts per second and have a natural background of 1 count per second. The most common ion detectors used in ICP-MS are Channeltron electron multipliers, Fig 2 The electron multiplier consists of an open glass tube with a cone at one end. The interior tube and cone are coated with a lead oxide semiconducting material. Electrical connections are made to the semiconducting coating through metal strips. For detection of positive ions, the cone is biased at a high negative potential ( $\sim -3$  KV) and the back of the tube is held near ground. When a voltage is applied across the tube a continuous gradient of potential exists within the tube.

Fig.2. Electron Multiplier



When a positive ion leaves the mass analyser and hits the surface of the multiplier cone, one or more secondary electrons are ejected. These secondary electrons move further into the tube region closer to the ground. As they travel along the tube they come into contact with other sections of the coating and emit more secondary electrons. This process is repeated many times along the length of the tube. This results in a discrete pulse containing as many as  $10^8$  electrons at the collector after an ion strike at the mouth of the detector.

## **1.3 ICP-MS Calibration Modes**

### **1.3.1 Mass Calibration**

Mass calibration of an ICP-MS instrument is required to match a pre-defined, software generated mass spectrum to the output of the quadrupole. Typically six elements are chosen across the mass range to produce the mass calibration.

### **1.3.2 Semi-quantitative Calibration**

Semi-quantitative data can be generated from ICP-MS instruments by correlation with a pre-determined response curve. The response curve is generated by collecting data for a number of elements across the mass range and producing a plot of mass against sensitivity. The response for each element is corrected for isotopic abundance, relative atomic mass and degree of ionisation. Once the response curve is established, the concentration of elements in an unknown sample can be estimated by reference back to the response curve. This calibration method is an ideal survey tool, particularly if an unfamiliar matrix is to be analysed or if the approximate levels of components in a sample are required. The accuracy of the data produced by this method is variable and matrix dependent, with accuracies typically in the region of 60-122 % across the mass range<sup>9</sup>

### **1.3.3 Quantitative Analysis**

#### **External Calibration**

The most common calibration method uses a set of external calibration standards. For solution analysis these would typically contain the analytes of interest in a dilute acid

matrix For direct solid sample analysis, standards would normally be matrix matched to the samples The fitting of a calibration line to measured standard data is usually achieved using least squares regression analysis. Under ideal conditions, measured data would form an exact linear function of concentration. However, errors are always introduced on real data and therefore a statistical procedure is used to calculate the best fit calibration line The goodness of fit of the line to the measured data is termed the correlation coefficient.

### Standard Additions

This alternative calibration strategy is performed by taking aliquots of the sample to be analysed and adding increasing quantities of the elements to be analysed. The increments are normally equal and the number of aliquots is at least three. The samples are analysed and a graph constructed of the integral of the isotope of interest versus the concentration of the element added. The intercept of the calibration line on the X axis gives the concentration in the unspiked sample This method can produce highly accurate data, but has the drawback of being time consuming to perform<sup>10</sup>.

### Internal Standards

Internal standards are commonly used in ICP-MS to monitor and correct for fluctuations in signal The effectiveness of an internal standard requires that its behaviour reflects that of the other elements to be analysed. For the analysis of samples in solution, the addition of internal standards is simple, using an internal standard with solid sample introduction is not so straightforward. The use of an indigenous internal standard is at present the most effective way of using internal standards in solid sample analysis. The internal standard should not suffer from an isobaric overlap or polyatomic interferences Two elements commonly used as internal standards are In and Rh, which lie in the central part of the mass range. Care must be taken when choosing an internal standard

to ensure that the elements of interest behave in a similar fashion to the internal standard in the matrix to be analysed.

### Isotope Dilution

Stable isotope dilution is another strategy which can be employed for elemental analysis. The basis of the technique is the measurement of the change in the ratio of signal intensities for two selected isotopes after the addition of a known quantity of a spike which is enriched in one of these isotopes. The method can be applied to any element with at least two stable isotopes.

## 1.4 Data Handling

There are two principle modes used for data collection in ICP-MS : (i) peak jumping and (ii) mass scanning

### Peak Jumping

In this mode, the mass spectrometer is used to collect data at a number of fixed mass positions (usually 1-3) for each isotope of interest. The location of the central position of the peak is particularly important, since it is used as the starting point for the acquisition of data. Ensuring that the instrument mass calibration is accurate is therefore a requirement. The advantage of this method is that data are only collected for the elements of interest, no time is wasted collecting data for elements that are not required. The amount of time data is collected at each isotope can be varied. These advantages help to improve counting statistics and allow optimisation of the acquisition time available. The disadvantages are that no data is available, should additional isotopes subsequently be required and interference and matrix effects are often missed as the spectrum is not available for examination.

## Mass Scanning

An alternative mode of operation is to collect data for a relatively large number of points so that the peak shape is defined for each isotope and the area under the curve is integrated. A complete spectrum containing information for all isotopes within the mass range 4-240  $m/z$  can be collected and stored. The advantage of the scanning mode is that data are available not only for the elements of immediate interest but also over a wider mass range for archival purposes. In addition, interfering peaks are more easily identified. A disadvantage is that data collection is generally slower and therefore longer acquisition times are required to improve counting statistics.

Single ion monitoring is an additional method of data collection. In this mode, data from a single isotope is collected and displayed. This mode is not widely used, as frequently the analyst is interested in more than one isotope present in a sample matrix. This type of data acquisition is useful when maximum sensitivity of a particular ion is required.

Time resolved analysis (TRA) is a specialised data acquisition tool. Data can be collected at specified time intervals whilst sample is being continuously introduced into the ICP-MS. This type of data acquisition is particularly useful for transient signals.

## **Chapter 2:**

# **Solid Sample Introduction**

### **2.1 Introduction**

The direct introduction of solid samples into atomic spectrometers offers a number of possible advantages from the analytical chemists viewpoint. These include, the reduction of time involved in sample pre-treatment, avoiding the use of potentially hazardous reagents and reducing the risk of sample contamination. In addition, separation or concentration steps may be avoided and there is less risk of diluting the analyte below a detectable concentration, or of losing volatile components during digestion procedures.

For ICP-MS, it is recognised that among the limitations of the technique are the isobaric interferences that occur due to the presence of molecular species derived from the solvents or reagents used in sample dissolution procedures. The desire to overcome these interferences has produced new interest in the development of reliable alternatives to sample introduction by nebulisation

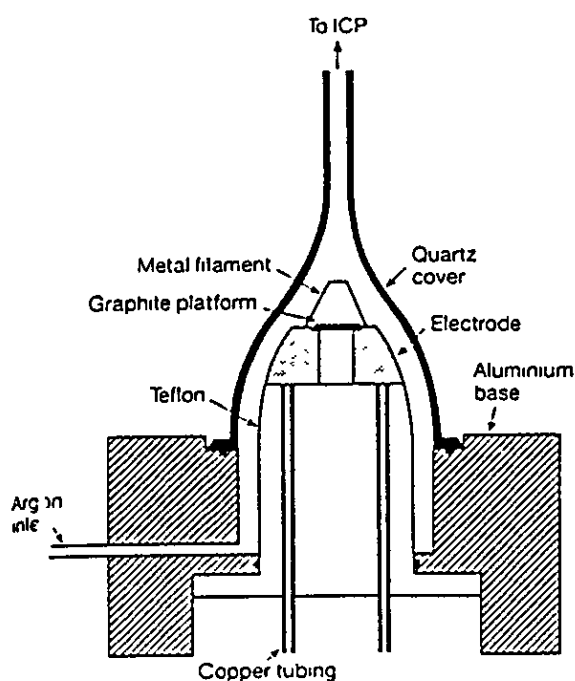
Various solid sample introduction systems have been developed, including electrothermal vaporisation (ETV), direct sample insertion (DSI), arc nebulisation, slurry nebulisation, and laser ablation (LA) and these have been reviewed in the literature in detail by Baumann<sup>11</sup>, Thompson<sup>5</sup> and Tyson<sup>12</sup>.

## 2.2 Electrothermal Vaporisation

ETV employs the use of a resistively heated graphite rod or furnace to vaporise a small volume of solution or solid. The technique was first described as an alternative sample introduction system for ICP-AES<sup>13</sup>. Various research groups<sup>13-18</sup> have developed modified versions of the original design Fig. 3 shows a vaporiser designed to be coupled to an ICP-MS<sup>19</sup> instrument. Argon flows through the device and carries the sample to the plasma with a transport efficiency of >80%. The filament vaporising temperature and the argon flow rate are critical parameters associated with this technique. Today most commercial systems made are of modified tube furnace atomisers of the type used for atomic absorption spectrometry.

The advantage of ETV over pneumatic nebulisation is the improved transport efficiency, the ability to separate analyte elements from the matrix with temperature programs, little or no sample preparation and low detection limits. A disadvantage is poor precision due to the reproducibility of the vaporisation process.

Fig.3. Electrothermal Vaporiser



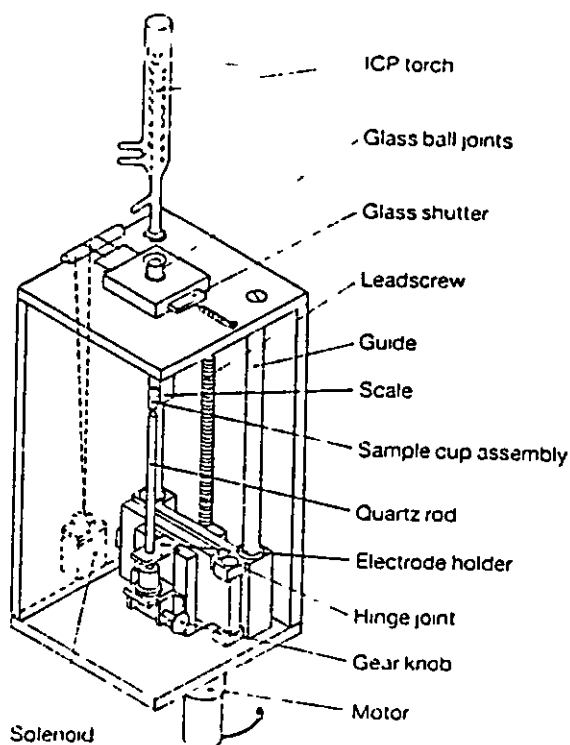


## 2.3 Direct Sample Insertion Devices

Direct sample insertion devices were first described by Horlick, Salin and Sing<sup>20,21</sup> for ICP-AES. Transport efficiency is effectively 100% as the whole sample is inserted directly into the ICP torch. The base of the torch is sealed by a glass shutter to avoid disturbance of the plasma. To insert a sample the glass shutter opens, the sample is introduced until the base of the torch is sealed with a teflon stop. The process is automated to improve reproducibility.

The benefits of ETV also apply to DSI devices, i.e. reduced matrix effects and improved detection limits. DSI does not afford the flexibility of ETV to deal with complex matrices. A typical DSI device can be seen in Fig 4.

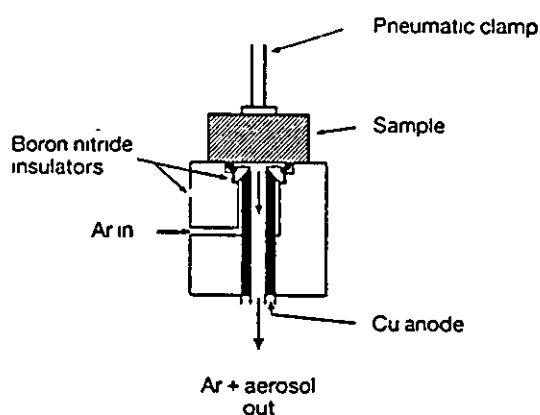
Fig 4. Direct Sample Insertion Device



## 2.4 Arc Nebulisation

Arc nebulisation uses an intermittent spark between a copper anode and the sample which acts as a cathode<sup>22</sup>. The arcing causes the sample to erode. The eroded material is then transported to the ICP by a stream of argon. The limitation of arc nebulisation is that the sample must be conducting. Fig 5 shows an arc nebulisation device

Fig. 5 Arc Nebulisation Device



## 2.5 Slurry Nebulisation

Slurry nebulisation is a technique allowing the introduction of solid samples suspended in aqueous solutions through the use of a Babington or V-groove nebuliser. This technique does not offer improvements in transport efficiency, but calibrations can be performed using aqueous standards<sup>23</sup>. The disadvantages of this technique are that the samples have to be reduced to particle sizes of  $<5 \mu\text{m}$  and grinding agents and dispersants can cause isobaric interferences.

## 2.6 Laser Ablation

Laser ablation for direct solid sampling has many of the beneficial features described for the other solid sampling devices and is also capable of providing spatially resolved information about the chemical composition of samples. To date, there seems to be little agreement on the fundamental design parameters of laser ablation systems, such as laser power, wavelength, frequency and spot size. Calibration is also of major concern, with matrix matching on all spatial scales being essential to produce accurate quantitative data.

The technique of laser ablation inductively coupled plasma mass spectrometry (LA-ICP-MS) was first described in the literature by Gray<sup>24</sup> in 1985. This paper described the use of a ruby laser, capable of producing laser energies from 0.3 - 1 J, for the sampling of rock samples which had been pelleted with a binder. Arrowsmith<sup>25</sup> followed on from the work of Gray, but used a Nd:YAG laser operating at 1.06  $\mu\text{m}$  and a pulse energy of 160 mJ. This work was unique in that it was the first application to use a high repetition rate of 10 Hz to analyse solid samples. Low repetition rates result in transient signals with precision limited by the pulse-to-pulse stability of the laser. The higher repetition rate used in this work, in conjunction with a suitable flow system for transportation of the ablated sample to the plasma, resulted in a continuous signal, giving improved precisions of the order of +/- 5%. Since these early applications of LA-ICP-MS, a variety of publications have appeared in the literature<sup>26-36</sup>.

Marshall<sup>30</sup> used LA-ICP-MS to analyse trace elements in polypropylene, polyester and nylon. The results showed that for semiquantitative analysis, values within a factor of two of the known value could be achieved for most elements. Perkins *et al.*<sup>31,32</sup> prepared synthetic standards, both as fused glass discs and pressed powder pellets for

the analysis of carbonates. The analysis of carbonate shell material from a marine bivalve demonstrated the potential use of LA-ICP-MS in pollution monitoring

Various authors have written reviews covering all aspects of the field. Moenke-Blankenburg<sup>33</sup> reviewed the use of lasers as a method of sub-sampling Sneddon *et al.*<sup>34</sup> investigated the interaction of laser radiation with the sample and concluded that it was a complex mechanism which was not fully understood. Denoyer *et al.*<sup>35</sup> gave an overview of laser sampling and also a survey of the practical applications of LA-ICP-MS Darke and Tyson<sup>36</sup> produced a comprehensive (1000 references), review of the interaction of laser radiation with solid materials and its significance to analytical spectrometry.

### **2.6.1 Processes Occurring During the Ablation Event**

When a laser beam is focused onto a solid surface, the irradiance in the spot can lead to a variety of effects including heating, evaporation, degradation and several non-linear phenomena. For most applications<sup>37</sup> power densities or fluences of between  $10^6$  and  $10^9$   $\text{W cm}^{-2}$  are common. When the fluence exceeds a threshold value of about  $0.4 \text{ GW cm}^{-2}$ , the formation of a plasma is observed expanding out from the surface of the solid and material is ejected from the sample due to the pressure generated by the expansion of gas in contact with the surface. The formation of this plasma is not thought to be beneficial as incoming radiation is absorbed, reducing its effectiveness in contributing to the ablation event. The formation of a laser induced plasma on the sample surface is dependent both on the wavelength of laser light and the nature of the sample being ablated. Sneddon *et al.*<sup>38</sup> compared the laser induced plasma formed on copper and lead targets. The plasma size and temperature were found to be different for the two metals

Huang *et al.*<sup>39</sup> postulated the occurrence of two different ablation mechanisms, a less efficient one occurring at higher fluences. The crater sizes produced by the higher

fluence laser pulses were larger than the calculated laser spot on the surface indicating the occurrence of an indirect ablation event such as heat conduction or laser shocks. Such a mechanism was believed to be less efficient in ablating or transferring materials than the direct interaction between laser and samples. The cross-over point from the more to less efficient ablation event was estimated to occur at fluences ranging from 130 to 330 J cm<sup>-2</sup>. This type of two stage mechanism was also observed by Fernandez *et al*<sup>40,41</sup> and Koppenaal<sup>42</sup> who proposed that at higher power densities, typically above 0.5 GW cm<sup>-2</sup>, the laser induced plasma at the sample surface was absorbing a proportion of the laser radiation

## 2.6.2 Models of the Ablation Event

Most of the work carried out on the processes occurring when laser radiation interacts with a solid surface can be found in the Physics literature. Most researchers agree on the presence of two mechanisms, photothermal and photochemical. The photothermal mechanism predominates in the infrared and the photochemical mechanism is increasingly evident for lasers operating in the ultraviolet region of the spectrum. It must be noted, however, that both these mechanisms occur simultaneously to a lesser or greater degree.

Srinivasan and Mayne-Banton<sup>43</sup> described the ablation of polyethylene tetracarboxylate (PET) at 193 nm and concluded that the ablation was purely photochemical in nature.

Srinivasan and Garrison<sup>44</sup> carried out further work in 1984 on modelling the laser ablation process. This study involved the ablation of organic polymers and concluded that at 193 nm, a photochemical mechanism is predominantly responsible for the removal of material. At 532 nm a thermal process that melts the sample as well as etching it is predominant.

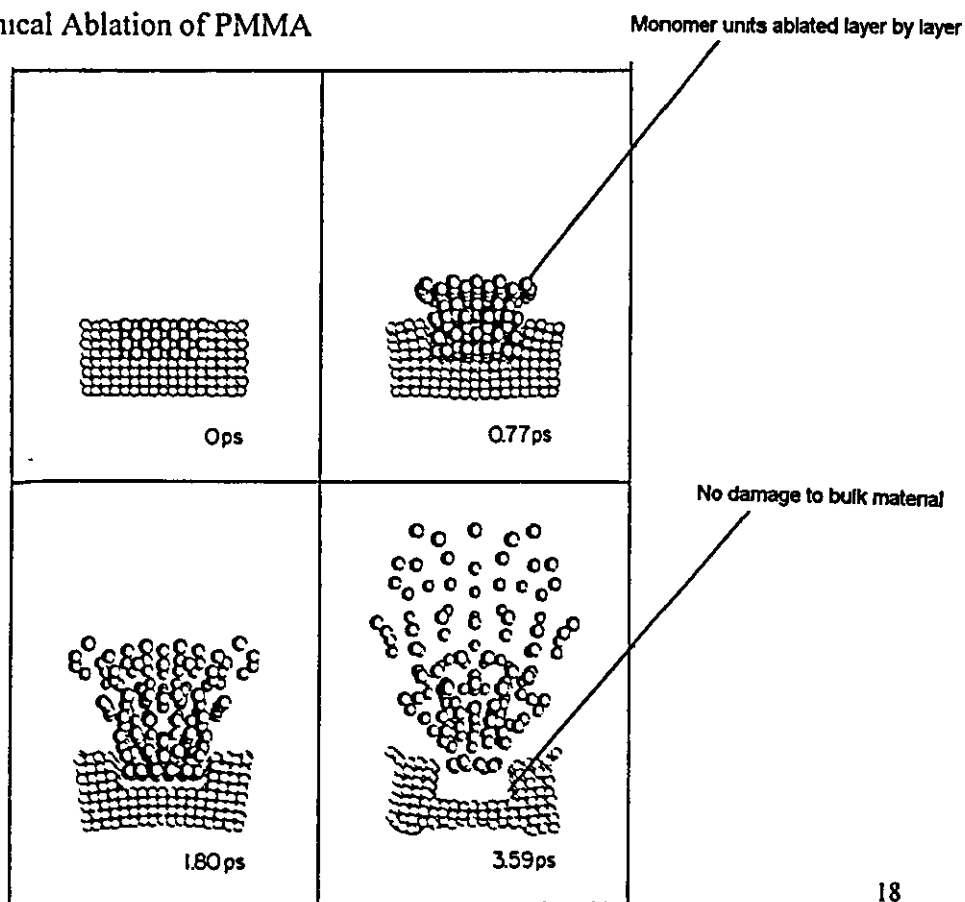
removal of material. At 532 nm a thermal process that melts the sample as well as etching it is predominant.

The absorption of UV radiation by organic molecules is known to involve an electronic transition to a higher state. If the photon energy is greater than the dissociation level then the molecule can dissociate immediately. Visible or infrared radiation is also able to ablate organic material. There is however, insufficient energy in one photon to break a bond. The energy is therefore absorbed into the vibrational modes of the molecule causing heating. Eventually a sufficient number of photons may be absorbed to initiate dissociation.

### Photochemical Model

Polymethylmethacrylate (PMMA) was the polymer used in the study<sup>44</sup>. Fig.6 shows a representation of the photochemical ablation process on a picosecond time scale.

Fig.6. Photochemical Ablation of PMMA

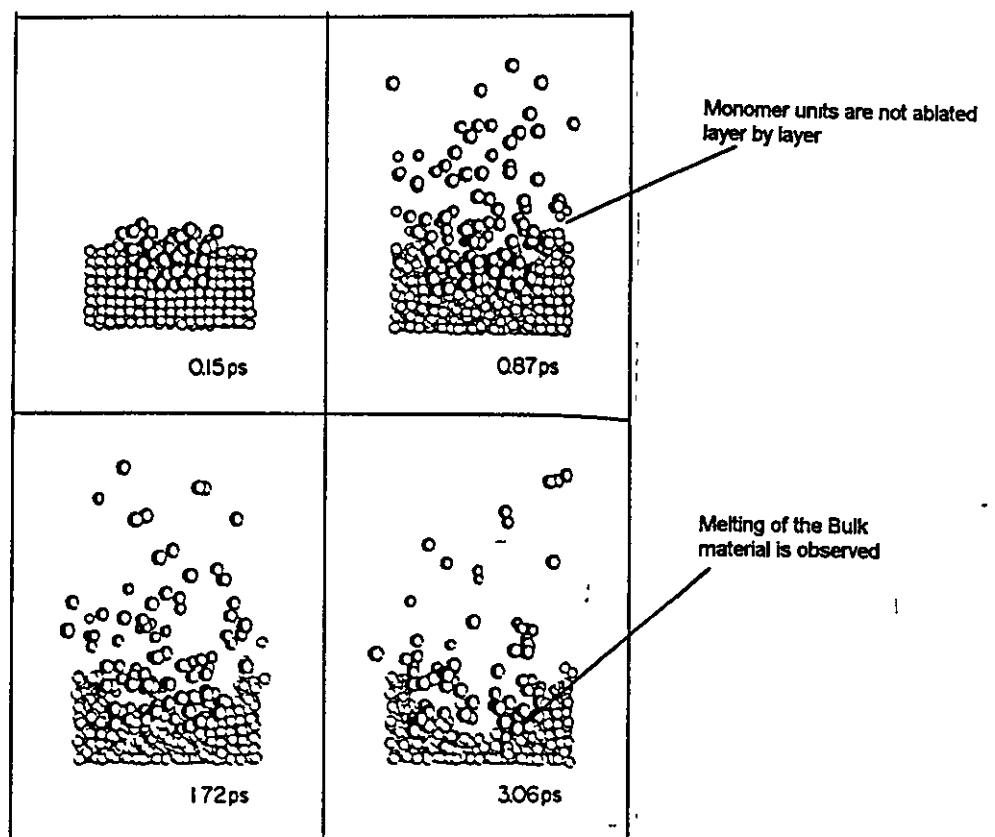


From the time sequence it can be seen that the reacted material ablates without melting the remainder of the sample and that the material ablates layer by layer.

### Thermal Model

Fig.7 shows the predicted thermal model for ablation of PMMA with laser light at 532 nm.

Fig.7. Thermal Ablation of PMMA

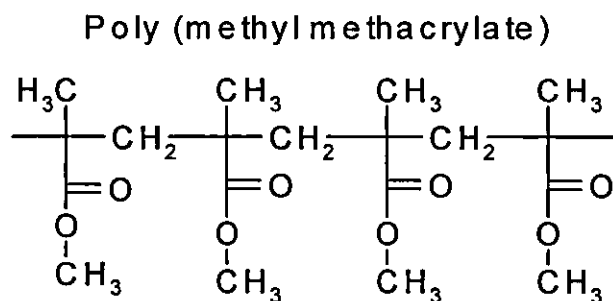


The ablation of material from the polymer is indicative of evaporation rather than volume explosion. Photon energy is absorbed into the vibrational modes causing a heating effect. Thermal ablation causes considerable melting and distortion of the remaining sample: It is also evident that the sample does not ablate layer by layer.

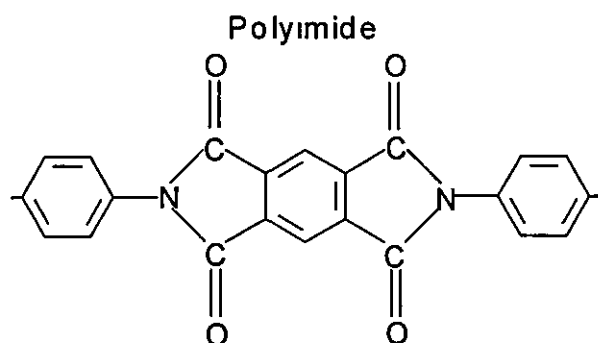
The precise wavelength at which photochemical, thermal or both processes occur is not yet understood, but will depend on the characteristics of individual materials.

A dynamic model for the UV laser ablation of organic polymer surfaces was postulated by Sutcliffe and Srinivasan<sup>45</sup>. The dynamic model was applied to the ablative photodecomposition (APD) of PMMA and a polyimide. These two polymers have different chemical compositions and spectroscopic properties see Fig 8.

Fig 8 Structure of PMMA and Polyimide







PMMA is a weak absorber compared to the polyimide. The first absorption maximum lies close to the ArF laser emission at 193 nm. At 248 nm the absorption drops by one order of magnitude and at 308 nm PMMA is almost transparent.

The study carried out involved modelling the etch depth of the polymer in  $\mu\text{m}/\text{pulse}$  against the fluence in  $\text{mJ}/\text{cm}^2$ . At 193 nm and at fluences above  $300 \text{ mJ}/\text{cm}^2$ , a threshold value on the etch curve was reached. Formation of a plasma above the surface absorbing the laser energy was attributed to account for this observation. At 248 nm, despite differences in etch depths and fluences, the threshold behaviour was reproduced as above. It was also predicted that at  $400 \text{ mJ}/\text{cm}^2$  more than 30 laser pulses were necessary to start etching. After which a transient signal should be achieved.

The intensity threshold ( $I_t$ ) is given as the energy required to eject material from the surface. The table below shows the intensity thresholds for PMMA at various wavelengths.

$I_t$ (193 nm)	$0.97 \text{ MW}/\text{cm}^2$
$I_t$ (248 nm)	$7.5 \text{ MW}/\text{cm}^2$
$I_t$ (308 nm)	$60 \text{ MW}/\text{cm}^2$

The strongly delocalised electronic distribution of the polyimide gives absorption coefficients that are two orders of magnitude larger than PMMA. The intensity thresholds for the polyimide can be seen below.

$I_t$ (193nm)	0.77 MW/cm <sup>2</sup>
$I_t$ (248nm)	0.98 MW/cm <sup>2</sup>
$I_t$ (308nm)	1.7 MW/cm <sup>2</sup>

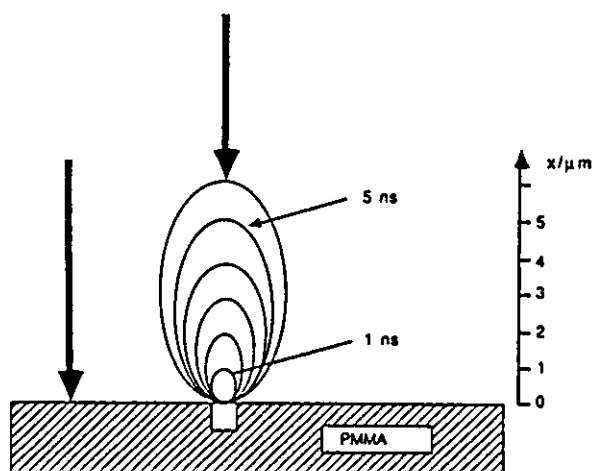
For the polyimide, at all fluences below the threshold level, energy is converted to heat. Beyond this point, at 193 nm and 248 nm, the thermal contribution rapidly reaches a steady state where only a small fraction of the absorbed light is transformed into heat. Thermal contributions become much more relevant when irradiating at 308 nm. For PMMA the thermal contribution is moderate at 193 nm, but is significant at 248 nm and dominates at 308 nm.

Photographic evidence from Simon<sup>46</sup> showed that laser ablation of polyimide was a layer by layer process, consistent with the photochemical model postulated by Srinivasan<sup>44</sup>.

Kuper and Stuke<sup>47</sup> carried out experiments on the ablation of PMMA with 300 fs pulse length excimer laser pulses at 248 nm. Standard excimer lasers have pulse durations in the region of 10-20 nanoseconds. At these pulse lengths, coupling of the laser energy into the sample, the ablation process and the removal of material all happen at the same time. The role of each part of the ablation process cannot therefore be clearly identified. This may not be of significance for many practical purposes, but is of importance for detailed investigations of the ablation process. At a typical etch rate of 1  $\mu\text{m}/\text{pulse}$  and a supersonic velocity of material removal of 1000m/s, corresponding to 1  $\mu\text{m}/\text{ns}$ , it can be seen in Fig.9 that for standard excimer laser pulses only the very first part of the pulse will contact fresh sample material. After 5 ns ablated material has moved 5  $\mu\text{m}$  away

from the sample surface and therefore may shield the remaining surface from laser radiation.

Fig.9 Typical Excimer Laser Pulse



Using 300 fs excimer laser pulses, energy coupling into the sample, incubation and removal of material can be separated. Ablated material will have only travelled 0.3  $\mu\text{m}$  in 300 fs.

It was found<sup>47</sup> that ablation was achieved at fluences five times lower for the 300 fs pulse duration laser compared to the 16 ns excimer laser pulses. This reduces considerably the thermal load on the sample.

### 2.6.3 Effect of Laser Wavelength

A comparison of infrared and ultraviolet radiation and its implications for solid sampling ICP-MS was carried out by Mermet et al<sup>48</sup>. The lasers used for this experiment were a Q-switched Nd:YAG and an excimer. The first experiment performed was to determine the amount of material removed from a copper target as a

function of laser wavelength. It was found that the excimer emitting in the UV ablated seven times more material than the Nd:YAG emitting in the IR for the same output energy of 200 mJ. Photographs taken with a scanning electron microscope of the craters were presented. In the case of the UV laser, a crater with well defined borders and minimal damage to the surrounding material was observed. With the IR laser, the craters were poorly defined. It was difficult to distinguish between the actual crater and the surrounding affected zone. In addition, the presence of a lip of metal that had flowed out of the crater before it solidified was visible, suggesting that significant heating was taking place. The conclusions which can be drawn from the paper were that UV laser sampling was superior to IR laser sampling in every analytical aspect, reproducibility, matrix effects, spatial resolution, quantification and sensitivity.

Geersten *et al*<sup>48</sup> also carried out a comparison of ultraviolet and infrared laser ablation. Three experiments were carried out to determine how ablated mass, ablated mass versus plasma temperature and plasma formation were affected by laser wavelength.

It was determined from the first experiment that the ablated mass per unit energy per unit surface area, as a function of laser fluence, was more than an order of magnitude higher for UV compared to IR ablation of a copper target.

It was concluded from the second experiment that, for the UV laser, a linear correlation existed between ablated mass and the melting temperature, for IR ablation no correlation existed

The final experiment indicated that plasmas produced above the surface during IR ablation were more complex and less reproducible than during UV ablation. The IR plasma was also found to be hotter, allowing less of the beam energy to interact with the sample surface

Laser wavelength is an important factor in the ablation of polymers. UV laser radiation is preferable to IR or visible radiation as less charring of the polymer surface occurs. Lower fluences can also be used with UV ablation, the penetration depth is less and only a short laser pulse length is required.

Ablation of polymers with a strong absorption band corresponding to the wavelength of the laser used require a lower fluence for ablation to begin. An advantage of using lower fluences is that the ablation depth can be accurately controlled. Dyer and co workers<sup>49</sup> demonstrated the effect of laser fluence threshold values using various transitions of excimer lasers. At 308 nm threshold values for polyimide and polyethylene tetraphthalate were 32 and 97 mJ/cm<sup>2</sup>. At 193 nm, the threshold values had fallen to 18 and 14 mJ/cm<sup>2</sup> respectively. The reason postulated for the differing degrees of reduction in the ablation threshold was that the polymers had different absorption characteristics.

A good indicator of the wavelength most suitable for the ablation of a particular polymer is obtained from the analysis of the UV spectra of the sample. This indicates which laser wavelength the polymer will absorb at. Spectra of some important industrial polymers were presented by Phillip<sup>50</sup>. Brannon and Lankard<sup>51</sup> used this type of information when ablating polyimide with a CO<sub>2</sub> laser. The laser could be tuned to either 10.6 or 9.2 μm. At 10.6 μm the polyimide only absorbed very weakly which resulted in poor craters with peripheral damage. At 9.2 μm, the polymer absorbed strongly giving craters with well defined edges, and a low threshold fluence was achieved.

If, as in many applications, it is not possible to tune the laser wavelength to a strong absorption band of the polymer then it is possible to change the absorption characteristics of the polymer. Kawamura *et al.*<sup>52</sup> carried out some doping work by the addition of benzoin to PMMA to increase the absorption of 248 nm laser radiation.

Srinivasan and Braren<sup>53</sup> modified the absorption of PMMA allowing ablation with radiation at 308 nm, a wavelength at which PMMA was previously transparent.

#### 2.6.4 Effect of Laser Parameters

Pulse energy, spot size and frequency are laser parameters of particular relevance to the generation of ablated material. Energies normally used in laser sampling range from a few to hundreds of mJ/pulse. Increasing the laser energy increases the analytical signal up to a threshold value. Laser sampling can therefore be used over a wide dynamic range with control of the laser energy. A low laser energy can be used when sampling concentrated analytes and the laser energy increased for weaker analytes. Prabhu et al.<sup>54</sup> noted, in their work on vaporisation of small volumes of solutions, that at high laser energies condensation of the test solution on the lens window of the laser cell could be observed. The condensation resulted in a decrease in the ion intensities over a period of time, due to the fact that the laser radiation reaching the sample was being attenuated.

Laser energy also affects the size of the crater sampled. However, the analytical signal is not a linear function of the radius of the sampled crater. Denoyer<sup>35</sup> reported that the use of a Nd:YAG laser in free-running mode resulted in an analytical signal that fitted to a cubic function of the area sampled, reflecting a dependence on the volume sampled. In the Q-switched mode, the analytical signal follows more closely the square of the crater radius, namely a dependence on area as opposed to volume. This is consistent with the fact that single pulse Q-switched craters are wide and shallow, whereas single pulse free running craters are deeper and more hemispherical in nature. The effective size of spot sampled is also dependent on the degree of focus of the sampling lens. Defocusing the laser beam can be used to reduce the power density of the beam impinging on the sample and also increase the depth of field providing more representative sampling of the bulk material.

Increasing the frequency of the laser increases the analytical signal, more of the analyte material is sampled increasing the load to the plasma. Initial studies<sup>24</sup> used lasers with maximum repetition rates of 1 Hz, but concluded that the use of high repetition rate lasers at lower laser energies would improve the uniformity of the delivery rate of the sample to the plasma and subsequently improve precision. Arrowsmith<sup>25</sup> confirmed this with a Nd:YAG laser running at 10 Hz. At this repetition rate, the signal was continuous and could be maintained over long periods by translation of the sample. Substantial improvement in precision was reported. Houk *et al.*<sup>55</sup> used a 100 Hz excimer laser and showed an improvement in precision in stepping from 10 Hz to 100 Hz. The improved precision was believed to be due to the generation of finer particles at moderate laser power and high repetition rates, increasing the sample transfer efficiency and reducing disturbance to the plasma.

### **2.6.5 Homogeneity and Sampling**

If bulk or average composition is to be determined, the sampling must be representative. Most commercially available laser sampling devices provide the capability of moving the sample underneath the laser beam during analysis, thereby rastering the beam over a wide sample area. Where depth gradients occur, a pre-analysis exposure of the order of 60 s is used to expose the bulk sample beneath the surface, resulting in a steady state signal.

For most materials, the major variability in LA-ICP-MS analysis is sample heterogeneity. This problem is not unique to this technique, but is an important consideration in all direct solid sampling devices. Heterogeneity implies the presence of a concentration gradient within the analytical sample that can occur along the surface or as a function of depth. Identification and characterisation of lateral or depth concentration gradients can provide valuable information about the nature of the

sample. This is a powerful capability of LA-ICP-MS and has direct application to the study of composite, natural and manufactured materials.

Measurement precisions achieved for homogeneous materials are typically in the range of 2-10% RSD. Reproducibility of the analysis depends on the variability resulting from analytical imprecision and sample heterogeneity. Although the analytical precision will be affected by ion counting precision as well as the stability of sample transport and ionisation, one of the most important sources of variability is the laser sampling process. Because laser sampling is a dynamic process, the specimen being sampled is constantly changing with time. This effect can be insignificant for many materials, but can be significant where sample removal rate is high as is the case with polymeric materials.

Internal standardisation is the technique commonly used for calibrating the analytical response. It also improves the precision of the results. It is not, however, always possible to identify an element in the specimen which is appropriate as an internal standard and that exists in the sample and standards alike. Where the sample is ground, mixed and made into pellet form, an internal standard of choice can be added. Otherwise a matrix element, such as calcium in bone samples, can be used as an internal standard. The distribution of the internal standard element in the sample must be the same as that of the analyte element to achieve the best accuracy and precision of results.

Several alternative approaches for signal normalisation have been proposed. One approach involved the measurement of the acoustic signal in the sampling cell generated by the laser pulse<sup>55</sup>. Another involved measuring the degree of light scattered by the ablated material in the sampling cell<sup>56</sup>. These techniques provide a measurement of the amount of material ablated independent of the ICP-MS measurement. Such independent measurements can be advantageous, however, both approaches depend on



the physical properties of the ablated material, such as particle size distribution and expansion distance. Because the physical properties of the ablated sample plume can be affected by the sample matrix type, these normalisation approaches may be vulnerable to matrix related effects.

### 2.6.6 Interferences

Laser sampling of solids removes the need for dissolution of the sample. This generates a dry plasma low in the components which form polyatomic ions and refractory oxide species i.e. O and H. It would be expected that the level of oxide interference would be reduced for laser ablation compared to solution nebulisation. Prabhu *et al*<sup>54</sup> demonstrated that for La and Ce with laser ablation the intensity of the  $MO^+$  peak is about 1% of  $M^+$  peak compared with 5% with the standard nebulisation technique. Data presented in the Handbook of ICP-MS<sup>9</sup> shows that the oxide and hydroxide levels are almost 2 orders of magnitude lower for laser sampling. It was also noted that the signal due to the formation of  $^{40}Ar^{16}O$  was indistinguishable from the background. This would be of particular value where the analysis of Fe is required. It must be noted, however, that O and H contribute to the total electron number density of the plasma. Table 1 shows the concentration of various species in atoms  $cm^{-3}$  for a wet plasma. Thus the removal of O and H may cause a reduction in the ionisation potential of the plasma.

Table 1: Concentration of Various Species in a Wet Plasma

Species	Concentration (atoms/cm <sup>3</sup> )
Ar	$9.4 \times 10^{17}$
H	$1.1 \times 10^{16}$
O	$5.4 \times 10^{15}$
N	$2.3 \times 10^{13}$

Handbook of ICP-MS, Jarvis, K E , Gray, A L. and Houk, R S , Blackie, 1992

## Chapter 3:

### Instrumentation

#### 3.1 ICP-MS

The ICP-MS used during these studies was a prototype PQ 1 instrument (V.G. Elemental, Winsford, Cheshire, UK). The plasma R.F. generator was a 27.12 crystal controlled supply (Plasma Therm Incorporation, Kresson, NJ, USA model HFP 2500F) with an automatic impedance matching network. A glass concentric nebuliser (J.E. Meinhard Associates, Santa Cruz, CA, USA, model TR-30-C2), peristaltic pump (Gilson Medical Electronics, Villiers Le Bel, France, model Minipuls 2) and V.G. Elemental water cooled spray chamber were used for sample introduction. The plasma was centred about the sampling orifice which was in the region of 12 mm above the load coil.

The ion extraction interface was a V.G. Elemental model of the type found in a V.G. PlasmaQuad. A modified version of the V.G. PlasmaQuad II ion lens stack was employed, in which lenses L3 and L4 were of reduced length. A quadrupole mass analyser (Micromass, Altrincham, Cheshire, UK, model 12-12S) having a mass range of 0-600  $\mu$  was used as the mass filter. The detector was a Channeltron electron multiplier (Galileo Sturbridge, MA, USA, model 4870V), positioned at right angles to the central axis

Data acquisition was computer controlled using PQ Vision software provided by V.G. Elemental. The PQ Vision software suite provides a user friendly interface between the ICP-MS and the user, allowing control of all analytical procedures.

A series of optimised ICP-MS operating conditions can be seen in Table 2. The plasma position, ion optics and gas flows, were optimised daily to obtain a maximum and stable signal at  $m/z$   $^{115}\text{In}$  for a  $50 \text{ ng ml}^{-1}$  standard solution. For this particular instrument, a typical count rate of  $4 \times 10^6$  counts / ppm was achieved.

Table 2: Optimised Operating Conditions

Incident power	1.30 KW
Reflected power	< 5 W
Outer gas flow rate	$12.0 \text{ l min}^{-1}$
Intermediate gas flow rate	$1.2 \text{ l min}^{-1}$
Central gas flow rate	$0.75 \text{ l min}^{-1}$
Solution uptake rate	$0.75 \text{ ml min}^{-1}$
Sampling distance	12 mm a.l.c.
Extraction potential	-300 V
Collector potential	-8.4 V
L1 potential	-7.7 V
L2 potential	-51 V
L3 potential	-5.6 V
L4 potential	-57 V
1st stage pressure	2.0 mbar
2nd stage pressure	$1.0 \times 10^{-4}$ mbar
3rd stage pressure	$2.5 \times 10^{-6}$ mbar

The software acquisition parameters used for collecting data were:

Peak jumping mode

3 points per peak

Total acquisition time of 30 seconds

### 3.2 Excimer Lasers

Excimer lasers are a group of lasers in which light is emitted by short lived molecules made up of one rare gas atom such as argon, krypton or xenon and one halogen atom such as fluorine, chlorine or bromine. First demonstrated in the 70's, excimer lasers have become important as they provide a powerful practical source of ultraviolet radiation. The most common excimer laser transitions are shown in Table 3.

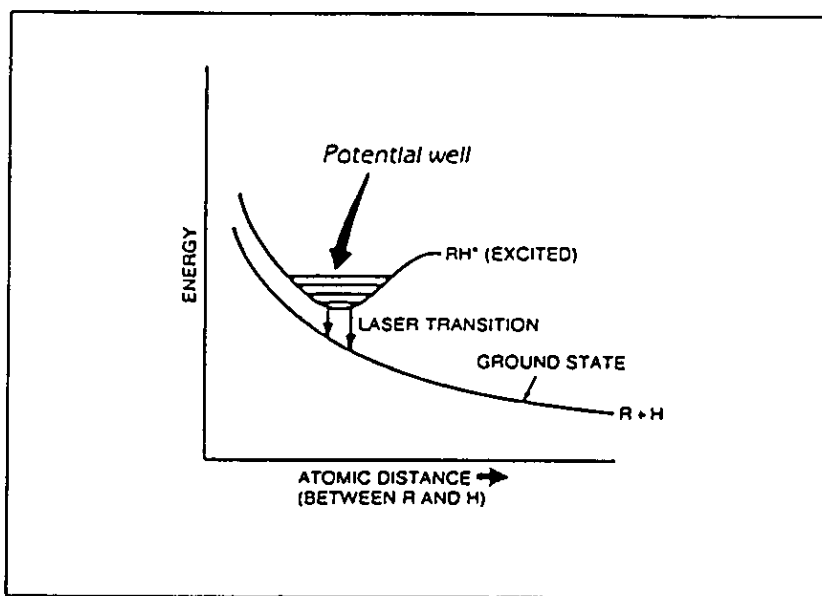
Table 3. Laser Transitions

Transition	Wavelength
ArF	193 nm
KrF	248 nm
XeCl	308 nm

Rare gas halides emit laser light from an unusual type of electronic transition. The two atoms are bound only when the molecule is in an excited state. That is the upper laser level. When the molecule drops to the ground state, the lower laser level, the molecule falls apart. This produces a population inversion in an unusual way, i.e. there are no molecules in the lower laser level as they are not bound together.

Fig.10 shows the energy levels of a typical rare gas halide as a function of the spacing between the two atoms in the molecule. R (rare gas) and H (halide). The dip in the excited state curve shows where the molecules are metastable. The absence of the dip in the ground state curve indicates the molecules fall apart. When the molecule is excited, the energy is at a minimum when the two atoms are a certain distance apart, trapped in a potential well. In the ground state with the lowest possible energy, there is no bonding energy to hold the atoms together and the molecule falls apart.

Fig 10 Energy Levels of a Rare Gas Halide



Excimer lasers are excited by passing a short, intense electrical pulse through a mixture of gases containing the desired rare gas and halogen. It is normal for 90% or more of the mixture to be made up of a buffer gas such as helium or neon, that does not take part in the reaction. Electrons in the discharge transfer energy to the laser gas, breaking up the halogen molecules and causing the formation of electronically excited molecules like krypton fluoride ( $\text{KrF}^*$ , the \* indicates excited state). The molecules remain excited for approximately 10 nanoseconds before dropping to the ground state and dissociating.

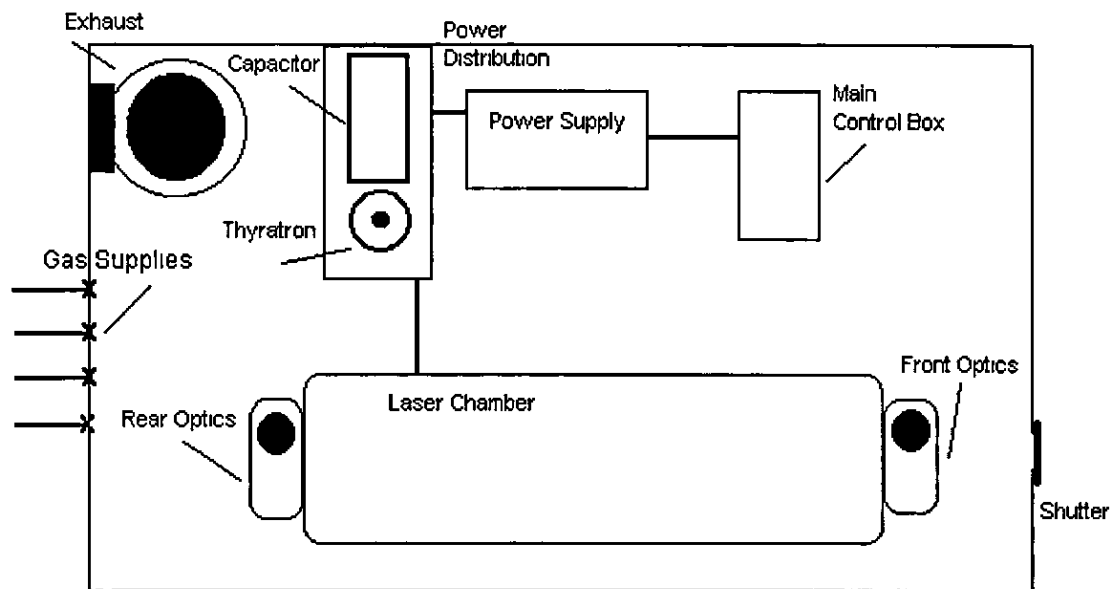
releasing a photon. The output energies involved are large and in the ultraviolet region of the spectrum.

Excimer laser repetition rates depend on the power supply rather than on the gas mixture. The major limitation is the speed of the high voltage switches. Typical repetition rates vary from tens to a few hundred Hertz. Pulse energies range from about 10 mJ to a few joules and differ for the various transitions, with KrF being one of the most energetic.

### 3.2.1 Structure of Excimer Lasers

Excimer lasers have such a high gain that they do not need reflective cavity mirrors. In practice they have fully reflective rear mirrors and uncoated output windows that reflect a few percent of the beam back into the cavity and transmit the rest. As in other high gain pulsed lasers, the discharge in an excimer laser is perpendicular to the length of the tube. A typical excimer design can be seen in Fig.11.

Fig.11. Excimer Laser Layout



Excimer laser tubes are filled with the laser gas mixture, sealed and operated for a certain number of shots until the gas needs to be replaced. The tube's total volume is much larger, typically 100 to 1000 times the volume where the discharge would excite laser action. The number of shots depends on the gas, and can be many millions for longer lived gases.

### 3.2.2 The Laser

A Lumonics EX-742 excimer laser was used to ablate samples. The laser was capable of operating at two transitions: KrF at 248 nm and ArF at 193 nm. All control functions of the laser were performed from a hand held keypad which continuously displayed output pulse energy and other relevant operating parameters of the laser. The laser incorporated a unique 'Stabilase' feature which automatically adjusted the voltage applied to the electrodes to maintain the required output energy.

Laser energy was coupled to the target by means of a simple optical system which consisted of a one metre optical bar onto which a 50 mm glass disc with a 4 mm hole, to act as a mask, and a fused silica lens with 100 mm focal length were mounted. The beam was turned through 90° by a fused silica prism to allow the samples to be mounted horizontally. Samples were mounted in an in-house constructed ablation cell with a fused silica window to allow transmission of the laser radiation. A transverse flow of argon was used to flush ablated material from the cell which had an internal volume of 40 cm<sup>3</sup>. The cell was mounted on slides on the optical bar allowing movement in the x-y-z planes by the use of hand driven micrometers. Fig.12. shows a photograph of the optical system and Fig. 12a shows a schematic of the laser cell and sample introduction system.



Fig.12. Laser Optical System

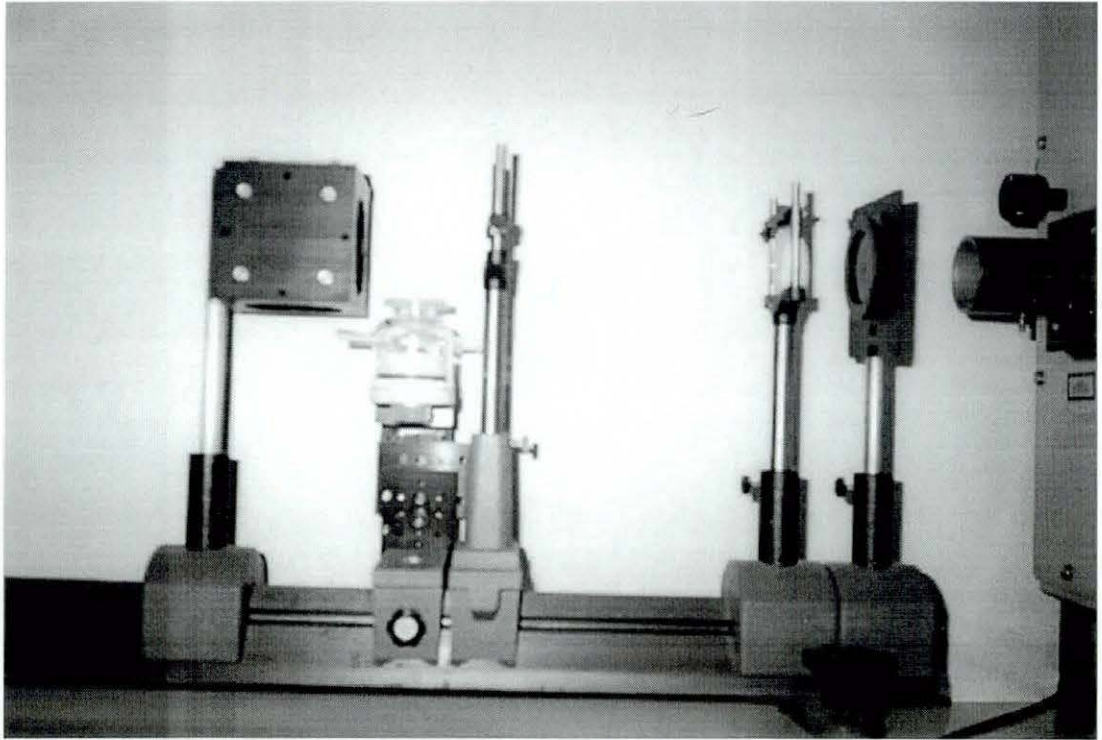
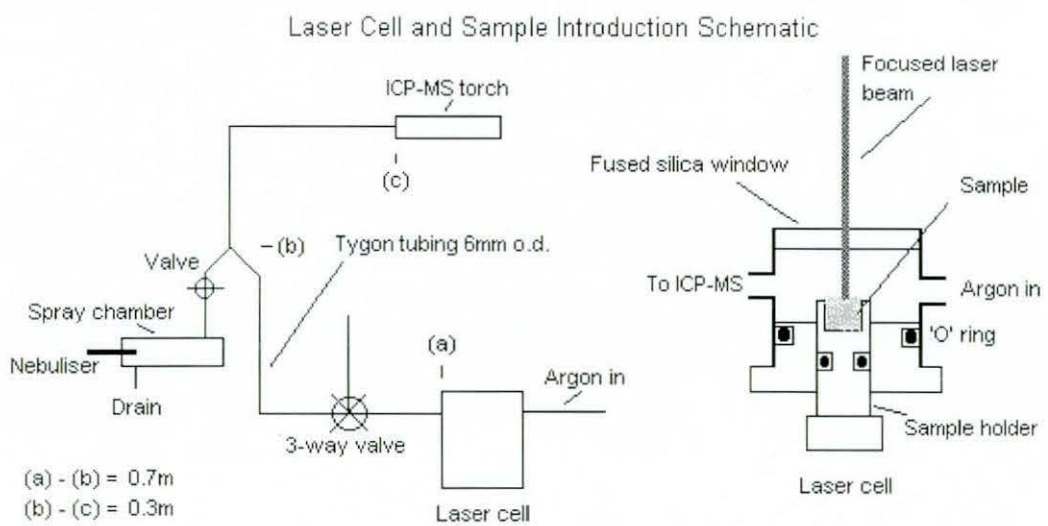


Fig.12A. Schematic of Laser Cell and Sample Introduction System



The resultant aerosol was transported to the ICP-MS via a one metre length of Tygon tubing having an internal diameter of 6 mm. Transport of both ablated material and nebulised solution was provided by a dual gas flow system. The two flows converged prior to the injector tube of the torch. The laser ablation system had a multiple port valve to allow the sample cell to be opened and then flushed with argon, preventing entrainment of air into the plasma.

Table 4 Typical Laser Operating Conditions

Wavelength	248 nm
Energy	40mJ per pulse
Repetition rate	5 Hz
Pulse duration	14 ns
Laser cell argon flow	1.0 l min <sup>-1</sup>

## Reagents

All solutions were prepared from 1000 ppm stock reagents (Johnson Matthey, Royston, Hertfordshire, UK, Grade Specpure). Dilution was made by the use of graduated flasks and auto pipettes with ultrapure 18 M $\Omega$  DI water (Elga, High Wycombe, Buckinghamshire, UK, Model Maxima). The polymer additive used for modification of absorption coefficients was poly sodium 4-styrene-sulphonate (Aldrich, Gillingham, Dorset, UK). Glass standard, NIST 613, was obtained from the National Institute of Standards and Technology and was used as a certified reference material.

### 3.3 Typical Run Sequence of the LA-ICP-MS System

The plasma was ignited and then allowed to stabilise for approximately 1 hour. The instrument operating conditions were then optimised in turn to obtain a maximum signal for In. The following parameters were optimised daily: Torch position relative to the sampling cone, ion optics and gas flows. A series of calibrations were then performed via the PQ Vision operating software and employing a multielement solution containing  $50 \mu\text{g l}^{-1}$  of the following elements: Be, Co, In, Ce, Pb, and U.

The first calibration performed was a mass calibration, during this procedure the software matches a pre-defined mass spectrum to the output of the quadrupole. This ensures that the masses acquired by the instrument are accurate with respect to the standard spectrum.

A summary of the mass calibration was as follows:

An element menu, method and procedure was created for Be, Co, In, Ce, Pb, and U. A tune solution containing the described elements was introduced into the ICP-MS. The data were collected and the calibration performed. The resulting mass calibration is then stored.

The laser was turned on and the appropriate gas fill introduced into the chamber. Standards for ablation were placed in the laser cell. The cell was then purged with a stream of argon to prevent air from being introduced, which would extinguish the plasma. The laser was then operated at the required laser energy and frequency settings and the analysis performed.

## Chapter 4:

# Calibration for Laser Ablation ICP-MS

### 4.1 Introduction

One of the greatest problems associated with LA-ICP spectrometry is the method of calibration. With laser sampling many samples can be analysed directly, without the need for any sample preparation. The extent to which the sample needs preparation depends on its nature and the information required.

For powdered samples it is beneficial to stabilise the sample by compacting it into a pellet, with or without the presence of a binding agent, or by fusing it to a borate glass. Samples that are not homogeneous may require grinding and mixing before stabilising.

Quantitative analysis by LA-ICP-MS is difficult to achieve for many sample types. This reflects the lack of suitable standards which ideally, but unobtainably, need to be identical to the sample both chemically and physically on all relevant spatial scales. Accurate results are generally only obtained when the sample and the standard are prepared in the same matrix. An example is the analysis of stainless steels<sup>57</sup>, where closely matched standards are available. In addition to matrix matching, the use of an internal standard appears to be essential due to the fact that the amount of sample ablated varies from shot to shot<sup>58,59</sup>. For any calibration method to produce accurate quantitative results some form of matrix matching is required as well as the use of an internal standard.

## 4.2 Calibration Strategies Currently in Use

Calibration strategies currently employed for LA-ICP-MS can be categorised into two broad groups. 1. Solid standard calibration and 2. Aqueous standard calibration. Most applications of LA-ICP-MS use a form of solid standard calibration, but there are a few interesting cases of aqueous calibration in the literature. Solid and Aqueous calibration strategies will be reviewed in the following sections.

### 4.2.1 Solid Standard Calibration

The most common calibration standards used for LA-ICP-MS today are the National Institute of Standards and Technology reference materials. The 600 series consist of a range of glasses containing of the order of 20 trace elements with concentrations from high  $\mu\text{g l}^{-1}$  to hundreds of  $\mu\text{g ml}^{-1}$ . Whilst these glasses are useful reference materials, it must be considered that one is restricted to the trace elements and the concentrations at which they are present in the glass. Recent work by Pearce *et al*<sup>70</sup> has shown that there is disagreement with the certified NIST values. A compilation of analyses from various laboratories was considered. Their results were collected and collated and a recommended working concentration for each element for NIST 610 and 612 was reported.

Hamilton and Hopkins<sup>71</sup> have produced an alternative set of homogenous glass standards by using a coprecipitated gel technique. A series of glasses were produced and their suitability assessed as standards for LA-ICP-MS by a collaborative study. The results were inconclusive showing a high degree of variation. It was felt that more work was required before any firm statement could be published on the composition of the glasses.

Other forms of solid standard calibration tend to focus on the production of matrix matched standards relating to the application being described. There has been very little work reported on calibration techniques that are universal or at least are applicable to a variety of sample matrices. This has resulted in a range of application specific solid sample calibration techniques.

Van Heuzen<sup>60,61</sup> studied quantitative elemental analysis of solids by LA- ICP-MS. Two different methods of sample preparation were investigated. The first method involved matching with a glass matrix. The solids were mixed with a flux and fused to a glass bead to give similar matrix composition. The second method involved matching with a pressed pellet. The solids were mixed with a binder material in a ratio of 1:10 and then pressed into a pellet.

Developments in the quantitative and semiquantitative determination of trace elements in carbonates by LA-ICP-MS were reported by Pearce *et al*<sup>32</sup>. An analytical technique was developed using a single multi-element standard to calibrate the instrument across the whole mass range. The same group<sup>31</sup> had previously described a quantitative technique for the analysis of carbonate materials. Standards were prepared as pressed briquettes using CaCO<sub>3</sub> as a base followed by the addition of oxides of the elements of interest.

Williams and Jarvis<sup>63</sup> carried out an assessment of LA-ICP-MS for quantitative multi-element determinations in silicates. Pressed powder pellets of silicate rock reference materials were used as calibrants.

Other solid sample calibration techniques including glass and polymer samples are described in the literature<sup>66-68</sup>.

## 4.2.2 Aqueous Standard Calibration

Aqueous calibration techniques presented in the literature may be used for a wide range of sample matrices. There are considerable problems associated with the use of aqueous solution standards for the calibration of ablated solids. The ablation of solids creates dry plasma conditions whereas nebulisation of solutions creates a wet plasma. The change from dry to wet plasma conditions will affect plasma zone structure, temperature, density and ionisation potential of the plasma. All these factors have an influence on the relative sensitivity and interferences of a particular analyte. The use of an internal standard can correct for differences in the mass ablated and transported to the plasma, but will not correct for fractionation or changes in interferences.

Weijer *et al*<sup>62</sup> described a technique for fast semiquantitative survey analysis by LA-ICP-MS. The procedure involved the calculation of a relative sensitivity factor (RSF) for each element. The RSF's were then used to correlate results obtained by laser ablation. The inaccuracy of the method was found to be greater than a factor of 2 in some cases.

Thompson *et al*<sup>59</sup> carried out a study to compare the use of laser ablated solids and aqueous standards for calibration purposes. Three matrices were investigated to study a variety of chemical and physical characteristics. Although matrix problems were encountered, they concluded that the advantages offered by calibration with nebulised solutions was worth further investigation.

Chenery and Cook<sup>64</sup> used the dual gas flow sample introduction system described by Thompson *et al*<sup>59</sup>, to allow calibration with aqueous standards for the determination of rare earth elements in single mineral grains. The laser used in this study was a frequency quadrupled Nd:YAG operating at 266 nm. Mineral grains are transparent to visible and near IR radiation and do not absorb significantly until the UV region of the

electromagnetic spectrum i.e. <300 nm. Therefore, conventional laser systems operating at 1064 nm will couple inefficiently with the sample and result in large poorly defined craters caused mainly by thermal shock.

Moenke-Blankenburg and Schuman<sup>65</sup> compared three calibration methods for the analysis of soil samples by LA-ICP-MS. Determination of heavy metals in soils by digestion with aqua regia and nebulisation into the plasma is time consuming. Direct sampling removed the need for digestion and reduced the analysis time. It was also noted that the digestion of soils with aqua regia was sometimes incomplete, which may introduce errors into the analysis. The three calibration methods used were:

External calibration with certified soil reference materials BCSS 1, SO 4, GSS 1, GSS 3 and GSS 8.

Calibration with aqueous standards.

Calibration by peak height measurement of the transient signal of a single external standard.

Comparison of the three calibration methods surprisingly revealed that the greatest accuracy and precision was achieved with the peak height calibration technique. This technique relies on the use of a single external standard and does not require the concentration of an internal standard to be determined in the samples. Results obtained compared favourably with the digestion technique and were within 10% of the certified value.

Moissette and co workers<sup>69</sup> described a calibration strategy for the elemental analysis of individual aqueous fluid inclusions by LA-ICP-MS. Elemental ratios were determined in natural fluid inclusions using three different calibration methods. These



were, synthetic fluid inclusions in halite, microvolume aqueous solutions and NIST standard reference material 611

Synthetic fluid inclusions were prepared by crystallisation from standard sodium chloride solutions. The microvolume calibration standards, 'microwells', consisted of small holes drilled into a perspex sheet, filled with a standard solution and then sealed with either Sellotape or 100  $\mu\text{m}$  thick glass coverslips

The results showed that microwells containing aqueous solutions and NIST reference materials were suitable as calibrants. The long term stability of the microwells was thought to be a potential problem and is the subject of further studies. The advantage of the microwells was that they approximated the ablation of the fluid inclusions. This type of calibration approach appears to be similar to the calibration technique described in this thesis, although the results obtained are different. The work carried out in this thesis shows that the coupling of laser energy with aqueous solutions is very inefficient without the addition of an absorbing species. The critical parameter of the microwell technique is the film covering the microwell. The nebulisation process is induced by coupling of the laser energy with the film.

A novel technique for the ablation of solids in a liquid medium was described by Iida<sup>29</sup>. A solid sample was held in a liquid medium in a flat bottomed beaker. Laser pulses were introduced from the bottom of the beaker and focused on the surface of the solid. Both the vapour and the particles produced by ablation were trapped in the liquid medium forming a suspension. The suspension consisted of fine particles of around 1  $\mu\text{m}$  in diameter and was found to be stable over a period of several hours. The suspension could then be introduced into the ICP without any additional operations.

Prabhu *et al*<sup>54</sup> used laser vaporisation to introduce small volumes of solutions into an ICP. The vaporisation cell was a modified version of the cell used for solid sample

introduction. Approximately 200  $\mu\text{l}$  of the test solution was dispensed into a PTFE boat. A graphite wheel was rotated in contact with the test solution. Laser radiation was focused onto the film of test solution that had adhered to the rotating wheel. Validation of the technique was achieved with NIST SRM 160b stainless steel. The reference material was dissolved in a mixture of acids and ablated by the method described. Good agreement with the certified value was achieved with precisions of less than 8% for all elements determined

It is clear from the work described that there is a need for a more universal calibration technique. Calibration with solid reference materials is adequate providing the sample and standard are matrix matched. All solid sample calibration standards tend to be application specific. It is felt that the technique would benefit from a set of standards that are easily prepared and of known concentration. Of the calibration techniques described, the ablation of solution standards holds great potential, but a degree of matrix matching is required if solid samples are to be analysed using an aqueous calibration technique.

## **Chapter 5:**

# **Analysis of Environmental / Biological Materials by LA-ICP-MS**

### **5.1 Review**

Laser ablation ICP-MS is well suited to the analysis of environmental samples, the amount of material is less than that required for traditional analysis using wet digestion. The minimal sample preparation saves time and reduces the chances of sample contamination. However, laser ablation sampling for the analysis of environmental / biological materials has not been widely accepted because quantitative measurements are difficult to perform. The poor accuracies and precisions observed are mainly due to the lack of matrix matched standards making calibration difficult. There are, however, some interesting examples of the use of laser sampling for environmental analysis.

Durant<sup>72</sup> used LA-ICP-MS for the analysis of several environmental matrices. A range of elements were determined in certified reference materials (CRMs) from the Japanese National Institute of Environmental Studies, the International Atomic Energy Agency and the Chinese Institute of Geophysical and Geochemical Prospecting. It was concluded from this fairly extensive study that biological matrices could be analysed by LA-ICP-MS, at least semiquantitatively. Trace analysis proved more difficult for the following reasons: A well characterised matrix-matched standard was not available. For the best calibrations, elements in the standard should be at similar concentrations to those in the sample. Many elemental concentrations in the CRMs are for information purposes only. Their accuracy can not therefore be guaranteed.

The analysis of Orchard Leaves NIST SRM 1571 and Tomato Leaves NIST SRM 1573 was carried out by Ward *et al.*<sup>73</sup>.  $^{13}\text{C}$  was used as an internal standard. Bowen's kale which has a similar physical composition to the materials under investigation and is well characterised was used for calibration. Fair agreement was achieved with the certified values without an internal standard. This indicated that there was negligible drift in laser output or instrument sensitivity. Results where an internal standard was used showed an improvement in absolute precision across most of the elements determined.

LA-ICP-MS was used for the semiquantitative analysis of several solid samples encountered in the environment<sup>74</sup>. The samples were mixed with a cellulose based binding agent and pressed into pellets. Semiquantitative results were generally accurate to within 20-40% with precision's ranging from 8% within single pellets to 14% between pellets. Sensitivity of the technique was good enough to provide detection limits at the  $\text{ng g}^{-1}$  level. Detection limits were estimated by measuring the background of the plasma with no laser, or whilst the laser was sampling a blank binder pellet. The first blank determination gives a best lower detection limit and the second method a worst case estimate. For Cu, detection limits of 0.2 and  $1.0 \mu\text{g g}^{-1}$  respectively were achieved with the two methods described.

Fuge and co workers<sup>75</sup> used LA-ICP-MS to study the minor and trace metal contents of the hard parts of shelly organisms from the west coast of Wales. Previous analysis of such samples had relied on the total digestion of the shell and then subsequent analysis.

Various elements were studied with detection limits for most elements of less than  $1 \mu\text{g ml}^{-1}$  and precisions of 10% or better. Mg, Pb, Cu and Zn were all distributed unevenly throughout the shell Mg variation was thought to be caused by seasonal changes in water temperature. Variations in Pb, Cu and Zn concentrations were thought to reflect major pollution events as well as regional geochemical differences Bulk shell

compositions would not reveal these features. This technique is therefore a powerful tool for following pollution events and building chronological profiles.

Chenery, Hunt and Thompson<sup>76</sup> studied the ablation of two simple mineral phases using a variety of laser conditions. The particulate products were examined using a scanning electron microscope and shown to have undergone a complex heating process.

Ulens *et al*<sup>77</sup> studied elemental distributions in weathered marble crusts. The presence of a naturally produced weathering crust on an artefact can be used in the authentication of marble objects. Depth profiles of Mg, Al, Mn, Fe, Zn, Sr, Ba, La, and Pb in the crusts were studied by LA-ICP-MS. <sup>43</sup>Ca was used as an internal standard. Matrix matched standards were produced by the addition of elemental standard solutions to CaCO<sub>3</sub> powder. A binder was then added and the standards freeze dried. The accuracy and precision achieved was sufficient to provide depth profiles of elements in the marble crusts. Large and highly significant trends for several elements were found.

Gold fingerprinting by LA-ICP-MS was demonstrated by Watling *et al*<sup>78</sup>. Trace element compositions of selected gold samples from Western Australia or South Africa were used to build up the 'fingerprint'. Quantitative results were not required. From the comparison of elemental associations it was possible to relate a gold sample to a specific mineralising event, mine or bullion sample. This is an important application of laser ablation as it is estimated that approximately 2% of gold in Western Australia is stolen. Considering that the annual income from gold is \$A2.5 billion, it is not an insignificant amount. The technique also benefits from the fact that only very small samples are needed for the analysis.

Environmental contaminants in calcified biological structures were investigated by Evans *et al*<sup>79</sup>. Calcified biological structures record changes in organism exposure to environmental contamination. Preservation of this information requires direct analysis

of the solid. Laser ablation offers the spatial resolution required to undertake such an analysis. The samples used were teeth collected from walrus and Beluga whales in the eastern Canadian Arctic. Cd levels were of particular interest to the researchers. It is known that the Cd level in the soft tissues of marine mammals is higher in the eastern Arctic than in more industrialised areas<sup>80</sup>. A typical example of Cd in Beluga's teeth showed very high levels at birth followed by a substantial decrease over the first few years of life and then a large increase later on in life. Using a Nd:YAG laser, operating at 1064 nm, for sampling, it was observed that at high repetition rates (10Hz) the teeth were showing severe scorching. The laser was therefore operated with a maximum frequency of 2 Hz. This example shows how useful laser sampling can be to produce spatial models of elements within a matrix.

Further studies<sup>81</sup> were carried out to determine the effect of laser parameters and tooth type on ablation characteristics. Two laser transitions were used for the investigation, the 2nd and 4th harmonics of a Nd:YAG laser giving rise to laser light at 532 and 266 nm respectively. <sup>43</sup>Ca, a major component in the tooth matrix, was used as an internal standard. Ablation craters in the tooth material did not exhibit the scorching or cracking observed with the infra-red ablation. <sup>43</sup>Ca response was measured as a function of laser energy. Distinct differences between the two types of tooth material were observed. For Beluga cement, <sup>43</sup>Ca displayed a linear relationship with energy for both green and UV wavelengths. For Walrus dentine, the <sup>43</sup>Ca signal was relatively constant with both types of laser. This difference could be due to the fact that a power density threshold exists that is necessary for the formation of an ablating plasma. Above the threshold level, increasing the energy does not result in an increased mass of tooth ablated. The absence of a threshold value for Beluga cement suggests the formation of a plasma that is enhanced by increasing laser energy. One of the unwelcome features reported was the deposition of a fine white powder on the sampler and skimmer cones. It would therefore seem advantageous to keep sample loading on the plasma to a minimum for ablating calcified material.

Raith *et al*<sup>82</sup> carried out zonation studies in minerals using infrared and ultraviolet laser ICP-MS. Two laser systems were used. The first incorporated a Nd:YAG laser operating at 1064 nm and the second a frequency quadrupled Nd:YAG operating at 266 nm. Pale minerals such as quartz have poor absorption efficiencies for IR light, but would be expected to absorb ultraviolet radiation at 266 nm.

In this study, a clinopyroxene mineral was analysed. A thin section with a thickness of 50 µm was analysed using the UV LA-ICP-MS system. The same mineral was then analysed as a sample block using the IR laser system. Silicon was used as an internal standard to correct for physical and chemical differences between the samples and NIST 612 which was used as a standard reference material for calibration. Data was collected as the laser traversed across the minerals to obtain elemental distributions. The data obtained with IR and UV lasers compared well. The distribution patterns for all elements was the same with both laser systems. Cr was detected at a level of 2000 ppm in the core of the bulk sample using the IR laser and at 1800 ppm in the thin section using the UV laser. It was concluded from this work that UV lasers can be successfully employed to analyse thin sections.

Wang *et al.*<sup>83</sup> carried out some interesting work on the application of LA-ICP-MS to the spatially resolved micro-analysis of biological material. With the infrared laser used, spatial resolution down to 30 µm was achievable. Calcium and magnesium in the samples were used as internal standards. Specimens studied included fish scales, rat kidney and pig femur.

Spatial distribution of bismuth in rat kidneys was investigated. The analysis suffered from two major drawbacks. Firstly, the spot size of the laser beam made accurate mapping of thin connective tissue at the kidney skin difficult. Secondly, the sample was not uniform across the section exhibiting a sponge like structure with many voids. This

made automatic line sampling difficult. Results, however showed that Bi was present at elevated concentrations in the cortex and was very high in the cuticle tissue surrounding the kidney.

A cross section of pig femur was analysed for Rb distribution by sampling from the inner to outer edge of the bone. Low levels of Rb were reported in the bulk bone with increasing levels at the bone-tissue interface. Precisions achieved were of the order of 9%.

Guo and Lichte<sup>84</sup> developed a method to determine several chalcophile elements in geological materials by LA-ICP-MS. Chalcophile elements are those that have a strong affinity for sulphur and include As, Se, Ag, Cd, In, Sb, Te, Tl, Pb and Bi. They are environmentally significant elements because of their toxicity to animals and birds at high concentrations. Recovery for most elements was greater than 95%. Detection limits ranged from  $<1 \mu\text{g l}^{-1}$  for Ag to  $100 \mu\text{g l}^{-1}$  for Te. Relative standard deviations ranged from 2-12%. Calibration was achieved by spiking elements of interest onto US Geological survey reference material PCC-1. The resultant mixture was then fused into a bead that could be mounted in the ablation cell for analysis. The authors concluded that the method was satisfactory and relatively fast to perform although improvements could be gained in the fusion process during formation of the bead.

Jeffries *et al.*<sup>85</sup> achieved spatial resolutions from 5 to 70  $\mu\text{m}$  using a frequency quadrupled Nd YAG laser operating at 266 nm. Various mineral grains were analysed by two laser probe systems. Laser radiation at 1064, and 266 nm was employed. The mineral samples investigated could be categorised into two major groups. The first, minerals with a strong absorption in the near-infrared and the ultraviolet region and second, minerals that absorbed poorly in the infrared, but strongly in the ultraviolet region. Using the IR laser system, craters of 20-30  $\mu\text{m}$  were observed with the first



group of minerals and larger 50  $\mu\text{m}$  craters for the second group. Craters of 5  $\mu\text{m}$  diameter were achieved with the UV laser system for both types of minerals.

These observations are consistent with work carried out by Geersten *et al*<sup>48</sup>, comparing IR and UV laser ablation. Plasmas formed above the sample surface during ablation are thought to be more complex with IR lasers, with a significant amount of material being removed by plasma erosion as opposed to direct absorption of the laser energy.

Detection limits in this study<sup>85</sup> for the UV laser varied from hundreds of  $\mu\text{g ml}^{-1}$  for craters of 5  $\mu\text{m}$  in diameter to sub- $\mu\text{g ml}^{-1}$  levels for 20-40  $\mu\text{m}$  craters. Crater diameter and thus the amount of material ablated was controlled by laser power. No control over resolution was achievable with the IR laser system. Detection limits were in the tens of  $\mu\text{g ml}^{-1}$  range. For the same crater diameter and power density, the UV system showed detection limits ten times lower than for the IR system. This suggests that ablation in the UV provides particles that are more suited to detection by ICP-MS

Proposed mechanisms for the ablation of biological materials include photochemical and photothermal processes. The photochemical model proposes that absorption of photons leads to the direct dissociation of molecular bonds. This model holds true in the far ultraviolet, but is not consistent with experimental results obtained in the near UV, visible or infrared in which photon energy is much lower than the molecular dissociation energy. In the photothermal model, ablation is initiated when enough laser energy is deposited into the sample material to cause vaporisation. Albagli *et al*<sup>86</sup> postulate a photomechanical model for the ablation of biological tissue with nanosecond laser pulses. Ablation takes place when the laser induced stress exceeds the strength of the material.

Other techniques for determining the spatial distribution of trace elements in solids include electron probe microanalysis (EPMA). This method has been used for major,

and some trace analysis in fish otolith<sup>87</sup>. However, LA-ICP-MS has the advantage of offering lower detection limits, a wider dynamic range and faster analysis times. Infrared laser ablation systems do not, however, offer the spatial resolution achieved by EPMA, typically 2-5  $\mu\text{m}$ .

From this review, it is clear that, as with laser sampling of other solid materials, characterisation of the ablation process and calibration are two very important considerations. Matrix matching of the sample and standard are required to produce quantitative data that has good accuracy and precision.

The choice of standard is difficult, even if suitable standard reference materials are available, the elements of interest may not be certified or may be present at concentrations significantly different to those expected in the sample material. The technique would therefore benefit from the development of a universal calibration procedure or the production of artificial standards.

There is great potential for laser sampling of biological materials especially in reduction of the time required for sample preparation. Muscle and liver samples require 1-2 hours sample preparation for analysis by solution nebulisation ICP-MS<sup>88</sup>. There is also the benefit, that, a spatial profile of the element distribution across the tissue surface is possible

The reduction of the occurrence of polyatomic interferences is another advantage of LA-ICP-MS that would be useful, particularly when determining elements with an  $m/z$  of less than 80. The determination of elements such as Si, S, Ca, Fe, Ge, and K should be improved

## **Chapter 6:**

# **Fundamental Studies on the Production of Aqueous Standards with Modified Absorption Coefficients.**

### **6.1 Introduction**

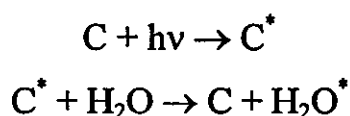
This chapter describes work on a new phenomena in which laser energy is coupled into aqueous media by the use of an absorbing chromophore. This principal has been previously used in the matrix assisted laser desorption technique (MALDI), coupling laser energy into glycerol to produce direct ionisation of organic molecules. Other workers<sup>44,45</sup> have also reported the modification of the absorption coefficients of polymers such as polymethyl methacrylate (PMMA). PMMA does not absorb readily in the UV. The addition of small amounts of organic substances such as benzoin results in a change in the absorption characteristics of the polymer. The change in absorption characteristics leads to better coupling of laser energy with the polymer sample, giving uniform ablation and allowing uniform etching of very small geometries. No work has been reported on the modification of the absorption coefficient of aqueous solutions or the use of such solutions as calibrants for laser ablation.

The goal of this work was to demonstrate that modification of the absorption coefficient of an aqueous standard solution was possible. Validation of the technique by comparison with certified reference materials and application of the calibration strategy to the analysis of various biological matrices without the requirement to quantify a component (internal standard) within the sample were demonstrated. It was also the aim to demonstrate that preparation of the standards was simple and easy to perform in any analytical laboratory.

To achieve these aims, the matrix matching of samples and standards by the addition of small quantities of polymer solutions that absorb in the UV was investigated. Various initial studies on the laser ablation system and polymer characteristics were carried out.

### **6.1.1 The coupling of Laser Energy into Aqueous Solutions Containing an Absorbing Chromophore.**

The laser energy is thought to couple with the aqueous standards by the following mechanism:



C = Chromophore      C\* = Excited state

For  $H_2O^*$  to lead to ablation,  $H_2O^*$  must have energy in translational and or vibrational modes to remove bulk water particles. Evidence to suggest that this is the mechanism of ablation were as follows:

- Droplets appear on the walls of the laser cell at high laser powers.
- Analytes appear to be ablated according to their bulk solution concentration.
- Their does not appear to be any evidence of fractionation.

### **6.2 Estimation of the Laser Power Density**

Power density, or fluence, is defined as the amount of power that is incident onto the sample per unit area with the units watts  $cm^{-2}$ . The power density was calculated for an incident beam of 120 mJ focused to a spot of 200  $\mu m$  in diameter. Typical laser running conditions are given in Table 5.

Table 5. Laser Operating Conditions

Laser energy	120 mJ
Laser Frequency	5 Hz
Pulse Duration	14 ns

$$\text{Total Power} = \frac{120 \cdot 10^{-3}}{14 \cdot 10^{-9}} = 8.57 \text{ MW}$$

Total beam area was  $3.24 \text{ cm}^2$ . Therefore in the total beam area there were  $2.65 \text{ MW/cm}^2$ .

The laser beam was sampled through a 4 mm diameter mask

$$\text{Area of beam sampled, } \Pi r^2 = 0.126 \text{ cm}^2$$

Assuming that the laser energy was distributed evenly throughout the beam, then in the area of the mask there were:-  $0.333 \text{ MW}$  of power.

The laser is focused by a fused silica lens to a spot  $200 \mu\text{m}$  in diameter.

$$\text{Area of spot} = 3.142 \cdot 10^{-4} \text{ cm}^2.$$

$$\begin{aligned} \text{Total power in spot} &= \frac{0.333}{3.142 \cdot 10^{-4}} = 1060 \text{ MW/cm}^2 \\ &= \underline{1.06 \text{ GW/cm}^2} \end{aligned}$$

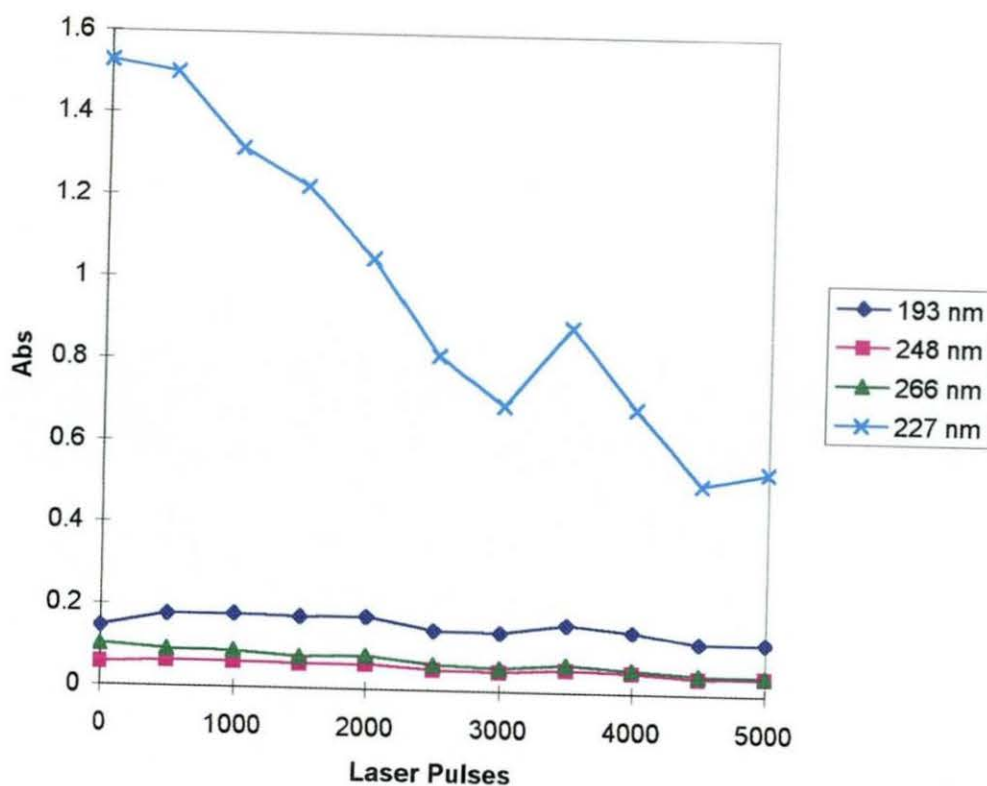
Assuming 100% transmission for the lens (in practice a figure of 80% is more realistic).

### **6.3 Investigation of the Absorption Characteristics of Poly (sodium 4-styrene-sulphonate) and Napthalene-2-sulphonic acid.**

Two polymers were selected for investigation, Napthalene-2-sulphonic acid (NSA) and Poly(sodium 4-styrene-sulphonate). The absorption spectrum of the polymers was measured in the ultraviolet region from 190-340 nm using a Unicam 8700 series UV/Vis spectrometer.

A 0.005 g dm<sup>-3</sup> solution of (NSA) was prepared. The initial absorption spectrum was measured in a 1cm path length cell. The solution was then exposed to a series of excimer laser pulses at 248 nm of output energy 40 mJ and frequency 5 Hz. The spectrum was re-measured at 500 pulse intervals. Particular interest was paid to the excimer wavelengths of 193 and 248 nm. The absorbance at 266 nm was also recorded as this wavelength corresponds to the emission of a frequency quadrupled Nd:YAG laser, which is the standard laser used for solid sampling in the ultraviolet region. The results can be seen in Fig.13.

**Fig 13 Effect of 248nm Laser Radiation on the UV Absorption Characteristics of Napthalene-2-Sulphonic Acid**



The peak at 227 nm was the major absorption peak. It can be seen that the absorption of this peak drops off rapidly on exposure to UV radiation. In a typical run sequence approximately 1000 laser shots were experienced by the sample.

A  $0.8 \text{ g dm}^{-3}$  solution of Poly(sodium 4-styrene-sulphonate) was prepared and its absorption characteristics investigated in the same way as above. The results can be seen in Table 6.

Table 6. Effect of 248 nm Laser Radiation on the UV Absorption Characteristics of a 0.8 g dm<sup>-3</sup> solution of Poly(sodium 4-styrene-sulphonate)

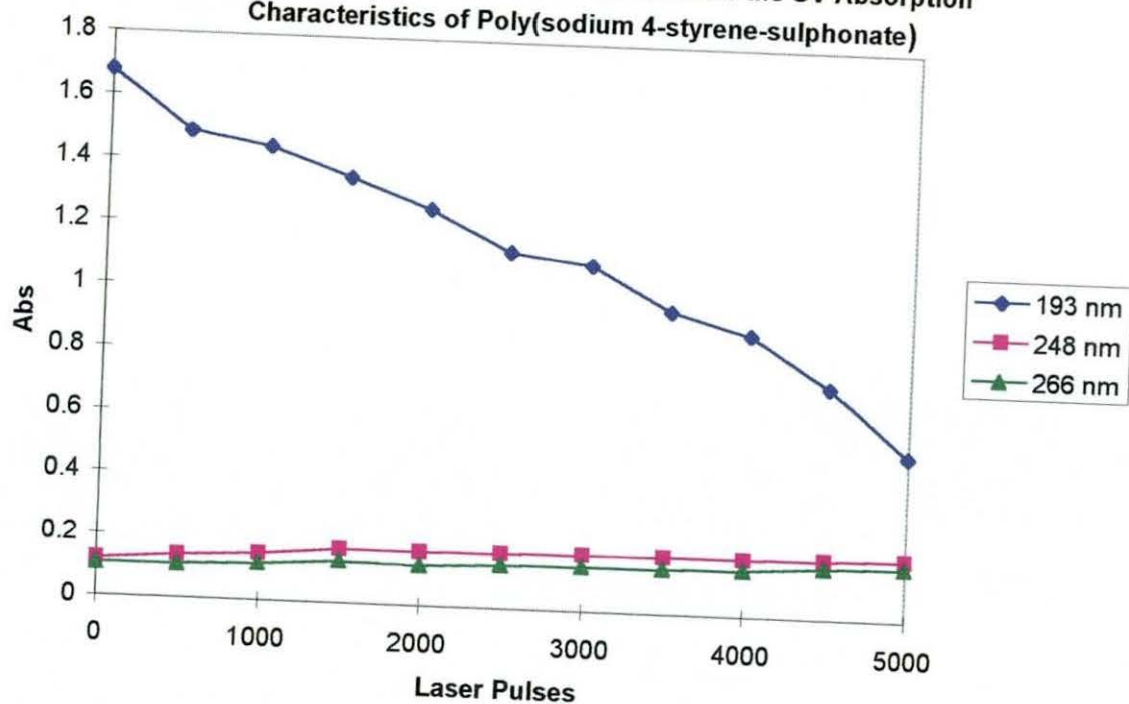
Absorbance @ (1 cm path length)

Laser Pulses	193 nm	248 nm	266 nm
0	>3	2.020	1.614
500	>3	2.234	1.774
1000	>3	2.586	2.039
1500	>3	2.563	2.022
2000	>3	2.732	2.150
2500	>3	2.879	2.271
3000	>3	2.935	2.315
3500	>3	>3	2.384
4000	>3	>3	2.507

Although at this concentration the absorbance of the solution was high at the wavelengths of interest, it can still be seen that on exposure to UV light the absorption of the solution appeared to increase. Fig 14. shows the results for a more dilute solution.

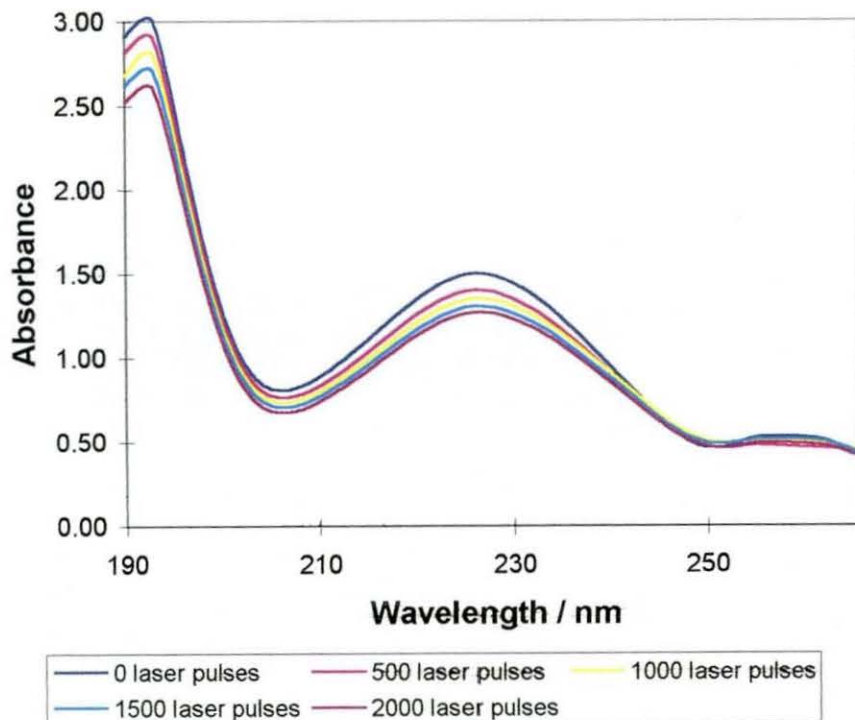


**Fig 14. Effect of 248 nm Laser Radiation on the UV Absorption Characteristics of Poly(sodium 4-styrene-sulphonate)**



At a concentration of  $0.02 \text{ g dm}^{-3}$  it was evident that there were two peaks in the far UV spectrum. One with a maximum at 194 nm and another at 224 nm. The absorbance of these peaks decreased on exposure to UV radiation. The apparent stability at 248 and 266 nm was due to the fact that the peak at 224 nm broadened and flattened on exposure to UV radiation. Although the absorption of the additive at 248 nm was low compared to the major peak at 224 nm, the important point was that the absorption at 248 and 266 nm remained quite stable for over 2000 laser pulses. The absorption spectrum and the effect of laser radiation at 248nm on a  $0.05 \text{ g dm}^{-3}$  polymer solution is shown in Figure 14A.

Fig 14A Effect of 248nm Laser Radiation on the Absorption Spectra of  
a  
0.05 g dm<sup>-3</sup> Poly (Sodium-4-Styrene Sulphonate) Solution



#### 6.4 Calculation of Absorption Coefficients

When monochromatic light of fluence ( $I_o$ ) strikes a homogeneous medium, a portion of the incident light is reflected ( $I_r$ ), a portion is absorbed within the medium ( $I_a$ ) and the remainder is transmitted ( $I_t$ ), then:

$$I_o = I_a + I_t + I_r$$

## Lamberts Law

This law states that when light passes through a transparent medium, the rate of decrease in intensity with the thickness of the medium is proportional to the intensity of the light. Thus any layer of given thickness of the medium will absorb the same fraction of the light incident upon it. This may be expressed by the differential equation:

$$-\frac{dI}{dl} = kI$$

where  $I$  is the intensity of the incident light of wavelength  $\lambda$ ,  $l$  is the thickness of the medium and  $k$  is the proportionality factor. Integrating this equation and making  $I = I_0$  when  $l = 0$ , then:

$$\ln \frac{I_0}{I_t} = kl$$

or stated in other terms,

$$I_t = I_0 \cdot e^{-kl}$$

where  $I_0$  is the intensity of the incident light falling upon an absorbing medium of thickness  $l$ ,  $I_t$  is the intensity of the transmitted light and  $k$  is a constant for the wavelength and the absorbing medium used. By changing from natural to common logarithms, then:

$$I_t = I_0 \cdot 10^{-0.4343kl} = I_0 \cdot 10^{-Kl}$$

where  $K = k/2.3026$  and is termed the absorption coefficient. The ratio  $I_t/I_0$  is the fraction of the light transmitted by a thickness  $l$  of the medium and is termed the transmittance  $T$ . The absorbance  $A$  of the medium is given by:

$$A = \log \frac{I_0}{I_t}$$

## Beers Law

Beer studied the effect of concentration of the coloured constituent of a solution on the light transmission or absorption. He concluded that the same relationship between transmission and concentration existed as Lambert had discovered between transmission and thickness of the layer. This may be written in the form:

$$I_t = I_o \cdot 10^{-K'c}$$

where  $c$  is the concentration and  $K'$  is a constant. Combining Lamberts and Beers equations gives the Beer-Lambert law which is expressed as:

$$\log \frac{I_o}{I_t} = ac l$$

If the concentration  $c$  is expressed in moles  $\text{dm}^{-3}$  and  $l$  in cm then  $a$  is given the symbol  $\epsilon$  and is called the molar absorptivity. The specific absorption coefficient  $E_s$  may be defined as the absorption per unit thickness and unit mass concentration.

$$E_s = \frac{A}{cl} \text{ or } I_t = I_o \cdot 10^{-E_s cl}$$

The absorption coefficient of certified reference material NIST 613 glass was established as outlined below. The concentration of polymer solution to give the same absorption coefficient as the NIST glass was then calculated.

NIST glass supplied as a reference material is opaque due to the poor optical finish of the surface. Accurate measurement of its absorbance at a particular wavelength is therefore not possible. The NIST glass was sent to an optical workshop to be optically polished allowing an accurate determination of the absorbance at 248 nm.

Thickness of NIST 613 wafer:-  $0.93 \times 10^{-3} \text{ m}$

The absorbance of NIST 613 was measured on a Unicam 8700 series UV/Vis spectrometer.

Absorbance @ 248 nm = 2.67

$$2.303 \log A = \ln A$$

$$I_t = I_o \cdot e^{-kl}$$

$$\ln I_t / I_o = -kl$$

$$A = kl / 2.303$$

$$K(\text{glass}) = 6612 \text{ m}^{-1}$$

The absorbance of a  $0.2 \text{ g dm}^{-3}$  solution of poly(sodium 4-styrene-sulphonate) at 248 nm was 0.623 using a cell with a path length of 1 cm.

$$A = Ecl$$

$$E = A / cl$$

$$E = 0.623 / 0.2 \times 0.01$$

$$E = 312 \text{ dm}^{-3} \text{ g m}^{-1}$$

Now we have to equate absorption coefficients, which is equivalent to equating the absorbances for equal lengths of the absorbing cell.

Thus:  $\log I_o / I = Ecl$

$$\ln I_o / I = 2.303 Ecl$$

but also:

$$\ln I_o / I = kl$$

Therefore:

$$2.303 Ecl = kl$$

$$c = k / 2.303E$$

$$c = 6611.8 / (311.5 \times 2.303)$$

Therefore concentration of polymer required to give an absorption coefficient matching the NIST glass was:-  $9.22 \text{ g dm}^{-3}$

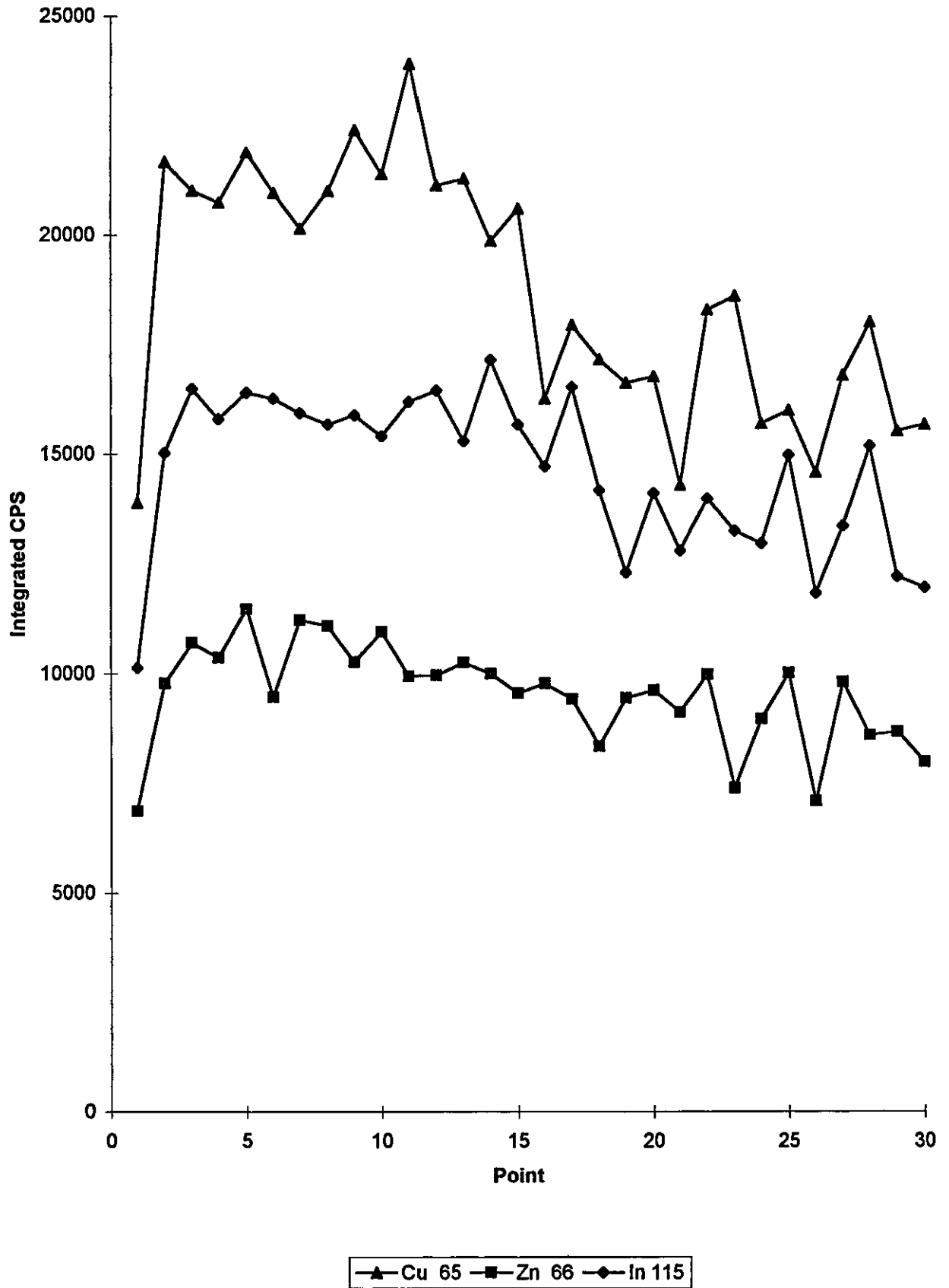
The absorbance of naphthalene sulphonic acid at 248 nm was 0.55 for a  $0.05 \text{ g dm}^{-3}$  solution. A  $2.61 \text{ g dm}^{-3}$  solution would be required to give an absorption coefficient matching NIST 613 using the same calculation as above. The maximum concentration of naphthalene sulphonic acid that could be dissolved was  $1.50 \text{ g dm}^{-3}$ . From the degradation results and the fact that it was impossible to achieve the desired concentration of additive in solution, it was decided that the naphthalene additive would no longer be investigated and that future experiments would use poly(sodium 4-styrene-sulphonate) as an additive.

## 6.5 System Optimisation

To optimise the instrument after ignition, a calibration solution was introduced into the plasma and the signal intensity of a particular element was maximised by fine adjustment of the plasma translation stage, the three plasma gas flows and the ion lens settings that focus the ion beam. For solution nebulisation,  $\text{In}^{115}$  was chosen as the element for optimisation as it was in the middle of the mass range. As indicated earlier, sensitivities for this instrument were of the order of  $4 \times 10^6$  counts per ppm per second, whereas sensitivities of  $40 \times 10^6$  counts per ppm per second and greater are achievable for modern instruments.

Fig.15

### Effect Of Laser Radiation On the Analyte Stability in Aqueous Solutions



Optimisation for sample introduction by laser ablation was normally carried out on La, at mass 139, which is present in the NIST standard reference glasses. Sensitivities of the order of 1000 counts per ppm per second were normally achieved. Optimisation of instrumental parameters for the ablation of solutions produced much higher sensitivities, of the order of 10000 counts per ppm per second, but more importantly showed optimum sensitivity at the same instrumental settings as for solid sample introduction

## 6.6 Determination of System Stability

The stability of the system was investigated by the acquisition of successive replicates of an aqueous standard solution containing  $50 \mu\text{g l}^{-1}$  of each element and  $9.2 \text{ g dm}^{-3}$  of polymer, see Fig.15. Each of the points represents the integrated count rate obtained for 150 laser pulses over a thirty second period, points were acquired contiguously. The total analysis time for acquisition of thirty replicates was fifteen minutes. From the graph it can be observed that it took approximately one minute after the laser was started before a quasi stable signal was achieved. The RSDs for the three elements used in this study can be seen in Table 7. The polymer, or at least its absorption at 248nm, appeared to remain stable throughout the fifteen minutes of the experiment, with RSDs in the expected range for analysis without an internal standard. This apparent stability was due to the flattening and broadening effect of the polymer absorption maximum described in section 6.3.

Table 7. System Stability Expressed as RSD for Cu, Zn and In in Aqueous Solutions.

Isotope	RSD	Isotope	RSD
Cu <sup>65</sup>	10.3%	In <sup>115</sup>	7.6%
Zn <sup>66</sup>	7.6%		



## 6.7 Effect of Laser Energy and Frequency on the Observed Count Rate

Initial experiments were carried out with the focal point of the laser on the liquid surface. The effect of laser energy and frequency on the observed count rate was determined for an aqueous standard solution containing  $30 \mu\text{g ml}^{-1}$  of each element and  $9.2 \text{ g dm}^{-3}$  of polymer. The data are shown in Figs 16 and 17 respectively. From the graphs it can be seen that increasing the laser energy and number of shots per second caused an increase in the count rate. The two stage mechanism described previously<sup>40-42</sup> is also evident. i.e. there is a tailing off of the slope at higher power densities due to the formation of a plasma above the surface causing shielding of the sample. This can be clearly seen in the energy data presented. It was also noted that at higher laser output energies, larger droplets were ejected from the sample surface. These droplets adhered to the cell window and may have been responsible for attenuating the laser beam and contributed to the observed tail off of the slope. An additional feature of the larger droplet sizes is that they would be transferred to the plasma less efficiently.

The precision of the laser energy experimental data varied from 5.5-11.1 % where  $n = 6$  for each data point. The best precisions were achieved for laser output energies of between 75 and 100 mJ per pulse which is equivalent to approximately  $0.5 \text{ GW cm}^{-2}$  on the sample surface. Again larger droplets were ejected from the sample surface at higher fluences which may account for the poor precisions. Precisions of between 3.1 and 13.7 were achieved for the laser frequency experiment, the best precisions occurring for laser frequencies of 5-7 Hz. This can be explained by the fact that the laser frequency has to be high enough to produce a quasi stable signal but not too high to induce large droplet formation. The results can be seen in Table 8.

Fig 16

Effect Of Laser Energy On the Analyte Signal of Aqueous Solutions

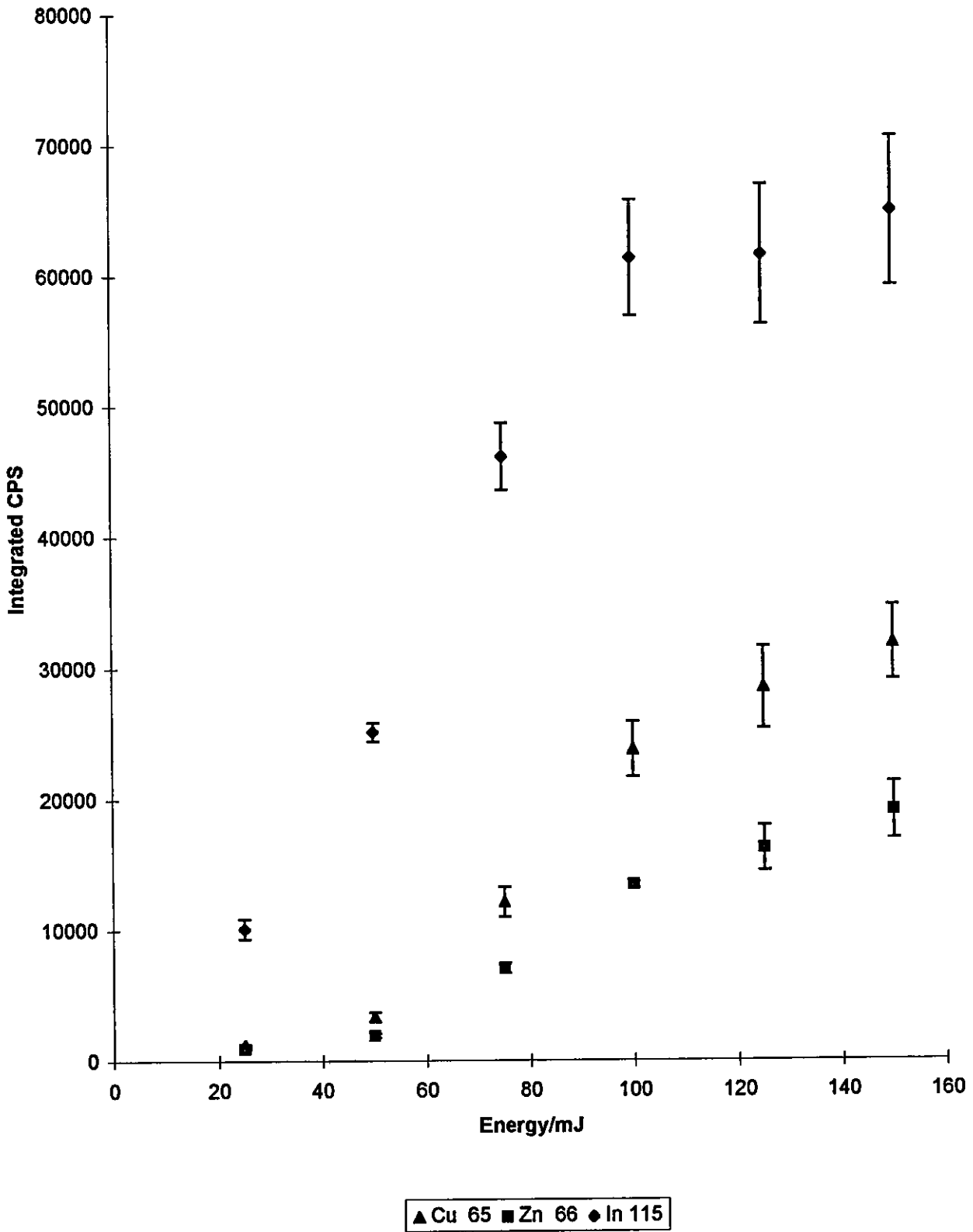


Fig 17

### Effect Of Laser Frequency On the Analyte Signal of Aqueous Solutions

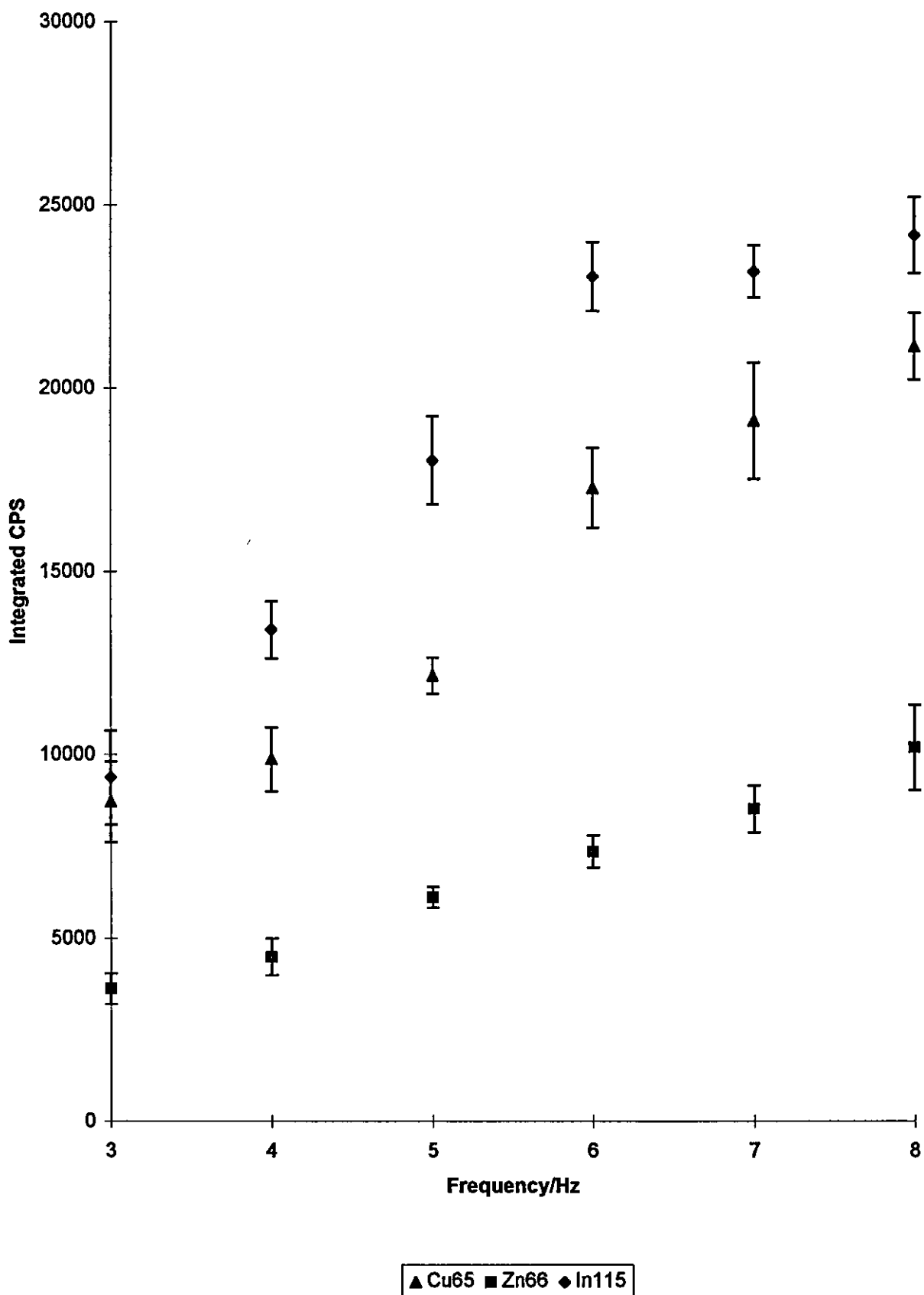


Table 8: Precisions Achieved at Varying Laser Output Energies and Frequencies

Energy/mJ	Cu <sup>65</sup>	Zn <sup>66</sup>	In <sup>115</sup>	Frequency/Hz	Cu <sup>65</sup>	Zn <sup>66</sup>	In <sup>115</sup>
25	7.0	6.8	7.6	3	12.6	11.6	13.7
50	11.1	9.2	2.8	4	8.9	11.3	5.8
75	9.4	5.5	5.5	5	4.1	4.6	6.6
100	8.9	1.8	7.2	6	6.3	6.1	4.1
125	11.0	10.6	8.7	7	8.3	7.5	3.1
150	8.9	11.4	8.8	8	4.3	11.5	4.3

## 6.8 Production of a Calibration Graph

Early attempts to produce a calibration graph using an aqueous standard were largely unsuccessful with poor correlation coefficients. This was due to the fact that it was impossible to return the ablation cell accurately and reproducibly to the same position after the change over of a standard. Calibration was therefore achieved by producing a count profile along the z axis of the translation stage which effectively alters the focal point with respect to the liquid surface. From the profile curves shown in Fig.18 for In<sup>115</sup>, it can be seen that for each elemental concentration there was a maximum sensitivity. This maximum value was plotted to give the calibration curve in Fig.19 which has a correlation coefficient of 0.9999.

Fig.18

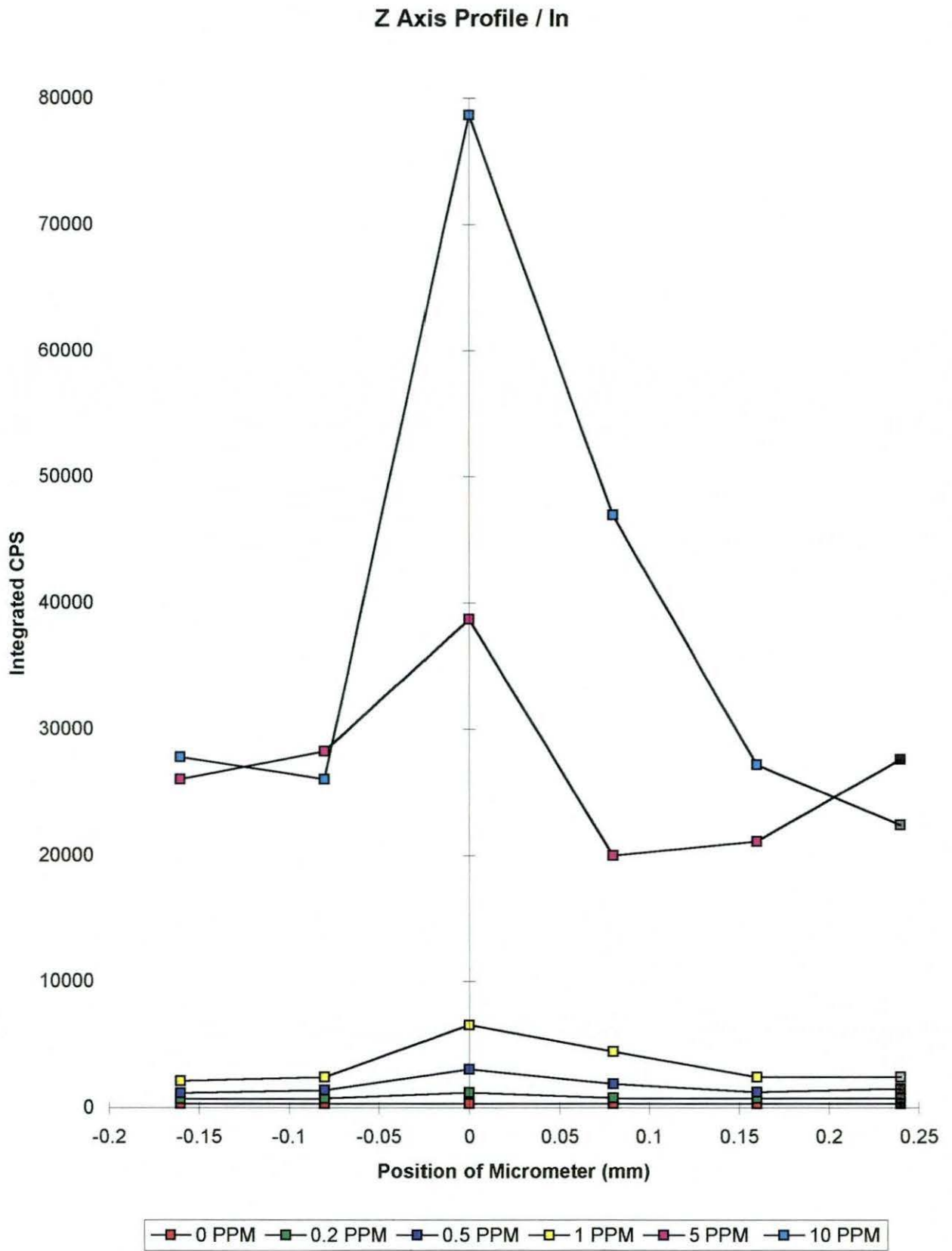
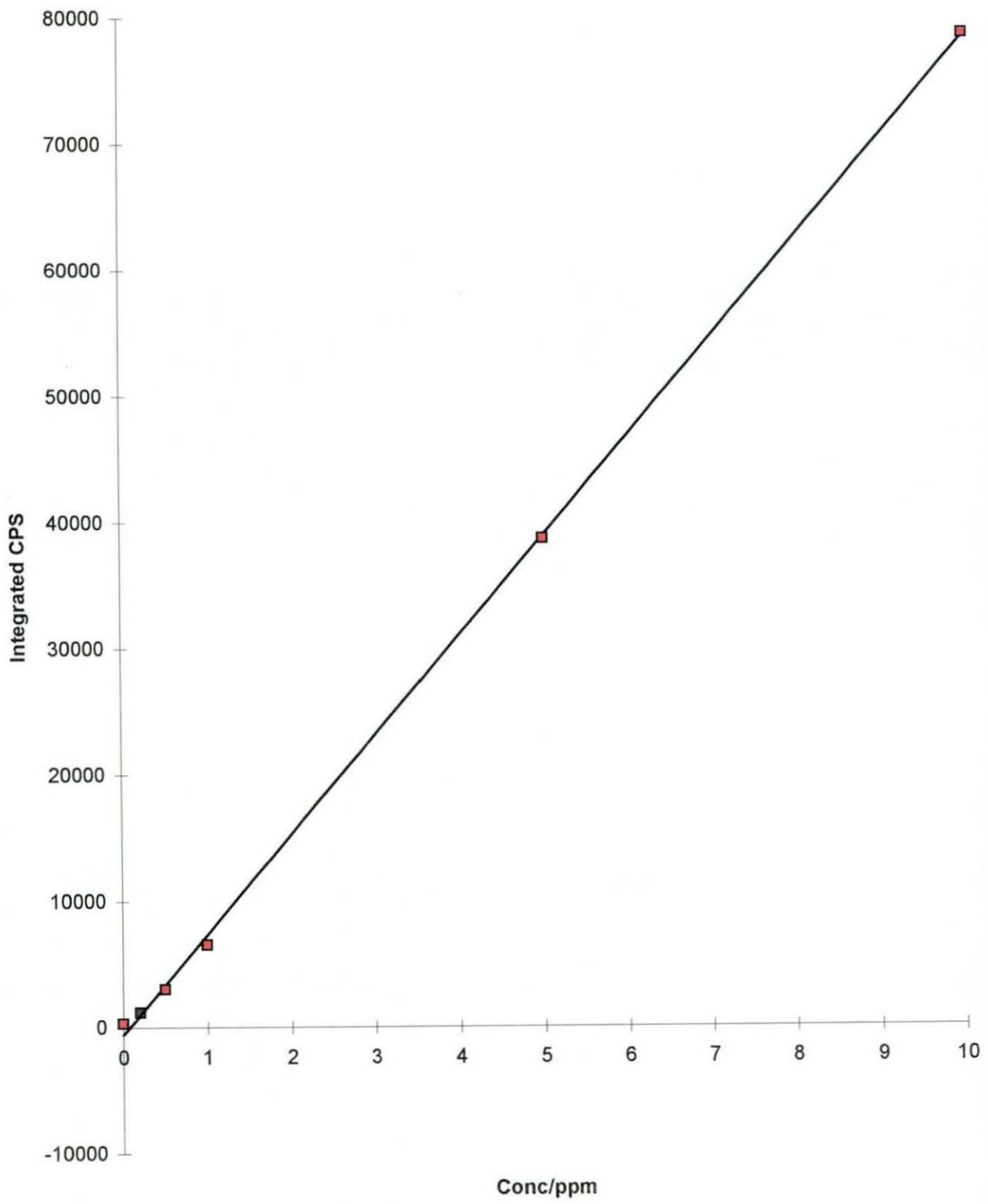


Fig.19

### Indium Calibration Graph



## **6.9 Effect of Polymer Additive Concentration on the Observed Count Rate**

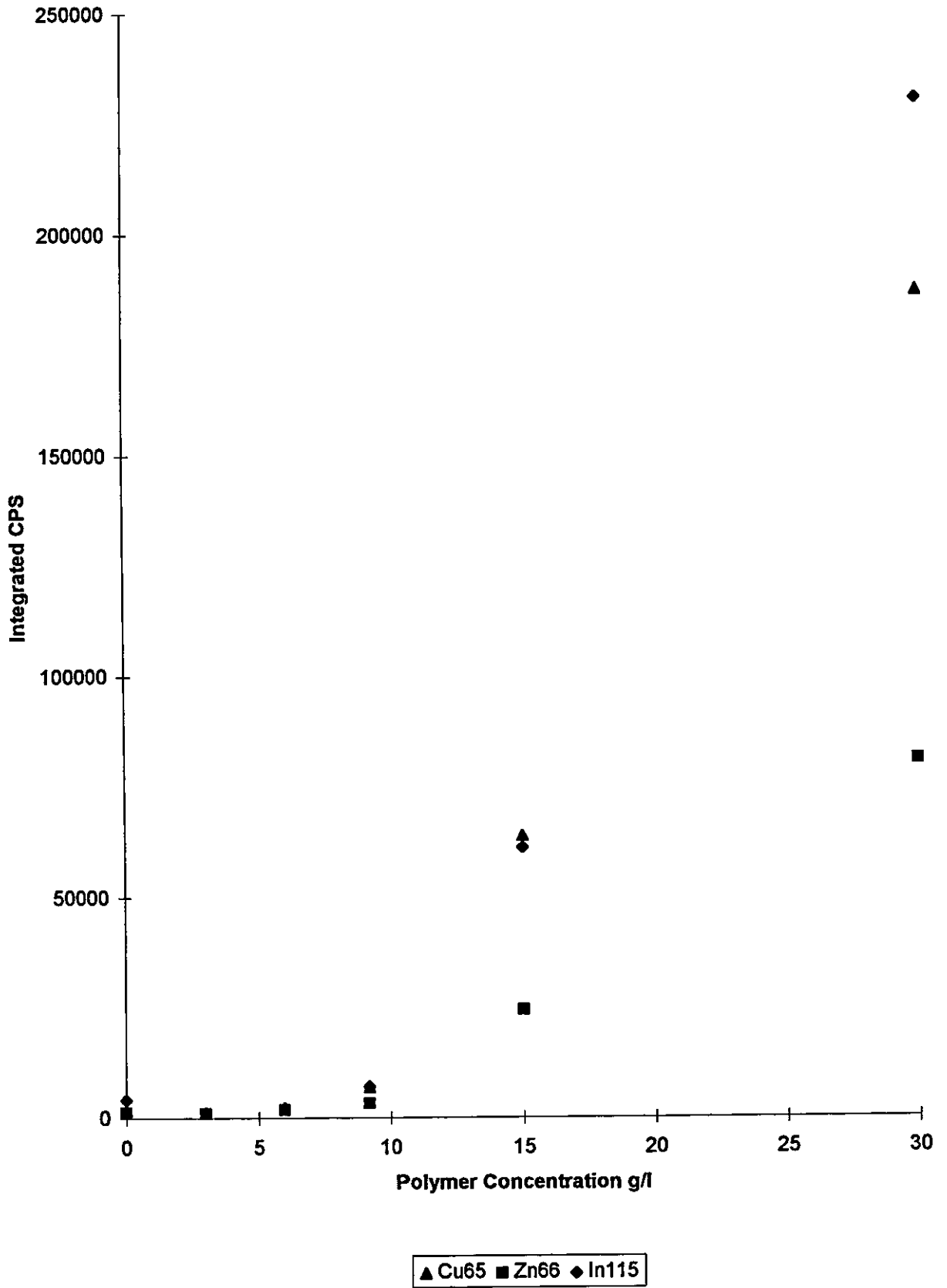
The effect of varying the polymer additive concentration can be seen in Fig.20. Standards containing Cu, Zn and In at concentrations of  $30 \mu\text{g m}^{-1}$  were used for this study. The observed count rate increased exponentially with an increase in polymer additive concentration. Addition of polymer altered the effective absorption coefficient of the standards. This resulted in better coupling of the laser energy into the sample causing more material to be removed per laser shot. It was therefore possible to control the count rate obtained with a standard solution by addition of differing concentrations of polymer.

## **6.10 Investigation of Fractionation**

When a solution is introduced into an ICP-MS instrument by standard nebulisation it is assumed that no fractionation takes place, i.e. for a given set of conditions the same amount of each element will be introduced into the ICP. Comparison of nebulisation and ablation results should indicate if any elements are being selectively removed during ablation. Elements were selected for this experiment that form complexes, such as Cu, Zn and In, Cs which do not. For the nebulised solution a concentration of  $50 \mu\text{g l}^{-1}$  was used. For the ablated samples a concentration of  $30 \mu\text{g m}^{-1}$  (Cu, Zn) and  $10 \mu\text{g m}^{-1}$  (In, Cs) was used with a polymer concentration of  $9.2 \text{ g dm}^{-3}$ . EDTA was used as a complexing agent to determine if the formation of elemental complexes had an effect on fractionation. EDTA was added to a ten fold molar excess which was equivalent to  $3 \text{ g dm}^{-3}$ . To study this effect a sensitivity ratio was calculated for each element, this takes into account the concentration of the standards used. The experimental results were ratioed to Cs to take into account slight differences in instrumental set up for the experiments and also because Cs does not form complexes with EDTA. The sensitivity ratio was obtained by calculating

Fig 20

Effect Of Polymer Concentration On The Observed Signal





the counts mole<sup>-1</sup> s<sup>-1</sup> for each isotope, compared to Cs<sup>133</sup>, see Table 9. Sensitivity ratio's are calculated for a normally nebulised solution, an ablated synthetic polymer standard and an ablated standard solution containing the complexing agent EDTA.

Table 9: Sensitivity Ratio's

Isotope	Nebulised Sample	Ablated Polymer	Ablated Polymer + EDTA
Cu <sup>63</sup>	0.203	0.420	0.417
Cu <sup>65</sup>	0.094	0.199	0.194
Zn <sup>64</sup>	0.101	0.153	0.157
Zn <sup>66</sup>	0.059	0.086	0.086
In <sup>115</sup>	0.991	1.384	1.374
Cs <sup>133</sup>	1	1	1

It can be seen from Table 9 that the addition of a complexing agent does not cause selective removal of elements. The sensitivity ratio's obtained by solution nebulisation do differ from the results obtained by ablation. An additional experiment to help confirm these results would repeat the ablated polymer solution experiment whilst nebulising water to simulate a wet plasma. This would indicate if the differences are due to dry v wet plasma conditions, i.e. atoms are being ionised earlier in the plasma under dry conditions. Gunther *et al.*<sup>89</sup> have produced a fractionation index for 59 elements across the mass range by laser ablation using a NdYAG laser at 266nm. All elements were ratioed to Ca.

## 6.11 Comparison of Wet and Dry Plasma Conditions

One of the claimed advantages that laser ablation has over solution nebulisation, as a means of sample introduction, is that laser ablation creates a dry plasma. This reduces the amount of oxygen introduced into the plasma and should therefore reduce the occurrence of interfering oxide species. It was unclear whether ablation of solutions created wet or dry plasma conditions and therefore this was investigated.

Glass tubes of 15 cm in length were packed with dry silica gel and sealed at each end with glass wool. The weight of the tubes was measured and recorded. The aerosol generated by laser ablation of a standard and solution nebulisation was allowed to pass through the tubes. The tubes were then re-weighed and the amount of aerosol generated per minute for each of the sample introduction methods was calculated.

Ablation of solution generated	626 $\mu\text{g min}^{-1}$
Standard nebulisation generated	23550 $\mu\text{g min}^{-1}$

It can be concluded that laser ablation of solutions under the conditions used here generated drier plasma conditions. This explains why the optimum operating conditions were similar for the ablation of the standard solutions and solids.

Wet plasma conditions for ablation were achieved using a design similar to the one described by Thompson *et al.*<sup>59</sup> Transport of both ablated and nebulised material was provided by a dual gas flow system. The aqueous nebulisation gas flow was arranged in parallel with the laser ablation nebulisation gas flow. The two flows converged approximately 30 cm before the injector tube of the ICP torch. Wet plasma conditions could be simulated by nebulising a de-ionised water solution at the same time as ablation.

Fig.21 shows the difference in signal for various elements under wet and dry plasma conditions. All elements were present at the concentration that is certified for NIST 613 glass standard.  $9.2 \text{ g dm}^{-3}$  of the polymer poly (sodium 4 styrene-sulphonate) was also present in each solution, (w) represents wet plasma conditions and (d) represents dry plasma conditions. The calculated % RSDs for each element can be seen in Table 10.

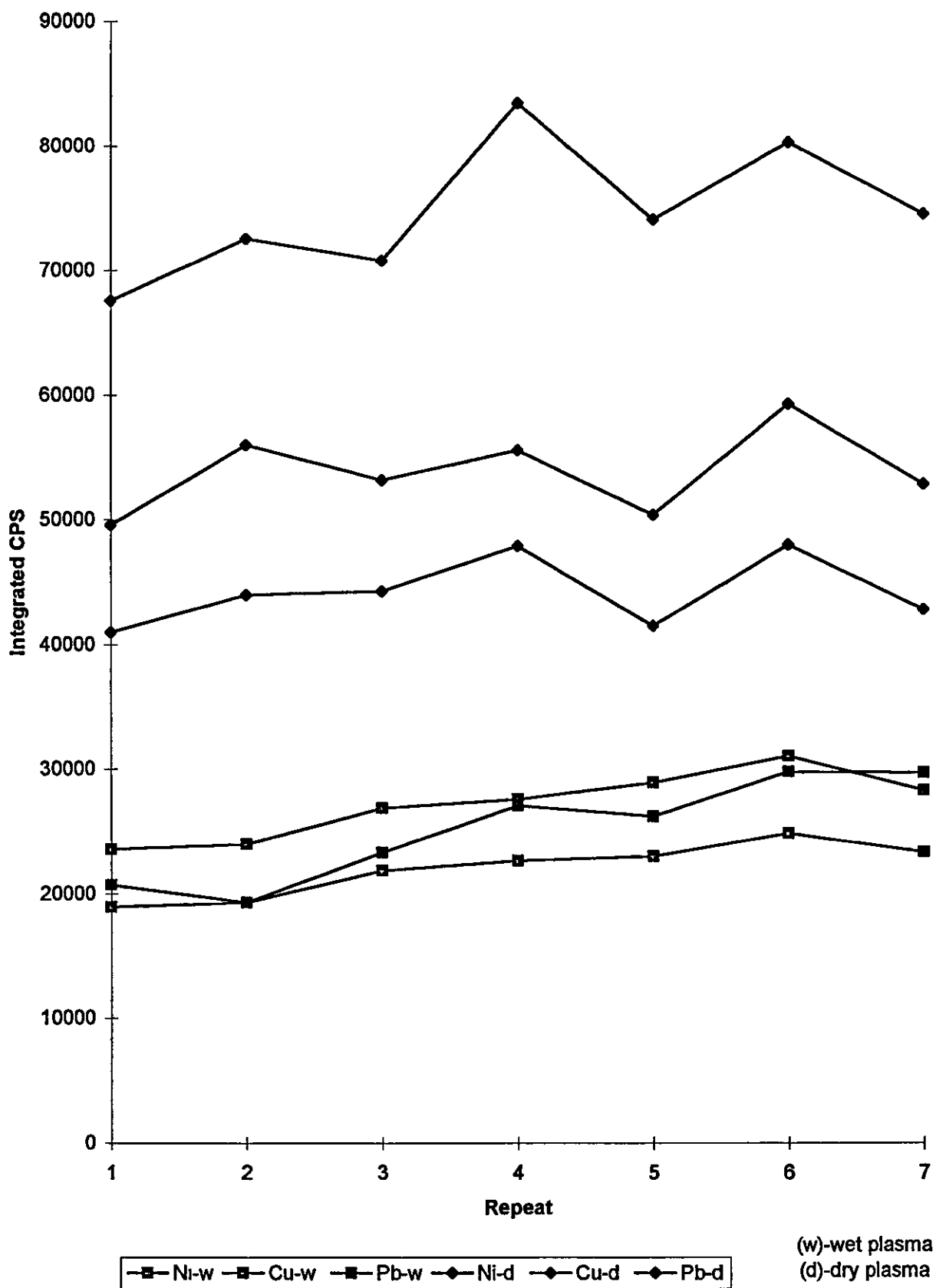
Table 10: Effect on % RSDs Wet and Dry Plasma Conditions on Precision

Isotope	Wet Plasma Conditions	Dry Plasma Conditions
Ni <sup>60</sup>	9.8	6.4
Cu <sup>65</sup>	9.8	6.3
Pb <sup>208</sup>	16.6	7.3

The RSDs for the dry plasma conditions appear to be better than those for wet plasma conditions. It can also be seen that for dry plasma conditions the observed count rate was greater. This was not the result expected, as O and H from the nebulisation of water would be expected to contribute to the electron number density of the plasma and thus improve ionisation efficiency. The relative count rate for each element also appears to alter from wet to dry plasma conditions. This can be explained by the fact that the instrument operating conditions were optimised for a dry plasma. This is an area that would benefit from more experimental work. However, from a practical standpoint it does show that it is vital to standardise plasma conditions for both standards and samples.

Fig 21

### Comparison Of Wet And Dry Plasma Conditions



## 6.12 Determination of Oxide Ratios for Dry Plasma Conditions

The oxide ratio for  $\text{CeO}^{156}:\text{Ce}^{140}$  was determined for dry plasma conditions, using the laser for sample introduction, and under wet conditions using normal solution nebulisation. A  $50 \mu\text{g ml}^{-1}$  Ce solution containing  $9.2 \text{ g dm}^{-3}$  polymer was ablated to give the oxide ratio for dry plasma conditions. A  $50 \mu\text{g l}^{-1}$  Ce standard was used to determine the solution nebulisation and hence the normal operating oxide ratio. The average results for five replicate analyses are shown in Table 11.

Table 11: Comparison of Oxide Ratio's for Wet and Dry Plasma Conditions

Sample Introduction Method	CeO/Ce Ratio
Laser (dry plasma)	1.2%
Solution Nebulisation	3.1%

The oxide ratio obtained for solution nebulisation is a typical result for the Loughborough PQ1 instrument. A modern instrument could be expected to achieve lower oxide ratio's. The general observation can be made that ablation gives lower oxide ratio's than nebulisation and was consistent with the finding that ablation of solutions constitutes drier plasma conditions, i.e. less water was introduced into the plasma.

## 6.13 Determination of Detection Limits

The analysis of a  $50 \mu\text{g ml}^{-1}$  standard solution was carried out to estimate the detection limits for a suite of elements by laser ablation. The polymer content of the solution was  $9.2 \text{ g dm}^{-3}$ . It would be possible to produce a solution with a higher polymer concentration that

would give a greater count rate for each element and hence a better signal to background ratio. The results from this experiment are for a polymer solution that had a matched absorption coefficient with that of NIST 613 glass.

The detection limit was determined by calculating the concentration of each element that would give a signal three times the standard deviation of the blank. A best and worst estimate are given for the detection limit of each element<sup>45</sup>. The best estimate was calculated with only a stream of dry argon being introduced into the ICP. The worst estimate was calculated by laser sampling a blank polymer solution containing no analyte. These two methods are different ways of measuring the blank contribution and will result in different values for the detection limits. The results are shown in Table 12.

Table 12: Detection Limits for Laser Ablation of Solution Standards

Detection Limit ng ml <sup>-1</sup>			
Element	Isotope	Best Estimate	Worst Estimate
Mg	24	22	102
Mg	25	78	127
Ca	44	659	2280
Fe	56	3446	2300
Fe	57	163	702
Cu	65	16	15
Zn	66	35	37
Sr	88	1.6	5.7
In	115	3.4	4.3
Ce	140	3.6	2.3
Pb	208	1.6	3.3

From Table 12 it can be seen that for some elements, the ablation of modified solutions produced a detection limit of the order of a few ppb. For most of the elements it is observed that there is no significant difference in detection limit for the two methods. This shows that ablation of an aqueous polymer solution does not add significantly to the blank level. Differences between isotopes of the same element can be attributed to differing abundances. Detection limits for Ca and Fe are high due to the expected spectral interferences for a quadrupole ICP-MS. The detection limits achieved compare favourably with the ablation of NIST standard reference materials<sup>90</sup> where detection limits in the ppm range are the best achievable. In these studies<sup>90</sup> less material was ablated due to smaller spot sizes and lower power densities.

## **Chapter 7:**

# **Results for the Analysis of Reference Materials and Biological Samples**

### **Introduction**

Following the initial studies using modified aqueous standards as described in chapter 6, it was important to attempt to validate the calibration technique using certified reference materials. This calibration strategy is unique and therefore validation using an existing calibration technique is required. The obvious choice of reference materials is the NIST glass range. This has the advantage of being well characterised and is also relatively transparent allowing its absorption coefficient to be measured and matched to that of the aqueous standards. The NIST glass range is also the most commonly used calibration standard for LA-ICP-MS, proving that the aqueous standards can perform at least as well as the most commonly used calibration standard would give credence to the new calibration technique. Validation was performed using NIST 613, although the analysis of a selection of reference materials would have been ideal, availability, time and polishing constraints did not permit this.

Following validation of the calibration method the technique will then be applied to the analysis of biological materials. Bone material was selected as the first specimen for analysis and liver samples were the second samples analysed.



## 7.1 Analysis of NIST 613 Using an Aqueous Calibration Procedure

A standard solution was prepared with the same elemental concentrations for Ni, Cu and Pb as NIST 613. A polymer concentration of  $9.2 \text{ g dm}^{-3}$  was used to match the absorption coefficients of the standard and the glass. Table 13 shows RSDs for the standard solution with and without  $\text{Pb}^{208}$  as the internal standard, where  $n=5$ . Both sets of RSDs were acceptable, with the use of an internal standard giving slightly better results.

Table 13: Precision's Achieved With and Without an Internal Standard for Aqueous Standards with Modified Absorption Coefficients.

Isotope	%RSD no internal standard	%RSD $\text{Pb}^{208}$ internal standard
$\text{Ni}^{60}$	4.7	3.9
$\text{Cu}^{65}$	5.4	3.9
$\text{Pb}^{208}$	4.2	--

Using the standard solution as prepared and Pb as an internal standard NIST 613 was analysed as a sample. Calibration was performed using the following calculation:

Select an internal standard whose concentration is known in the sample and the standard, calculate a correction factor as follows:

$$\text{Correction Factor} = \frac{\text{Sample CPS}}{\text{Std CPS}} * \frac{\text{Conc of Std}}{\text{Concin Sample}}$$

The correction factor was then applied for the determination of other elements in the sample.

$$\text{Element Concentration} = \frac{\text{Conc element in std}}{\text{Correction factor}} * \frac{\text{CPS element in sample}}{\text{CPS element in std}}$$

The results for n=5 replicate analyses can be seen in Table 14.

Table 14: Analysis of NIST 613 Using Modified Absorption Coefficient Aqueous Calibration Standards.

Isotope	Calculated Conc / ppm	+/-	NIST Certified Conc /ppm	Ref <sup>70</sup> Conc / ppm	+/-
Ce <sup>140</sup>	36.3	2.6	39*	38.2	1.7
Cu <sup>65</sup>	36.5	1.4	37.7*	36.8	2.9
Fe <sup>57</sup>	44.7	6.3	51	55.6	15.8
Pb <sup>208</sup>	int std	-	38.57	38.7	1.7
Ni <sup>60</sup>	35.2	3.1	38.8	37.8	4.1
Sr <sup>88</sup>	77.6	2.0	78.4	76.4	2.0
U <sup>238</sup>	35.8	0.4	37.38	36.9	1.1

(\* not certified, given for information only.)

The initial experiments showed that calibration using the modified aqueous standards produced excellent results.

The absorption coefficient of the polymer standard and the NIST glass were matched, but it was found that the signal intensity of the polymer standards was of the order of ten

times greater than the intensity achieved for the NIST glass. The integrated count rate for 37.7 ppm in the glass was 6419 compared to 62386 for the polymer standard solution.

The actual count rates per second for the NIST glass and standard were expected to be similar as the absorption coefficients had been matched. It was therefore decided to employ time resolved analysis (TRA) which is a data acquisition programme within the PQ Vision software suite. TRA is a specialised application that permits data to be acquired at specified intervals for a sample that is being continuously introduced into the ICP-MS.

The TRA software was used to follow the count rate for the isotopes of interest over the full thirty seconds of data acquisition. Data was acquired for the standard polymer solution and NIST 613 and is presented in Fig 22.

It can be seen from Fig. 22 that the signal intensity for elements in the glass fell off very sharply after the start of ablation. The signal intensities for elements in the polymer standard remained fairly constant over the whole acquisition period. The apparent loss of signal in the NIST glass may have been due to the fact that the laser channelled into the solid sample causing a loss of focus and hence a lower observed count rate. The polymer standard did not suffer from this problem as the solution provided a constantly renewable surface. This problem had been addressed by Cousin<sup>91</sup>. The group developed an active focus system for solid sample introduction. As the laser etched into the sample, the translation stage was adjusted to keep the laser in focus. An interesting point to note from these studies was that the initial count rates for ablation of solids and solutions were indeed similar despite the fact that the ablation mechanisms are thought to be different.

Fig.22

### Comparison Of NIST 613 And Polymer Standard By TRA

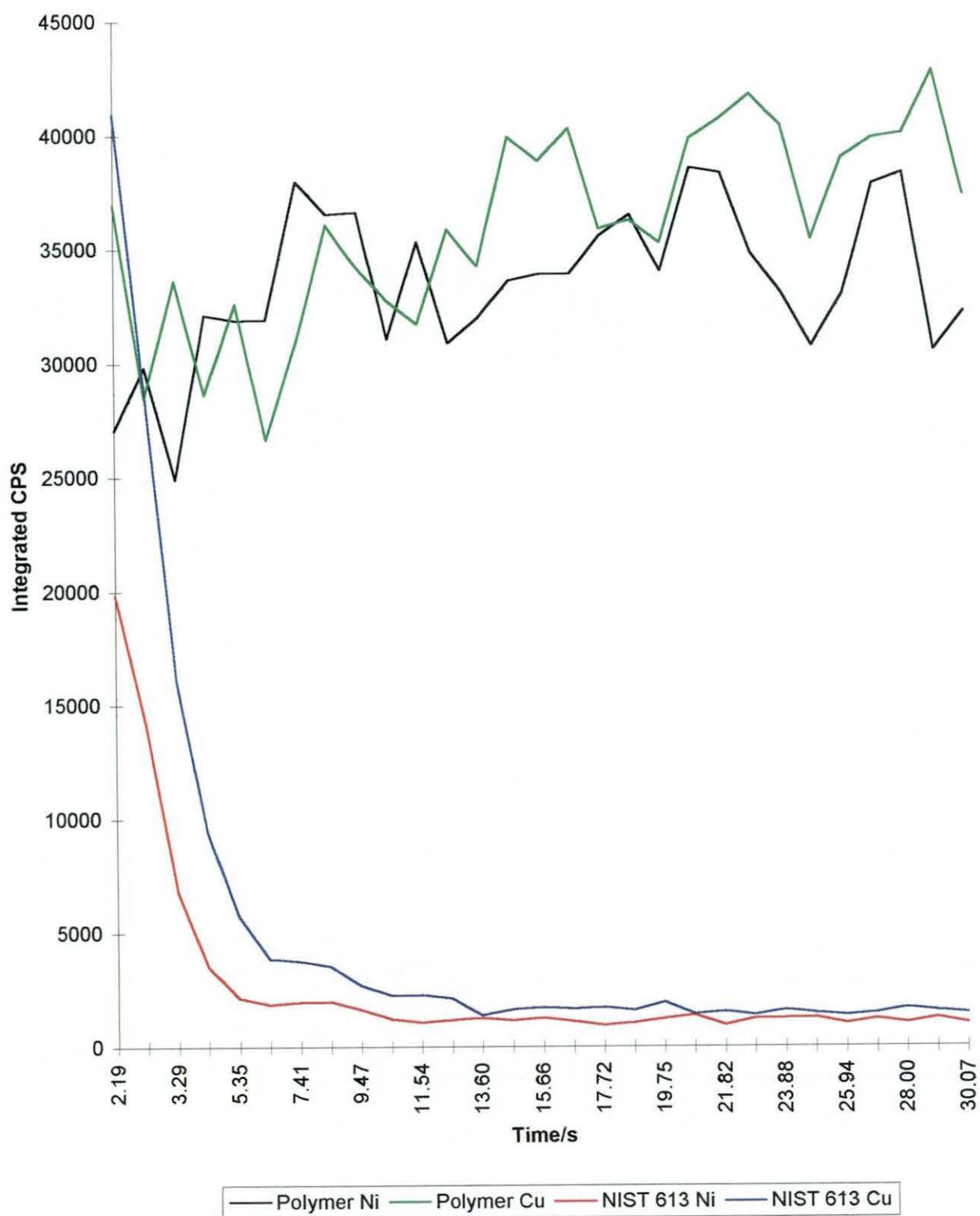
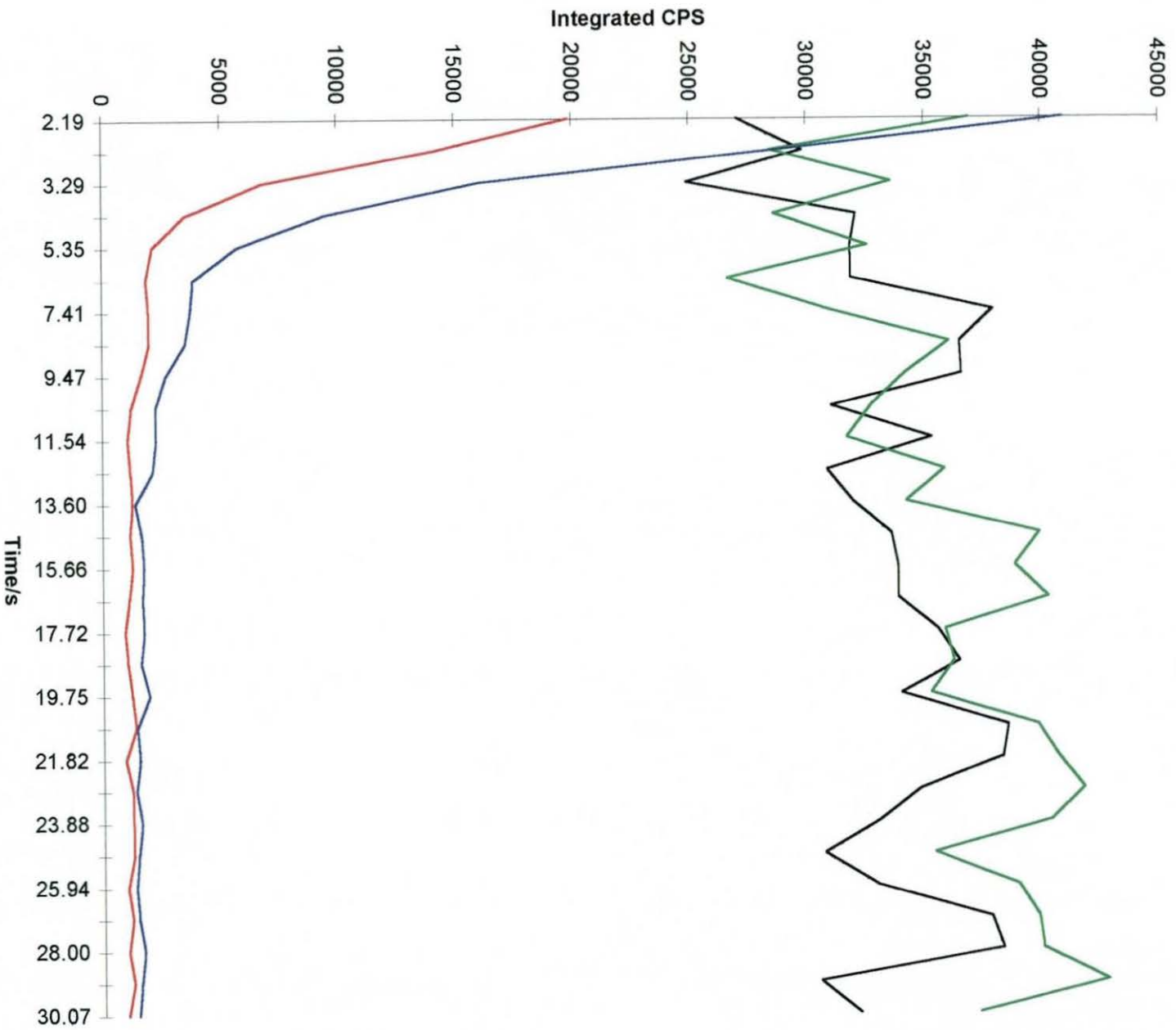


Fig.22

### Comparison Of NIST 613 And Polymer Standard By TRA



— Polymer Ni — Polymer Cu — NIST 613 Ni — NIST 613 Cu

Work carried out by Dyer<sup>92</sup> has shown that the mechanism of ablation is different for liquids when compared to solids. During the ablation of liquids, shock waves were observed to pass through the solution. These shock waves were thought to be responsible for removal of more material from the sample surface, a form of laser nebulisation. This effect was certainly observed in the experiments on laser energy, see section 6.7, as large droplets were ejected from the surface. However, whereas Dyer was interested in the *ablated mass*, ICP-MS responds only to the *transported mass*. The larger droplets produced by the shock wave at higher powers are not transported to the plasma and therefore the mass transported is similar for both solids and solution standards. The results presented here suggest that shock wave removal of material is less of a problem at lower fluences.

In practice the use of an internal standard to relate the signal intensities, can correct for differences in observed count rates for samples and standards. This does, however, move away from the original concept that a universal calibration procedure should not rely on the fact that the concentration of one component in the sample must be known.

## **7.2 Osteoporosis**

Osteoporosis is defined as thin or porous bones and is a major cause of suffering and disability among elderly women. Although bones generally become thinner in everyone with advancing age, some individuals develop osteoporosis so severe that their risk of breaking bones increases. Osteoporotic hip fracture is one of the most serious consequences of bone thinning. As many as 20% of individuals who suffer a hip fracture die within one year, usually as a result of complications of the fracture. Osteoporosis is a major cause of morbidity and mortality. At least 1.2 million fractures occur each year in

the United States as a direct result of osteoporosis with medical and social costs estimated at \$6.1 billion annually<sup>93</sup>.

Bone is active, living tissue, continually remodelling itself and constantly participating in a wide range of biochemical reactions. Bone tissue consists of both cells and an intercellular matrix. Osteoblasts are the cells within bone involved in laying down new bone tissue. Osteoclasts on the other hand participate in the breakdown of old and damaged bone tissue in a process called resorption. The formation and resorption of bone is a dynamic process which helps keep bones young by replacing old and weakened areas with new bone tissue<sup>94</sup>.

The intercellular matrix of bone consists of an organic component, primarily collagen and other proteins and an inorganic component which is responsible for the rigidity of the bone. The inorganic component is composed of mainly calcium phosphate and calcium carbonate, with trace amounts of magnesium, fluoride, sulfate and other minerals. These minerals form crystals known as hydroxyapatites. Some of the elements found in bone and their connection with osteoporosis will now be discussed.

### Manganese

Studies in both animals and humans provide evidence that Mn provides an important role in bone health. Rats fed on a Mn deficient diet showed a reduction in the calcium levels in the femur bone, indicating that Mn deficiency caused the bones to be thinner than normal<sup>95</sup>.

Mn stimulates the production of a group of protein like molecules in the bone called mucopolysaccharides<sup>96</sup>. These compounds provide a structure upon which calcification can take place.

### Magnesium

As much as 50% of all the Mg in the body is found in the bones. A study of Mg deficiency<sup>95</sup> showed that all patients deficient in Mg had abnormally large calcium crystals in the bone. Mg deficiency was shown to be common in women with osteoporosis and associated with abnormal calcification which may be one of the factors that increases the risk of fracture. Healthy well formed crystal will be inherently stronger than bone containing abnormal crystals.

### Zinc

Studies with rats have provided evidence that Zn is essential for normal bone formation<sup>97</sup>. Zn further enhances the biochemical actions of vitamin D, which itself is involved in Ca absorption and osteoporosis prevention<sup>98</sup>. Zn is responsible for the formation of osteoblasts and osteoclasts, as well as the synthesis of various proteins found in bone tissue. Zn levels have been found to be low in the serum and bone of elderly individuals with osteoporosis<sup>99</sup>.



### Strontium

Sr has an affinity for bone tissue, tending to migrate to sites where active remodelling is taking place. In a study of mice, administering 0.27% Sr in the drinking water increased the rate of bone formation and decreased the rate of bone resorption<sup>100</sup>. The bone density of the mice given the extra Sr dose was higher than that of mice given normal drinking water. This suggests that Sr levels may influence the likelihood of developing osteoporosis.

### Aluminium

As well as accumulation in the brain and kidneys, ingested Al can also accumulate in bones. The accumulation of Al in bones appears to reduce the formation of new bone and increase the amount of bone resorption<sup>101</sup>, thereby increasing bone loss. One of the effects of Al is to bind P in the intestinal tract, inhibiting the absorption of P. This leads to bone loss as P is an essential component of bone crystals<sup>102</sup>.

### Lead

Pb has been linked by various studies to abnormalities in bones<sup>103,104</sup>. The injection of lead salts into animals caused the appearance of large numbers of osteoclasts causing an increase in bone resorption. The lead doses in these studies was high, but it can not be ruled out that prolonged exposure to low levels may contribute to osteoporosis.

The determination of elements in human femoral bone using ICP-AES and ICP-MS was carried out by Roberts<sup>105</sup>. Samples were taken from the head of femur bone. Adhering muscle and fat was removed using a hydrogen peroxide / ethanol wash and the clean

dried bone then dissolved in a mixture of mineral acids. Al, B, Ca, Fe, K, Mg, Na, P, Pb, Sr, and Zn were quantitatively determined.

This study was carried out to determine if the composition of major and trace elements in femoral bone differed from healthy to osteoarthritic bone. Osteoporosis is thought to be a compounding factor in fractures of the proximal neck of femur, a significant cause of morbidity and mortality in the elderly. Traditionally, osteoporosis has been defined as a quantitative reduction in bone mass. The authors suggested that osteoporosis may not only be a reduction in bone mass, but also a change in bone composition.

Inhomogeneity of the bone samples was found to be a potential limiting factor in the interpretation of data from different patient groups. The sampling site was found to be critical, care was taken to ensure that samples were taken from the same bone site for comparison.

The results obtained suggested that there was no clear evidence of any differences in the composition of both major and trace elements in femoral bone from osteoarthritic patients, patients with fractured head of femurs, or patients who had died from other causes. Pb levels were found to be lower in osteoarthritic bone compared to other bone which could indicate an increased bone turnover in this condition. The authors concluded that the tendency for femoral fractures to occur was not related to an abnormality in bone composition.

LA-ICP-MS would offer a solution to the problem of sample inhomogeneity. It would be possible to produce elemental profiles across the bone and fracture site and remove the need for any sample pre-treatment.

### 7.3 Analysis of Biological Materials

To date, the vast majority of applications of LA-ICP-MS have been in the geological field<sup>106-113</sup>. The analysis of biological materials opens up another exciting area for investigation. A profile map of an element across a biological material would be useful in providing information as to the areas of accumulation of that element.

In this study, various biological materials will be investigated using the novel calibration method described in previous chapters. Semi-quantitative and ultimately fully quantitative results will be presented.

Thin bone sections of patients who had undergone hip replacement operations were mounted in the ablation chamber. An elemental profile map was built up by sampling at different points across the bone section. This type of analyses had never been reported before and it was therefore uncertain as to what significance the results would have. Unfortunately bone samples from healthy subjects were not available for comparison. Future work could involve the analysis of bone from a person who had died from other causes and who, to all knowledge, had a healthy hip bone.

The effect of trace metal concentration in the liver has not been studied or aroused as much interest as bones. However, some diseases of the liver are linked with the accumulation of trace metals.

Wilson's disease is associated with the accumulation of Cu in the liver. A healthy person would be expected to have Cu concentrations of less than 100  $\mu\text{g/g}$  dry weight, but a person suffering from Wilson's disease could have concentrations up to 3000  $\mu\text{g/g}$ <sup>114</sup>.

High concentrations of Fe in the liver have been associated with Cirrhosis<sup>114</sup>.

Sections of pig liver were prepared for analysis by LA-ICP-MS. 2cm square sections of liver were frozen between microscope cover slips in order to produce a flat surface for laser sampling. The coverslips were removed just prior to analysis to reveal a uniform flat surface onto which the laser could be focused. Fresh pigs liver samples from a local butchers shop were used in this study. Results were compared with Bovine liver reference material SRM 1577a and also with bulk analysis results of the liver following microwave digestion of the samples.

## 7.4 Experimental

The laser operating parameters for the bone and liver samples can be seen in Table 15.

Table 15: Laser Operating Parameters

Parameter	Setting
Laser Transition	248 nm
Estimated Laser Energy	40 mJ into a 200 $\mu$ m spot
Laser Frequency	5 Hz
Crater Diameter	200 $\mu$ m
Acquisition Time	30 s

The laser output energy was reduced for the analysis of the biological materials. At high laser output energies, severe damage was observed on the sample surface. Using the calculation described in section 6.2, the estimated power density on the sample surface was  $0.35 \text{ GW cm}^{-2}$ .

Bulk analysis of the liver samples involved microwave digestion and then subsequent analysis on the ICP-MS. 4 g liver samples were frozen and then dried under vacuum. The average water content for five replicate samples was 69.6 %.

0.5 g samples of the dried liver were then digested in 10 ml of Aristar grade 70% nitric acid using a microwave digester (CEM, Buckingham, UK, Model MDS 81D). The microwave oven was operated at 60% (600 W) power for 10 minutes followed by a further 10 minutes at 30% power. The resultant solution was then diluted with deionised water in a 100ml graduated flask and then stored in a poly ethylene bottle prior to analysis.

Standards for the analysis of the bone and liver samples were prepared in the same manner as described previously. The amount of polymer added and hence the degree of modification of the absorption coefficient of the standards was calculated by matching the signal of an element of known concentration in the sample with the signal for the same element in the standard. This was an alternative procedure to matching the absorption coefficients which are not readily obtainable for biological materials. This was in effect a tuning procedure, whereby the standard and sample were matched by count rate comparison.

## 7.5 Analysis of Bone Samples

Bulk analysis of the bone samples was not possible as the bone samples had to be returned after analysis. Table 16 gives an estimate of the elements likely to be encountered and the concentration they are likely to be present at<sup>115</sup>.

Table 16: Estimated Composition of Bone Samples

Element	Estimated $\mu\text{g/g}$	Element	Estimated $\mu\text{g/g}$
Ca	250	K	0.08
P	120	Fe	0.075
Na	4.6	Sr	0.038
Mg	2.8	Pb	0.020
Zn	0.2		

Thin sections of bone approximately 5 cm in diameter were received for analysis. Elemental distribution profiles from the centre of the bone outwards were obtained using the laser as a means of sampling. Samples were taken at 1 mm intervals over a range of 1 cm which was the maximum permissible travel of the translation stage. Results for elements of interest are shown in Figs. 23 a,b,c,d. Figs 23 a and b represent different elements at the same bone site. Figs 23 c and d represent analysis for the same elements as 23 a and b but carried out at a different site on the bone. The graphs show elemental profile maps for P, Ca, Na, Al, K, Fe, Zn, Sr, Pb across the bone sample. Mg was used as an internal standard and assumed to be at a concentration of 2.8 ppm in the bone. The analysis of elements with atomic masses below 80 is difficult with a quadrupole ICP-MS

Fig.23a

Bone 323/91 Profile 1a

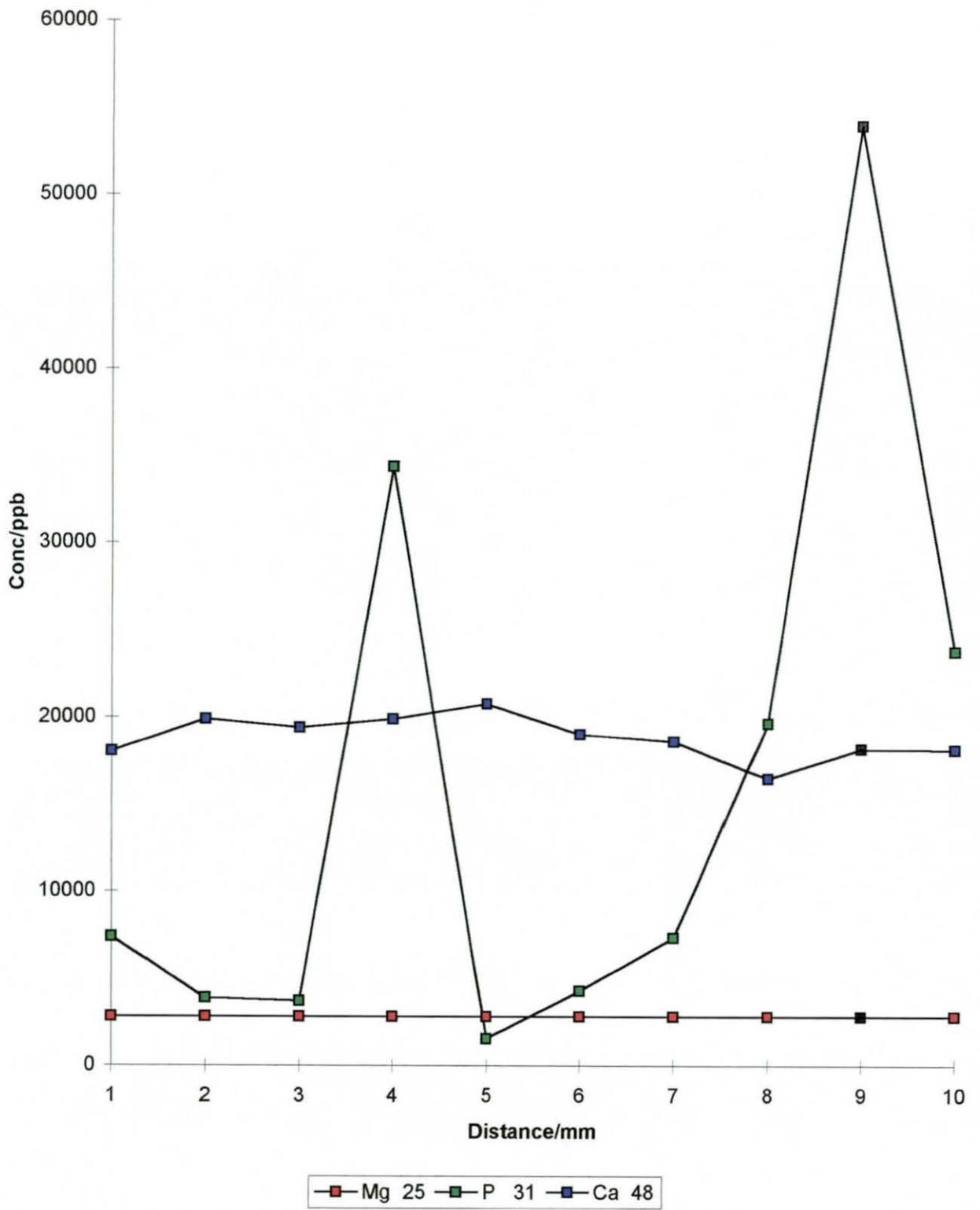


Fig.23b

Bone 323/91Profile 1b

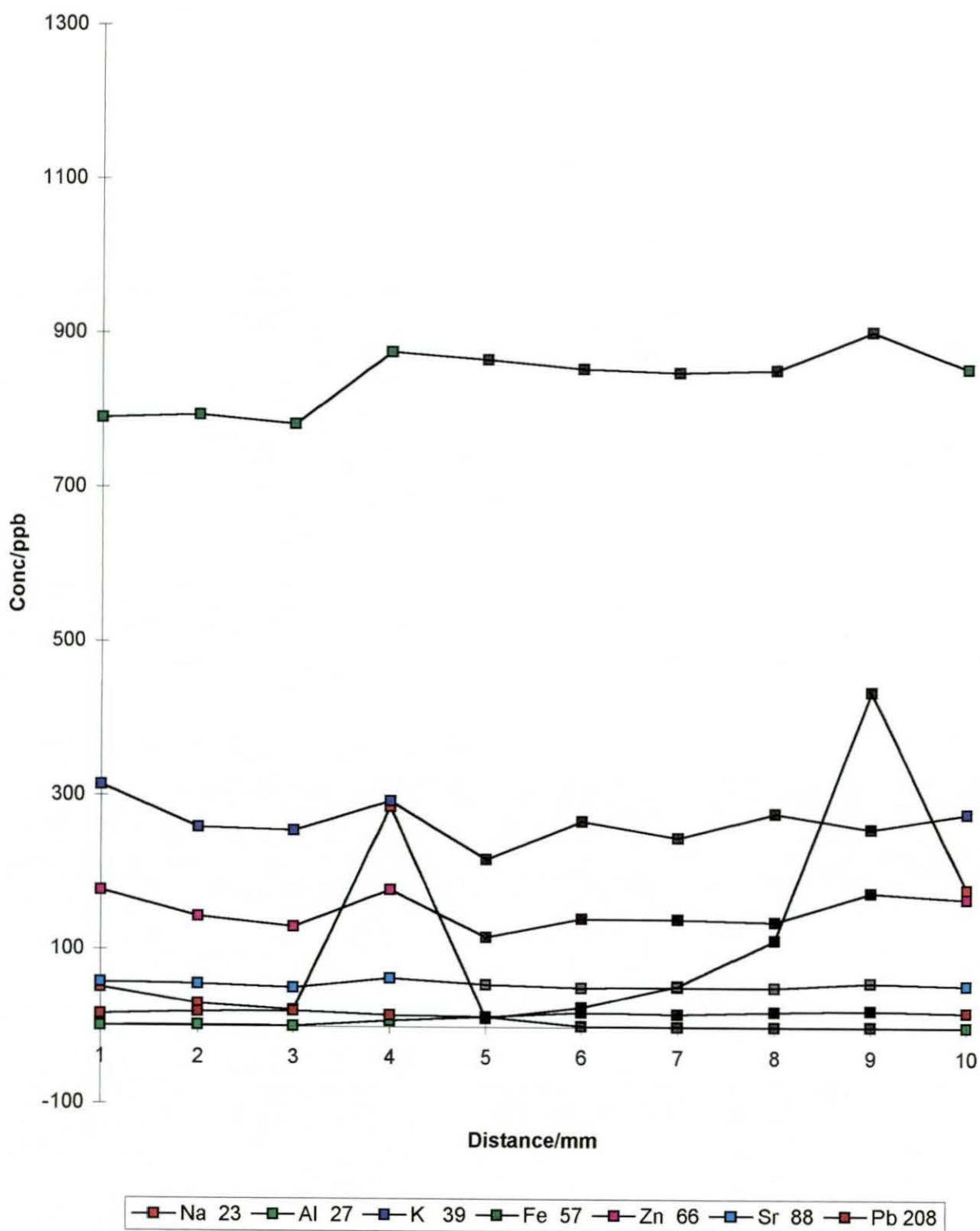




Fig.23c

Bone 323/91 Profile 2a

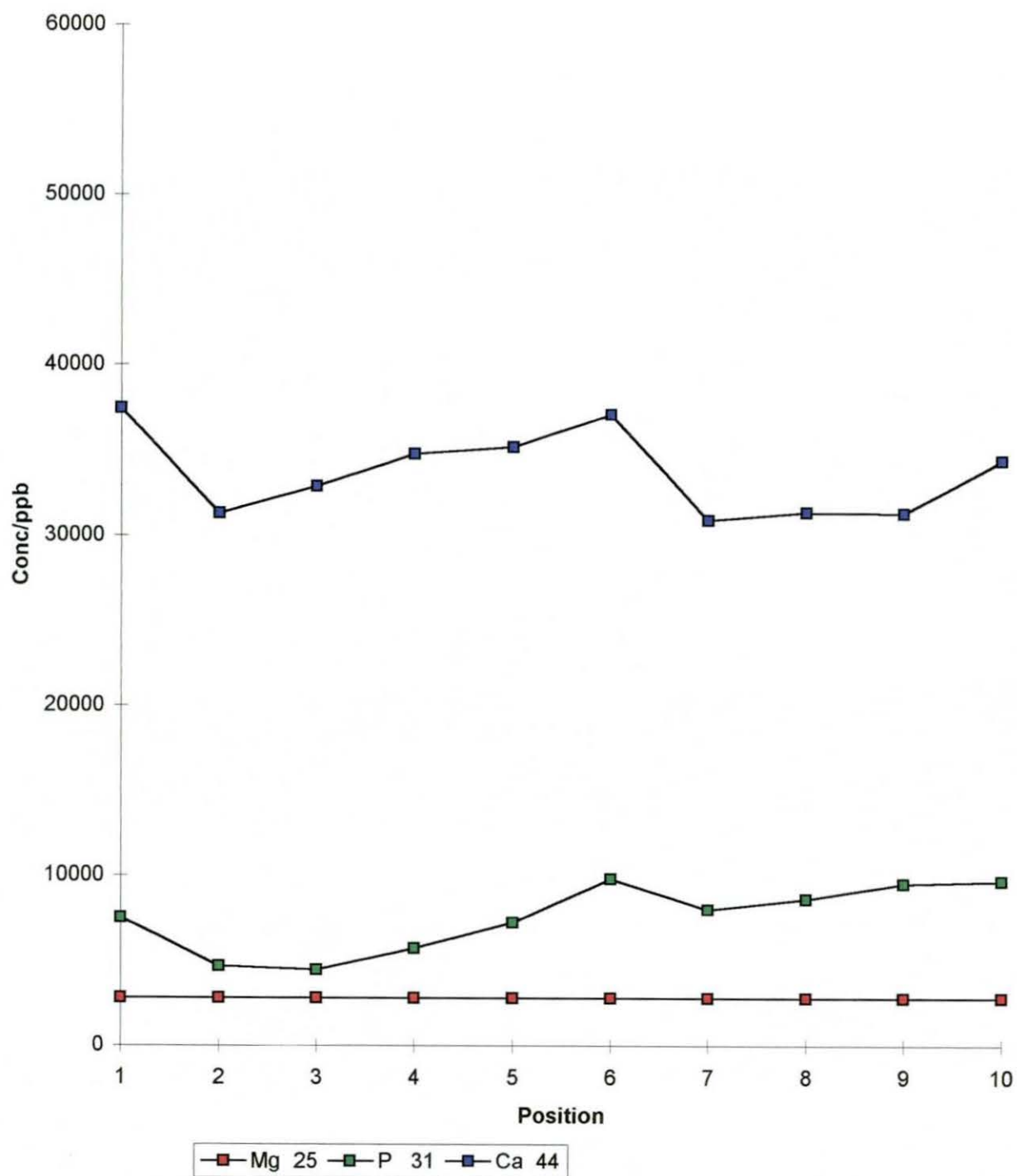
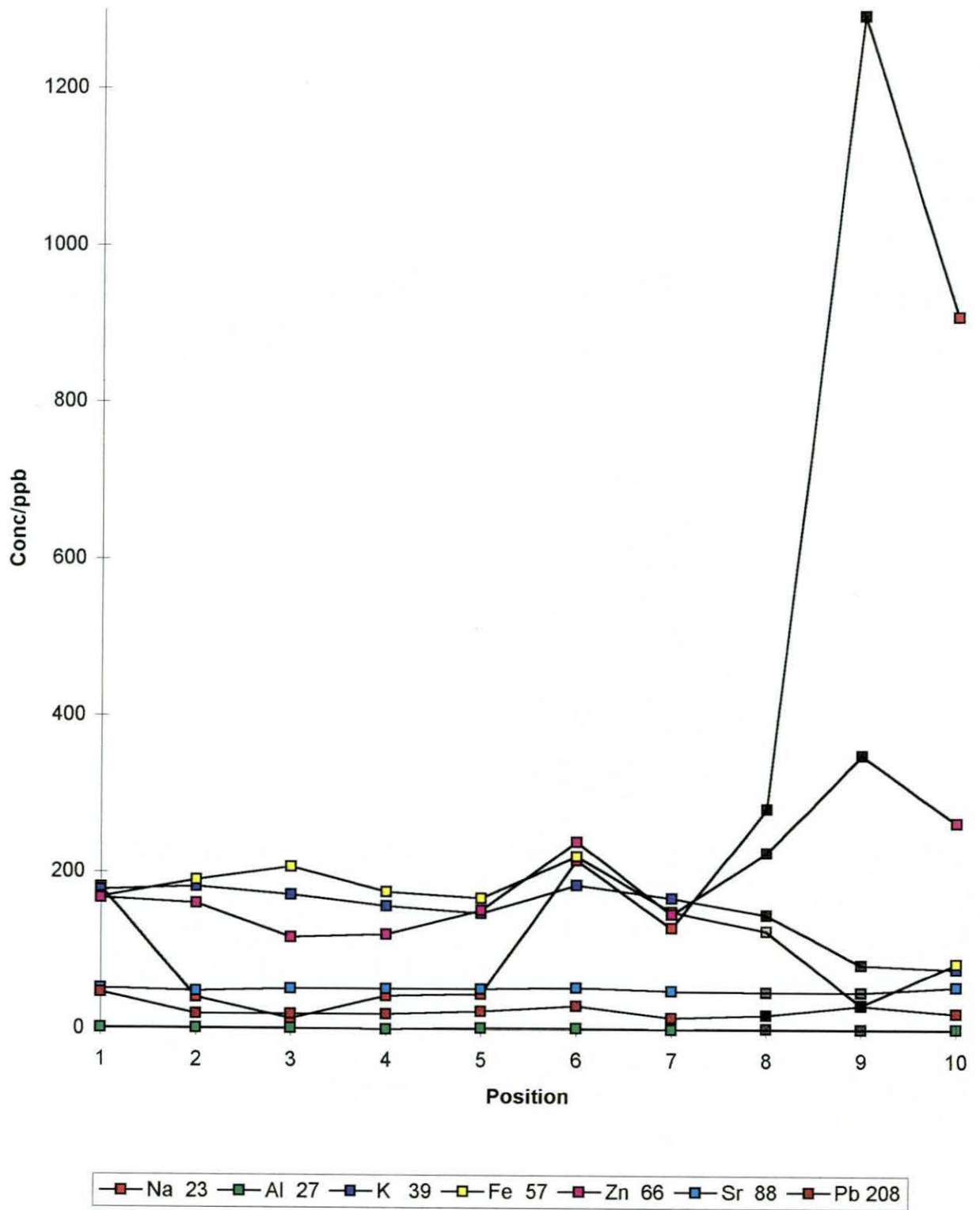


Fig.23d

Bone 323/91 Profile 2b



due to spectral interferences. At these relatively high concentrations it was hoped that general concentration trends could be identified.

Further analysis was carried out by sampling the same position of the bone continuously for 5 minutes using the TRA software available from the PQ Vision suite. This allowed a depth profile to be built up of element concentration as the laser channels deeper into the bone. The results can be seen in Figs. 24 a,b,c.

From the profiles shown in Figs. 23, which were taken from the centre of the bone outwards to a distance of 10 mm, it can be seen that the concentration of most elements remained fairly uniform. The spatial differences could be on a smaller scale than the 200  $\mu\text{m}$  spot size for the laser. Small variations in concentration can be seen for elements such as Fe, K and Zn. However, at various points across the transects the Na and P concentrations increased and are correlated. It would be useful to use smaller spot sizes with closer sampling intervals to actually monitor the rise and fall of the correlated spikes. This was not possible with the Loughborough system as the quality of the optics was not sufficient to produce reproducible craters below 200  $\mu\text{m}$ .

Discussions with Dr N. Roberts from The Royal Liverpool Hospital suggested that the effect could be due to surface contamination from a phosphate buffer used to prepare the bone samples. An alternative and more interesting possibility was that the effect was mobilisation of sodium phosphate, but why this should happen was unclear.

TRA was used to determine if the observed effects were due to surface contamination. Data was acquired for five minutes at a single point on the bone. The analysis was carried out at the sample point where the apparent increase in Na and P had occurred. The inaccuracy in the manually driven laser translation stage may have meant that the same

Fig.24a

### TRA Analysis Of Bone 323/91

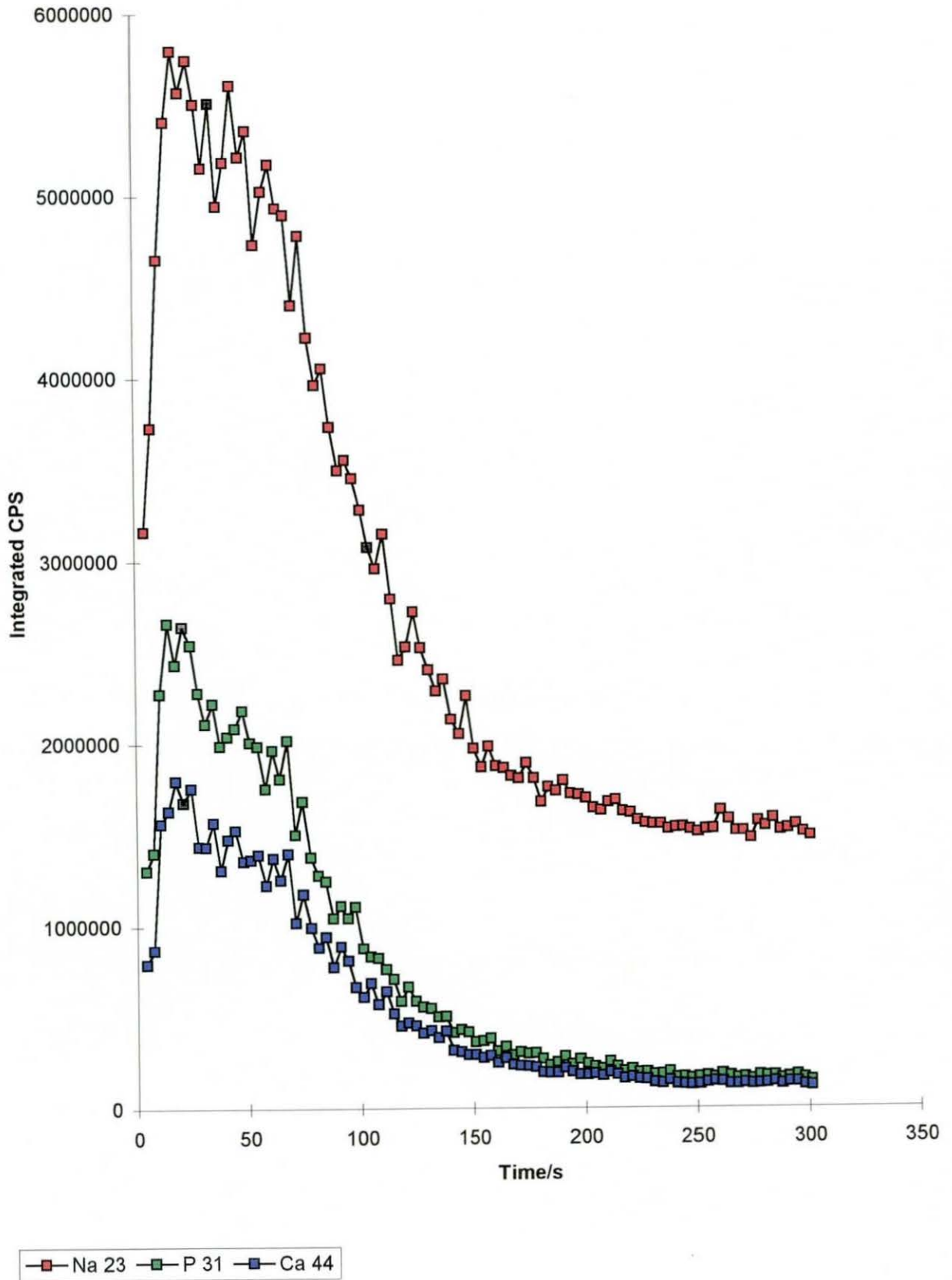


Fig.24b

### TRA Analysis Of Bone 323/91

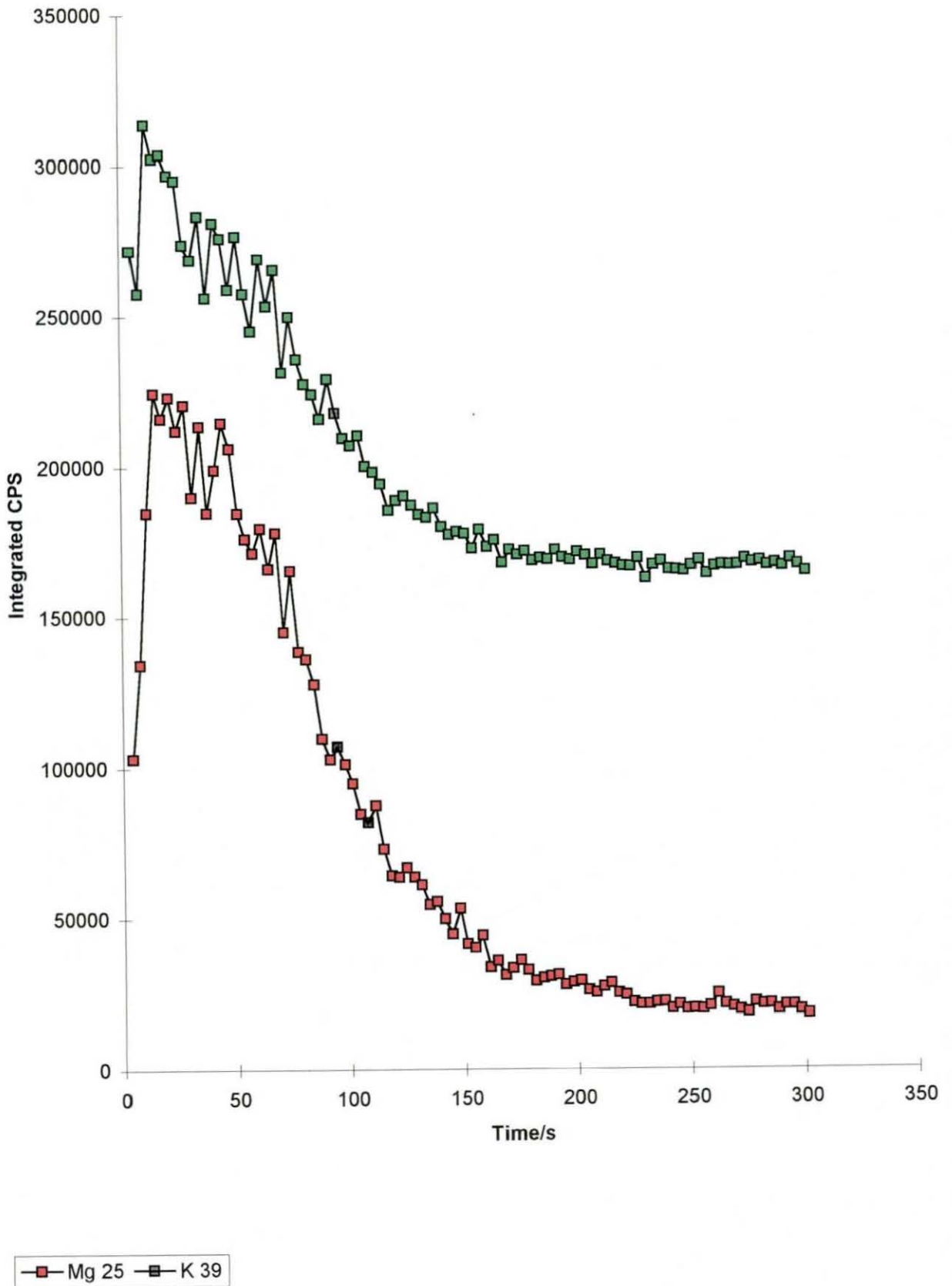
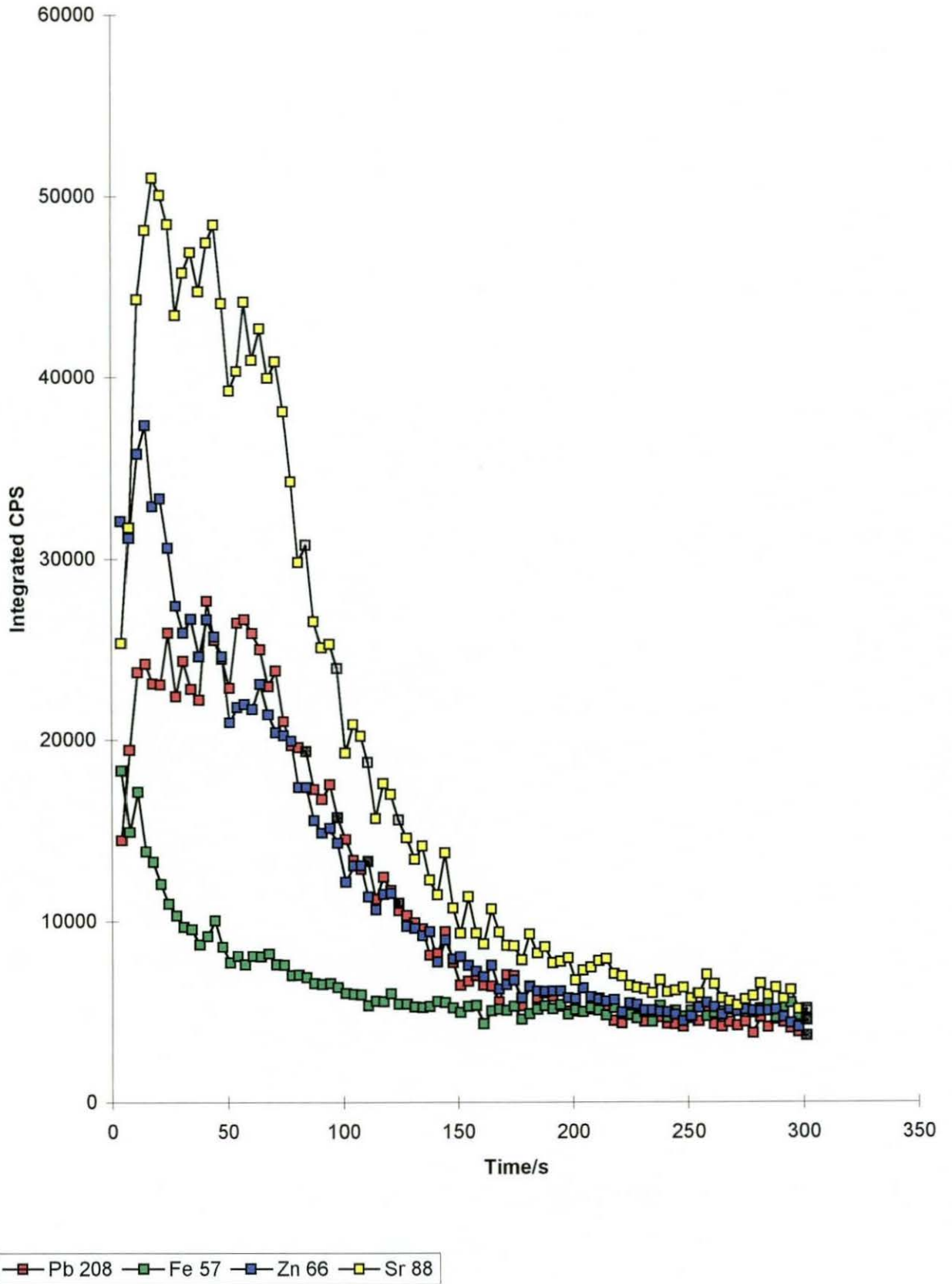


Fig.24c

TRA Analysis Of Bone 323/91



point was not sampled. The TRA profiles shown in Figs.24 show that the concentration of elements remains uniform throughout the bone. The Na and P depth profiles show no variation from other elements. The observed drop in signal was believed to be caused by loss of focus as the laser samples and channels deeper into the bone. It can therefore be assumed that the Na and P spike was not due to surface contamination.

## 7.6 Analysis of Liver Samples

Bulk analysis results for five replicate pigs liver samples and the certified values for bovine liver SRM 1577a can be seen in Table 17. The samples were prepared as described previously. The concentrations reported were for the dried sample. The mean and standard deviation for five different samples are also reported.

Table 17: Bulk Composition of Liver Samples

Element	Concentration $\mu\text{g/g}$	
	Bulk Analysis	Certified value NIST SRM1577a
Mg	$647 \pm 28$	$600 \pm 15$
Zn	$114 \pm 4$	$123 \pm 8$
Cu	$37.4 \pm 1.9$	$158 \pm 7$
Mn	$8.6 \pm 2.7$	$9.9 \pm 0.8$
Cd	$0.16 \pm 0.05$	$0.44 \pm 0.06$
Pb	not detected	$0.135 \pm 0.015$

The results of bulk analysis of the porcine samples showed similar concentration ranges as the bovine certified values. Porcine liver was chosen for this study as it is thought to bear the closest resemblance to human liver. Unfortunately the only reference material available was bovine liver.

A profile across the liver samples was then obtained using the laser as a means of sampling. Samples were taken at 1 mm intervals over a range of 1 cm which was the maximum permissible travel of the translation stage. Results for the elements of interest can be seen in Figs. 25 a,b,c,d. Figs 25 a and b represent different elements at the same liver site. Figs 25 c and d represent analysis carried out for the same elements as 25 a and b but at a different site on the liver. The graphs show elemental profile maps for Mg, Mn, Cu, Cd, Pb across the liver samples. Zn was used as an internal standard.

The profiles in Figs.25 show the elemental concentration gradients. No striking correlations between elements can be seen for the liver samples. The results obtained for Mn and Cu at the two sites on the liver are in good agreement with the bulk analysis results (Table 17). The Mg concentration varies significantly at different sites on the liver samples with concentrations ranging from 400-150  $\mu\text{g/g}$  over a 1cm interval. These concentrations are lower than those obtained for the bulk analysis and suggest that Mg is stored at specific sites within the liver cells. At the second liver analysis site, Pb levels appear to be high. The high levels could be due to contamination during the sample preparation stage or a site of heavy metal storage. It can however be noted that for profiles taken at different sites the elemental concentration can vary significantly. This work has demonstrated that it was possible to produce elemental concentration gradient results using aqueous polymer standards for calibration.



Fig.25a

### Liver Profile 1a

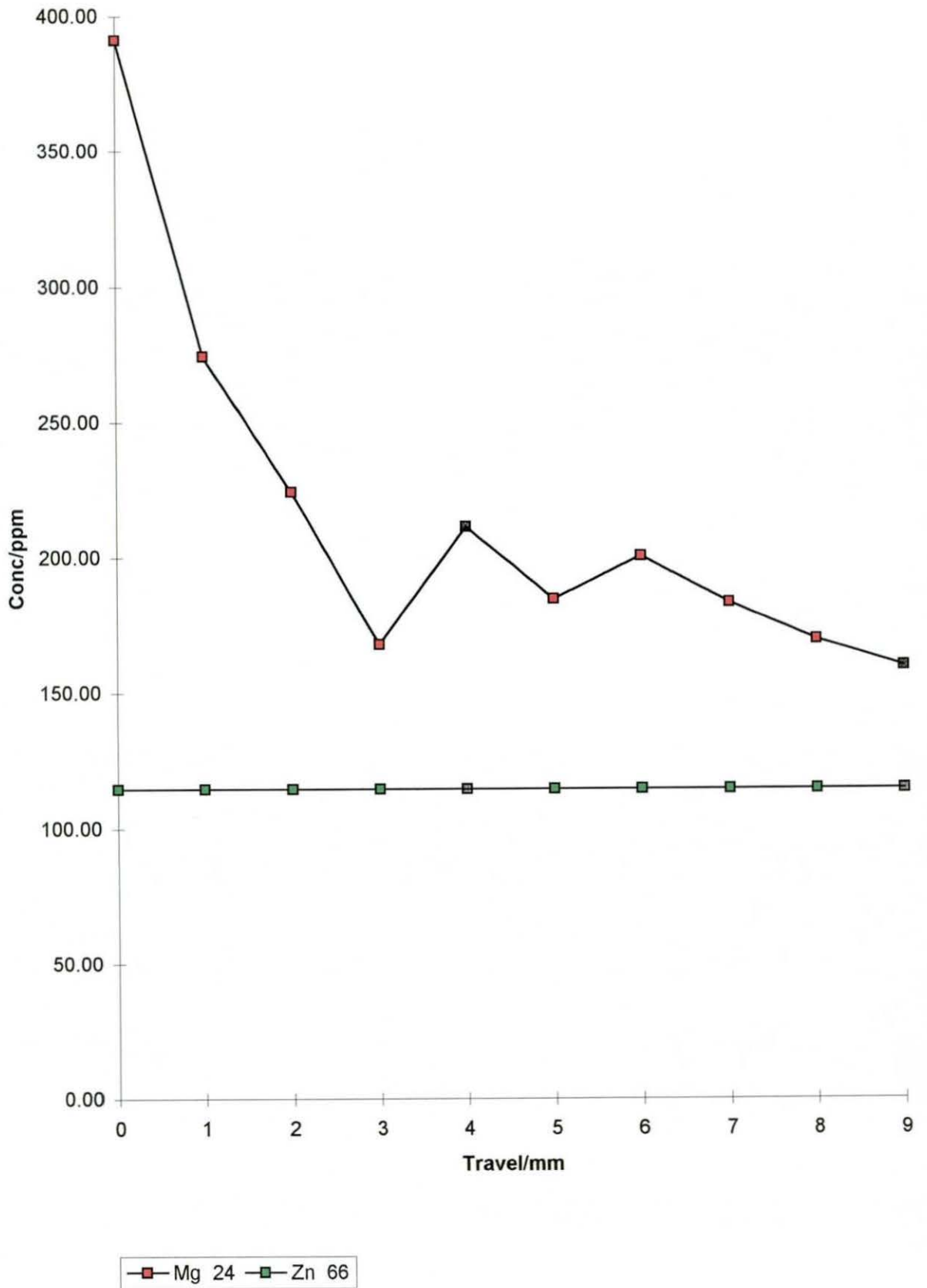


Fig.25b

### Liver Profile 1b

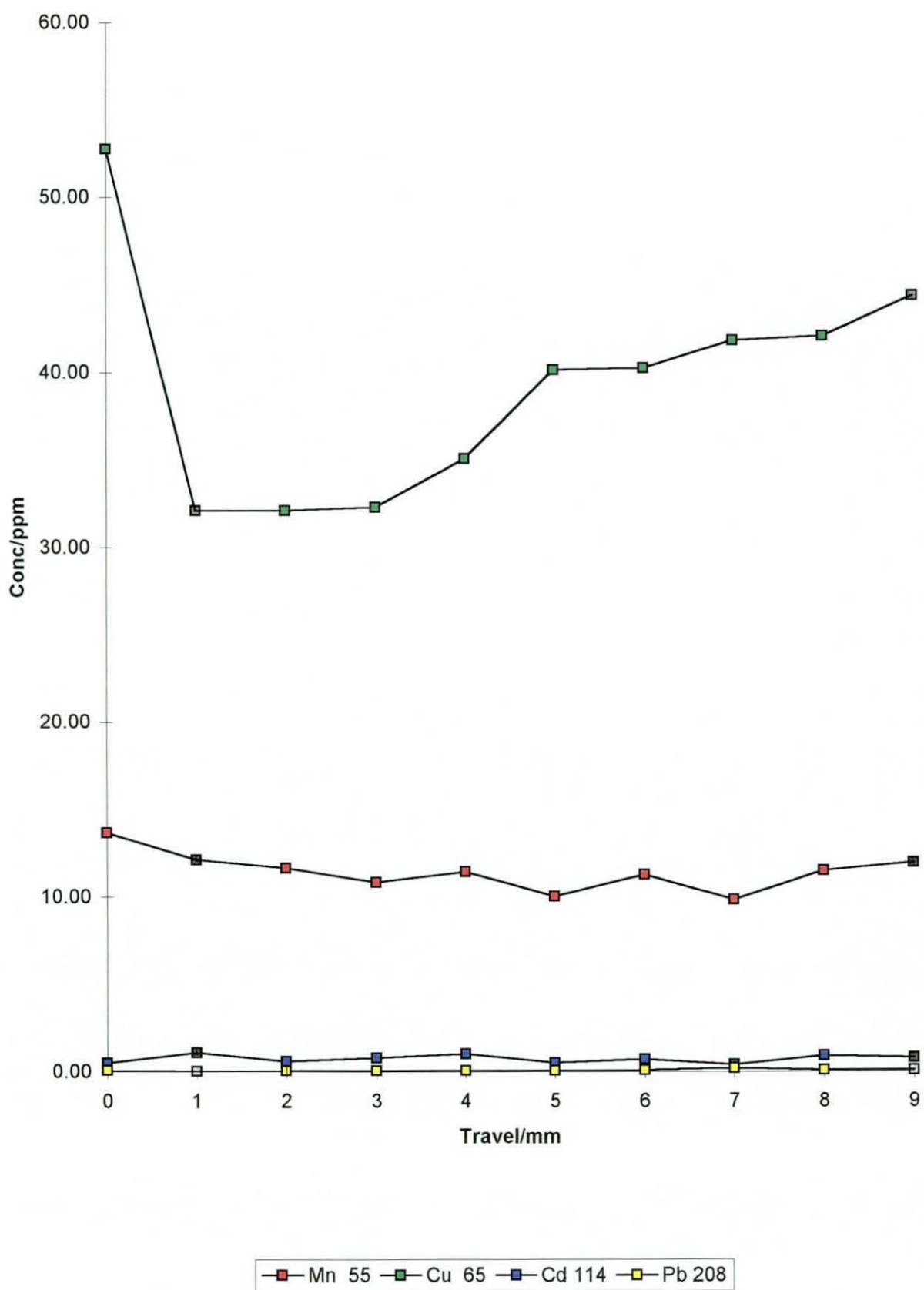


Fig.25c

### Liver Profile 2a

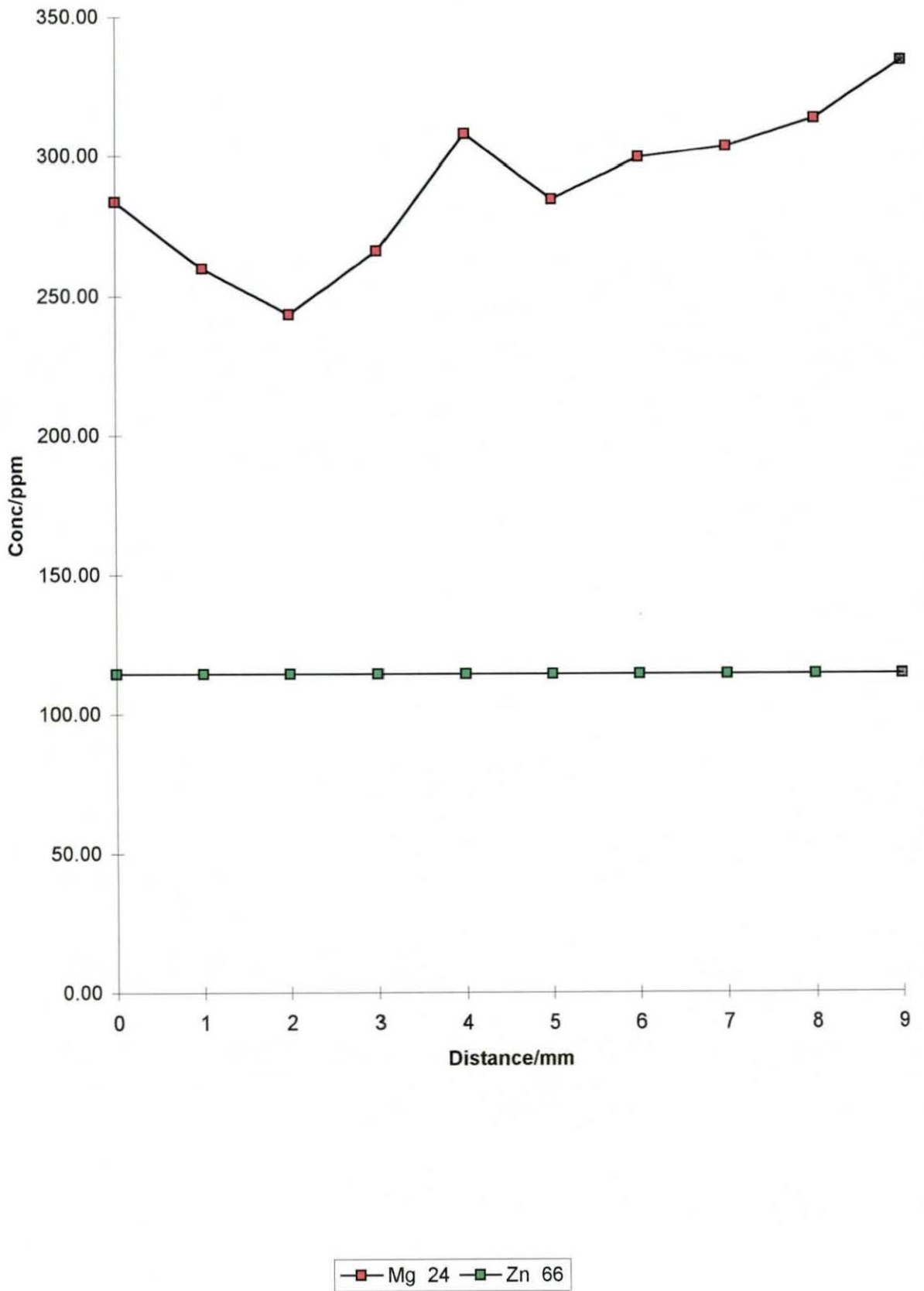
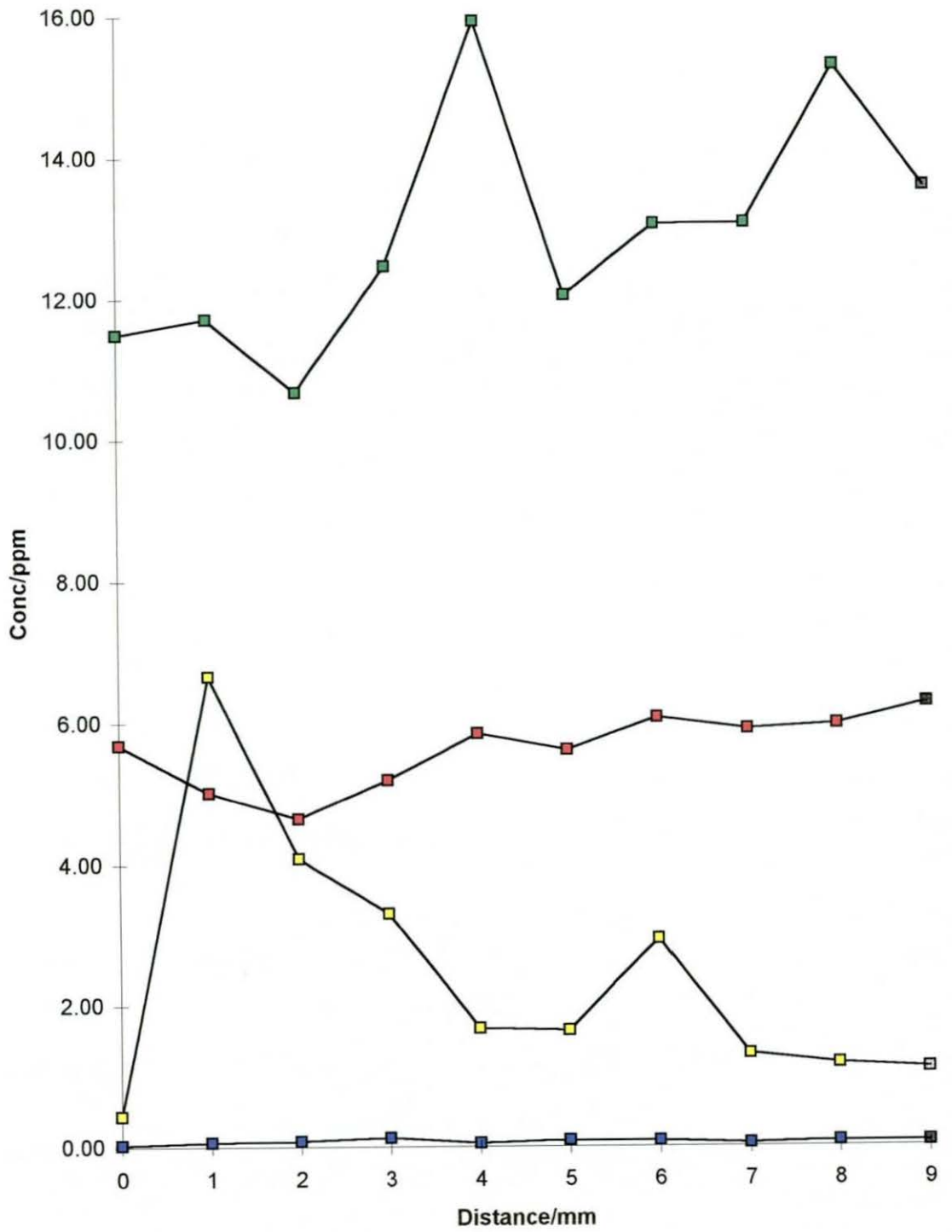


Fig.25d

### Liver Profile 2b



—■— Mn 55 —■— Cu 65 —■— Cd 114 —■— Pb 208

## **7.7 Experiments on a Commercial Laser Microprobe ICP-MS System**

Following on from the work on the Loughborough University laser ablation ICP-MS system, a visit was made to Fisons Instruments in Winsford Cheshire to use a commercially available UV MicroProbe laser system.

The UV MicroProbe is the first commercial UV laser to be fully integrated with its ICP-MS instrumentation. The laser used was a compact, frequency-quadrupled Nd:YAG, operating at 266 nm. It was not clear if the modification of the absorption coefficient of the standards at 266 nm would produce similar results to those seen at 248 nm.

The UV MicroProbe had a number of advantages over the Loughborough laser system that made sampling easier.

- High quality viewing optics and sample illumination
- High performance precision x:y:z stage
- Fully software controlled laser

The viewing optics allowed the ablation target to be viewed in-situ through a colour CCD camera for precise location of the analysis site. The quality of the optics also allowed craters with diameters of less than 10  $\mu\text{m}$  in diameter to be ablated. The computer controlled translation stage was ideally suited to profiling across the bone and liver samples.

### 7.7.1 Experimental

The samples and standards were prepared as described in previous sections. The laser and instrumental set-up were essentially the same as for the Loughborough instrument. The laser used was a UV MicroProbe (V.G. Elemental, Winsford, Cheshire, UK) which employed a frequency quadrupled Nd:YAG laser giving output at 266 nm. The ICP-MS was a commercially available PQ-XR (Fisons Instruments). The laser cell had an internal volume of 38 cm<sup>3</sup> with a cross-flow of argon to carry the ablated material to the ICP. The operating conditions for the analyses carried out in this section are shown in Table 18.

Table 18: UV MicroProbe Operating Conditions

Parameter	Setting
Laser Transition	1064 nm
Laser Energy	2 mJ
Laser Frequency	8 Hz
Crater Diameter	80 μm
Acquisition Time	60 s

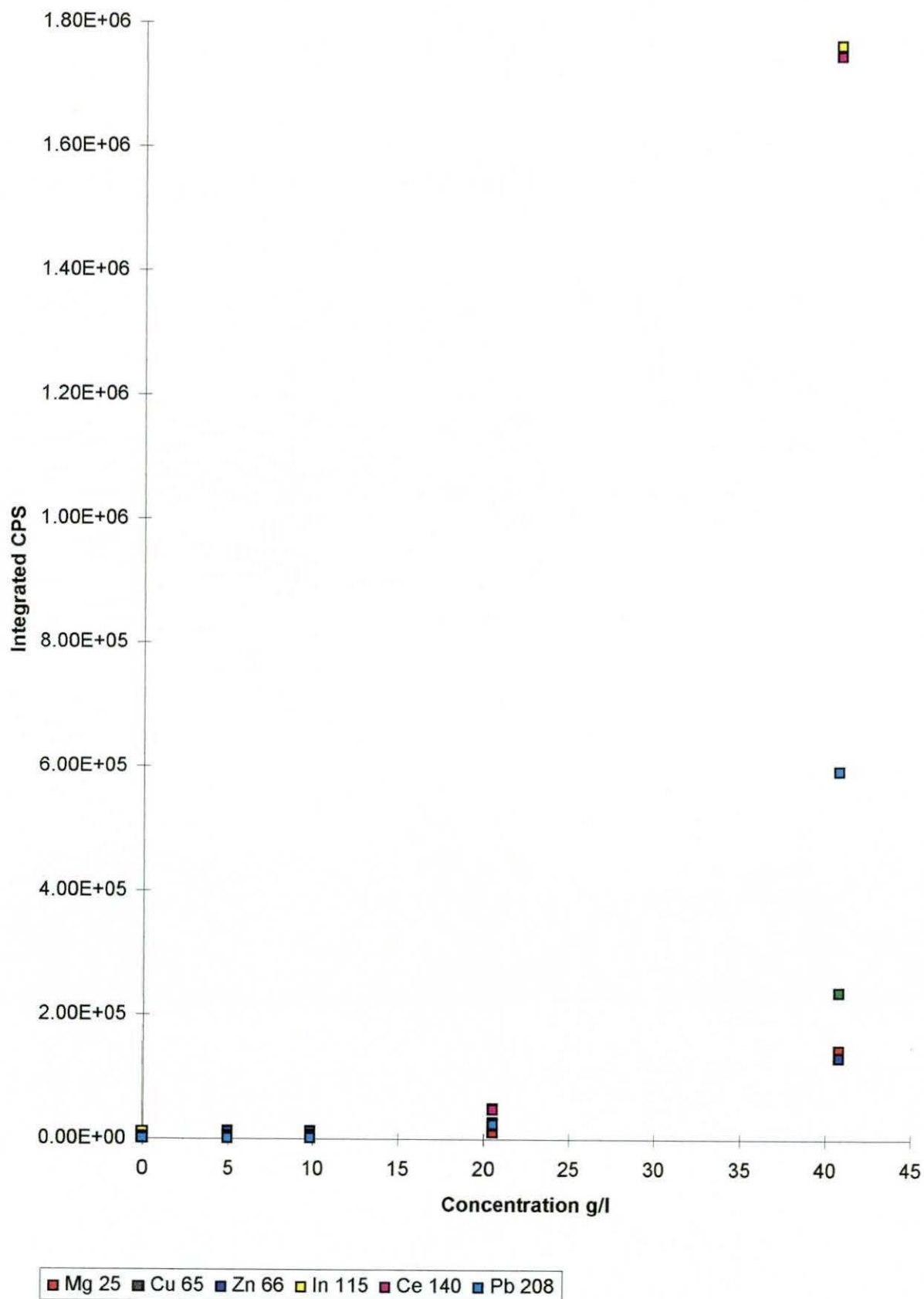
Using the calculation described in section 6.2, the estimated power density on the sample surface was 0.26 GW / cm<sup>2</sup>.

### 7.7.2 Polymer Additive Concentration

Initial experiments were carried out to determine if coupling could be achieved between the Nd:YAG laser and the modified standard solutions. A range of solutions containing

Fig.26

### Effect Of Polymer Concentration for Laser Radiation at 266nm



#### **7.7.4 Calibration Graphs**

Accurate repositioning of the translation stage after sample change-over made production of a calibration graph difficult on the Loughborough LA-ICP-MS system. The excellent repositioning accuracy of  $<4 \mu\text{m}$  for the computer controlled stage made production of calibration graphs easier. It was also possible to load several samples into the cell. This allowed analysis of standards and samples without the need to remove the laser cell which could affect the stability of the plasma. Accurate focusing on the sample surface was achieved using the monitor images and the incident illuminator beam. Figs 27-31 show calibration graphs produced for a suite of elements. Calibration graphs are also produced for elements that are traditionally difficult such as Fe and K.

Good calibration was achieved for most elements as can be seen for Cu and Zn in Figs. 27 and 28. Correlation coefficients of better than 0.999 were achieved. Acceptable calibration graphs were produced for traditionally difficult elements such as Fe and K. Correlation coefficients in the region of 0.850 were achieved for these elements. As indicated previously, these elements are particularly difficult to analyse due to spectral interferences. The large positive intercepts for these elements show that blank level is high. This was due to a combination of spectral interferences and elemental contamination of the system.

#### **7.7.5 Analysis of Bone Samples**

Bone samples were prepared and analysed by the same method described previously. Calibration was quantitative as opposed to the single standard calibration used for the Loughborough results. A profile across a bone sample of 5 cm in diameter was determined using the laser as a means of sampling. Fig 32 shows a typical bone sample.



Fig.27

### Cu (65) Calibration Curve

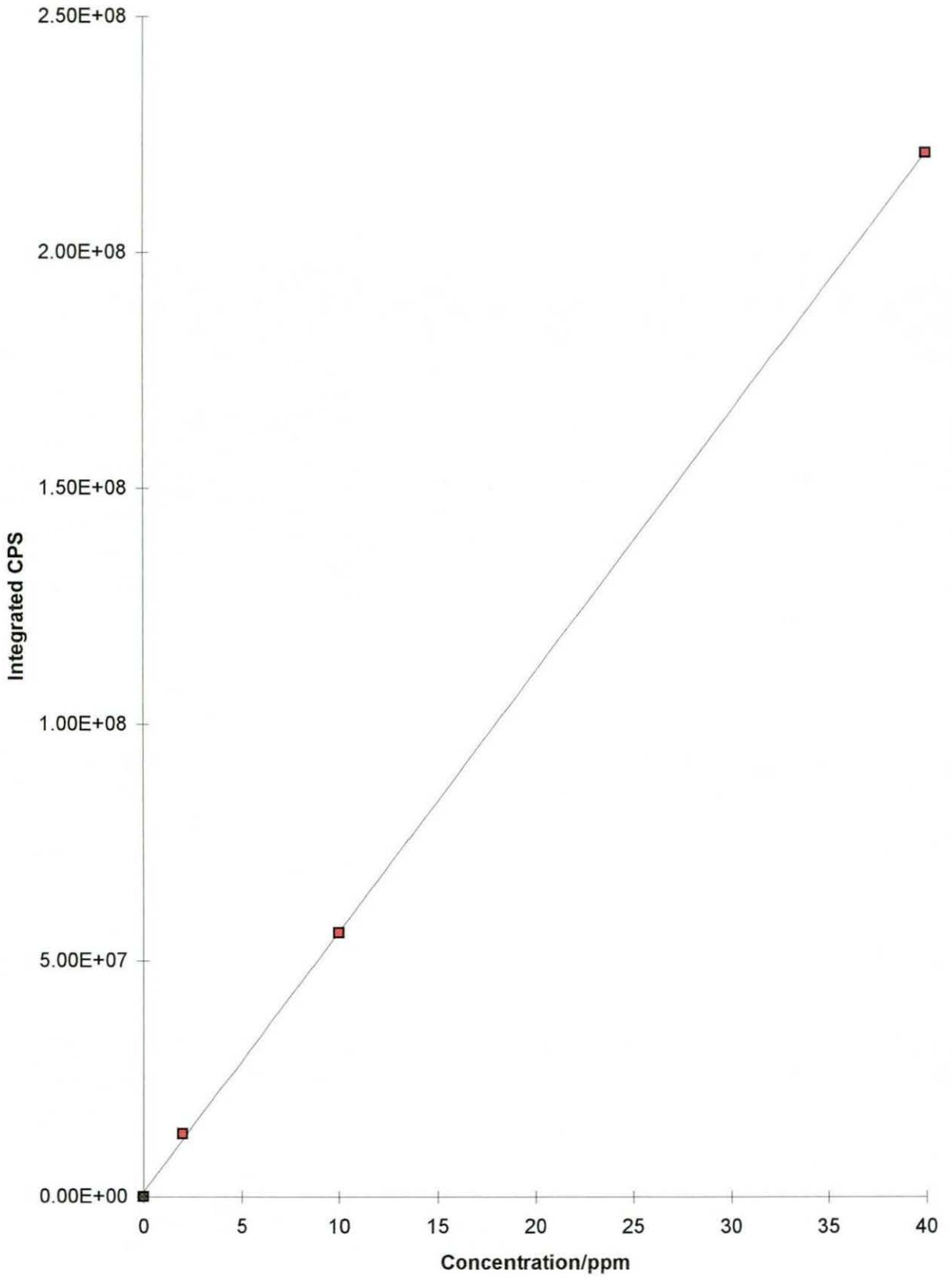


Fig.28

### Zn (66) Calibration Curve

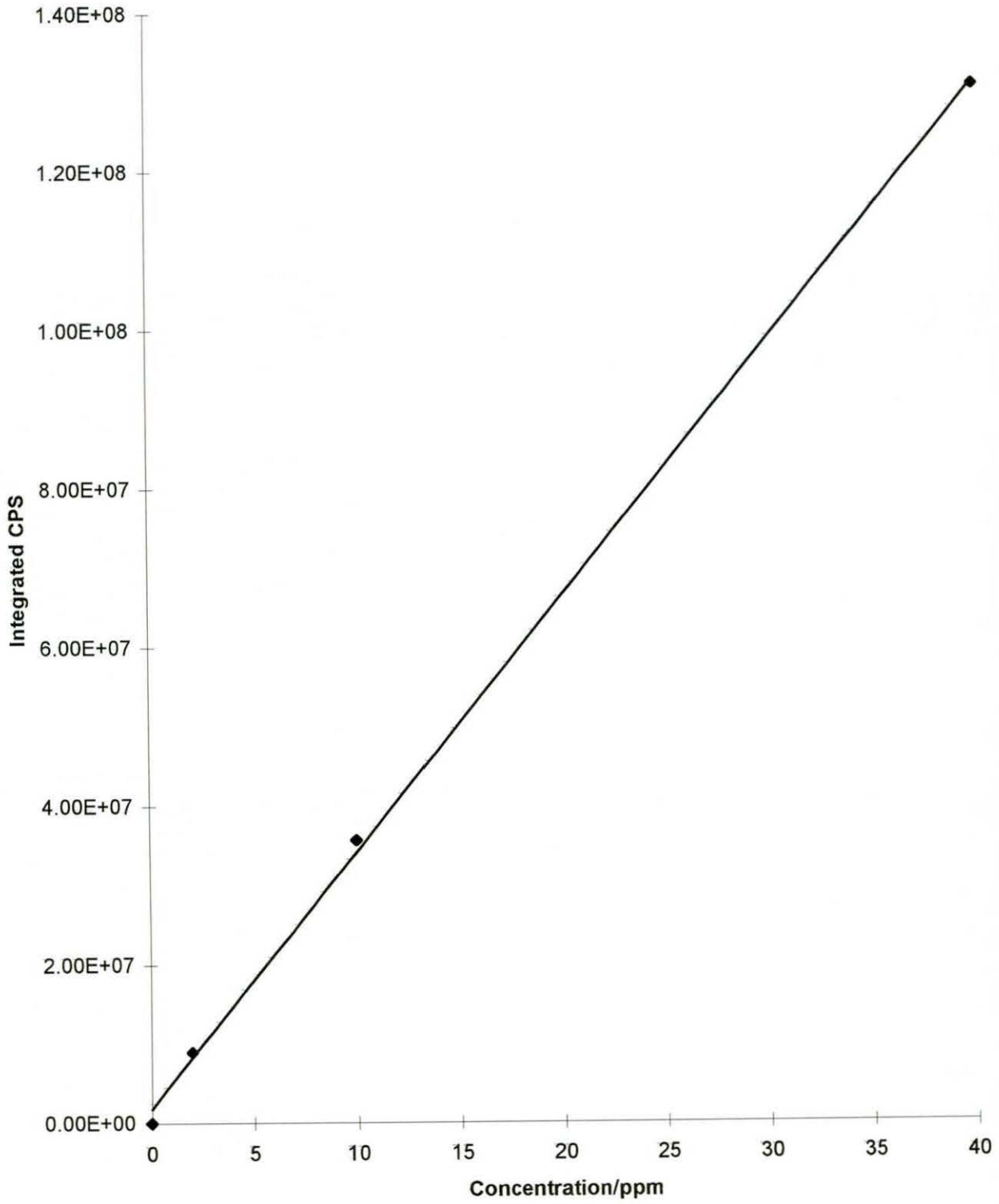


Fig.29

### Cd (114) Calibration Curve

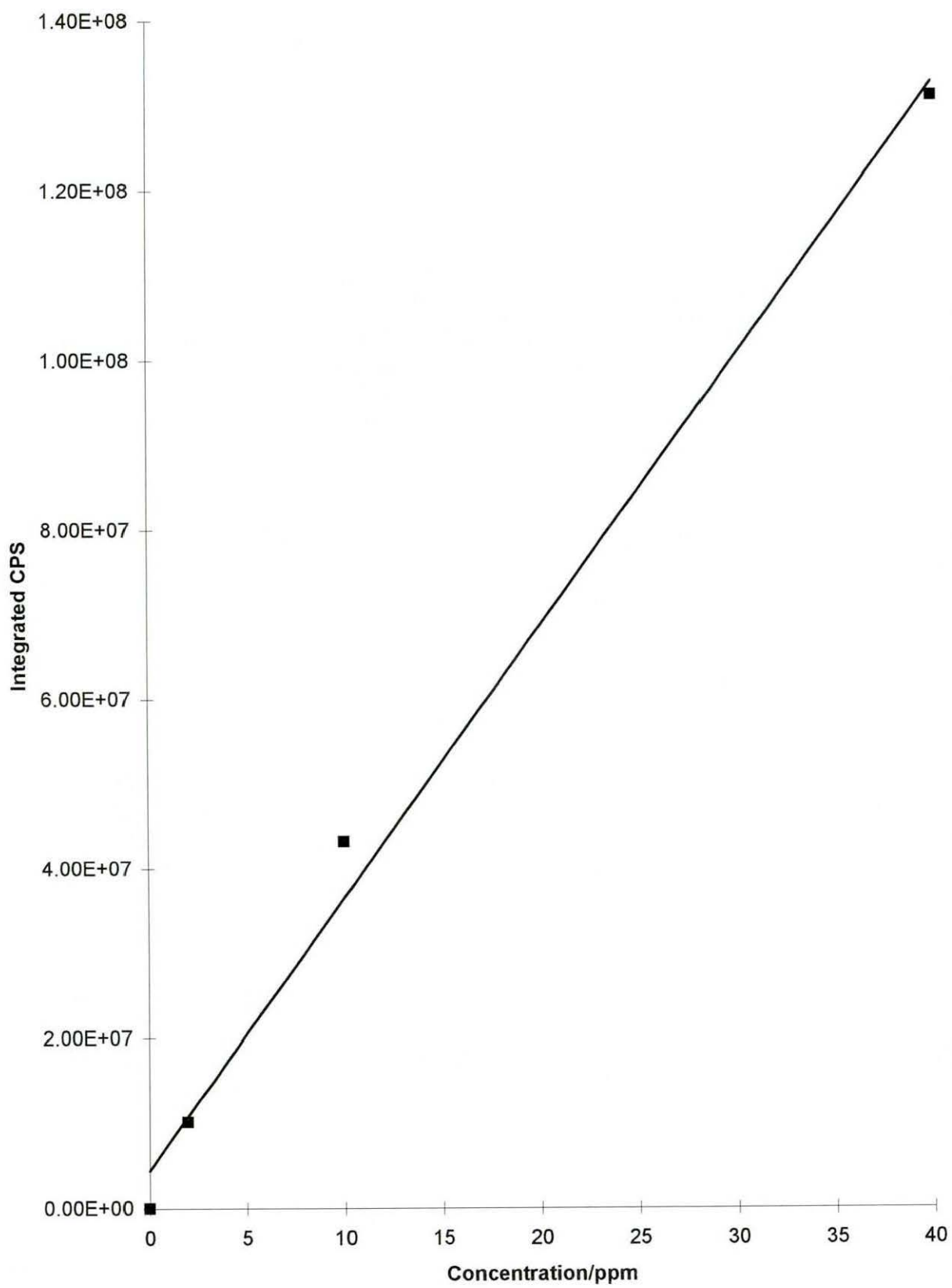


Fig.30

Fe (56) Calibration Curve

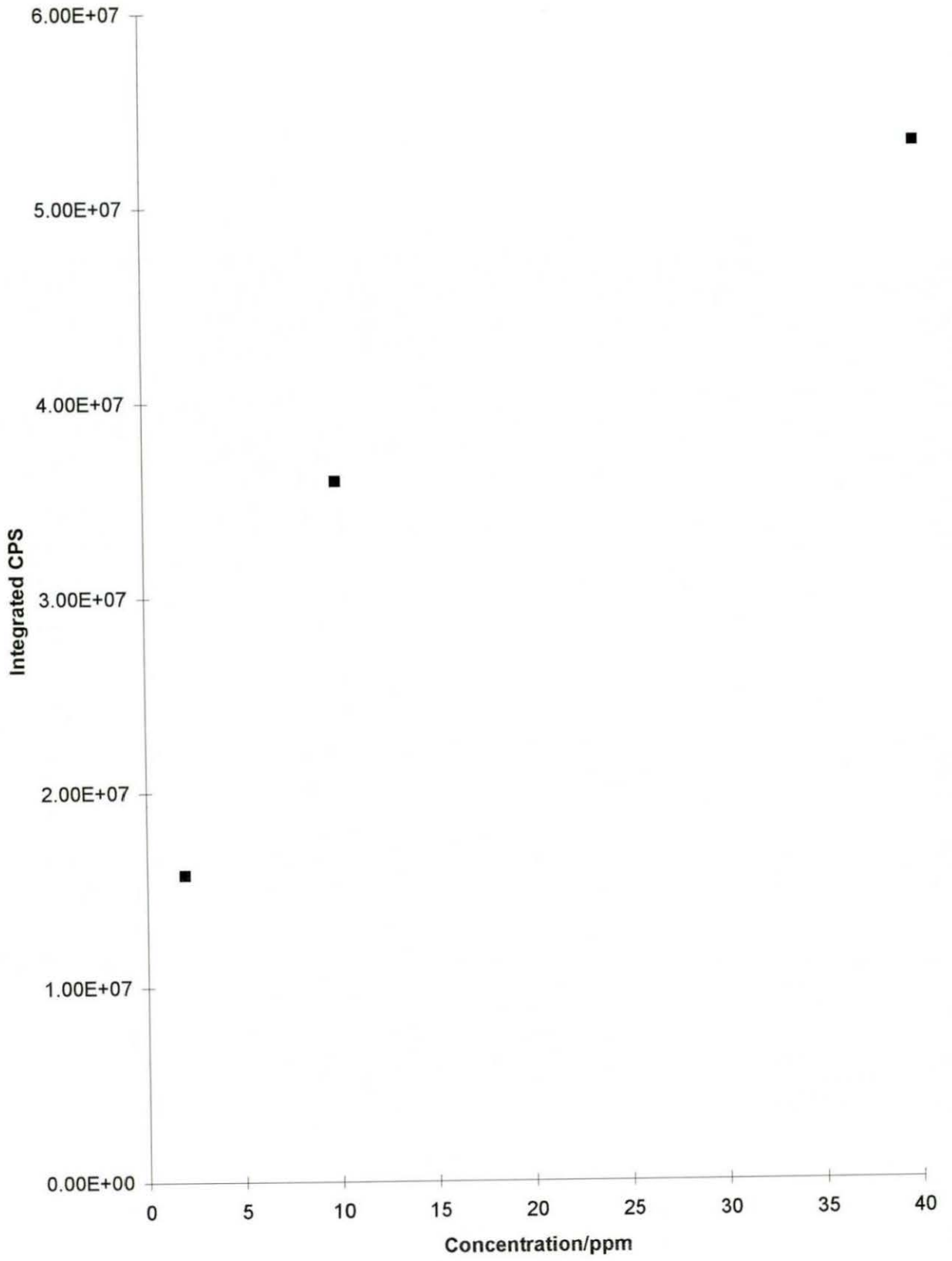
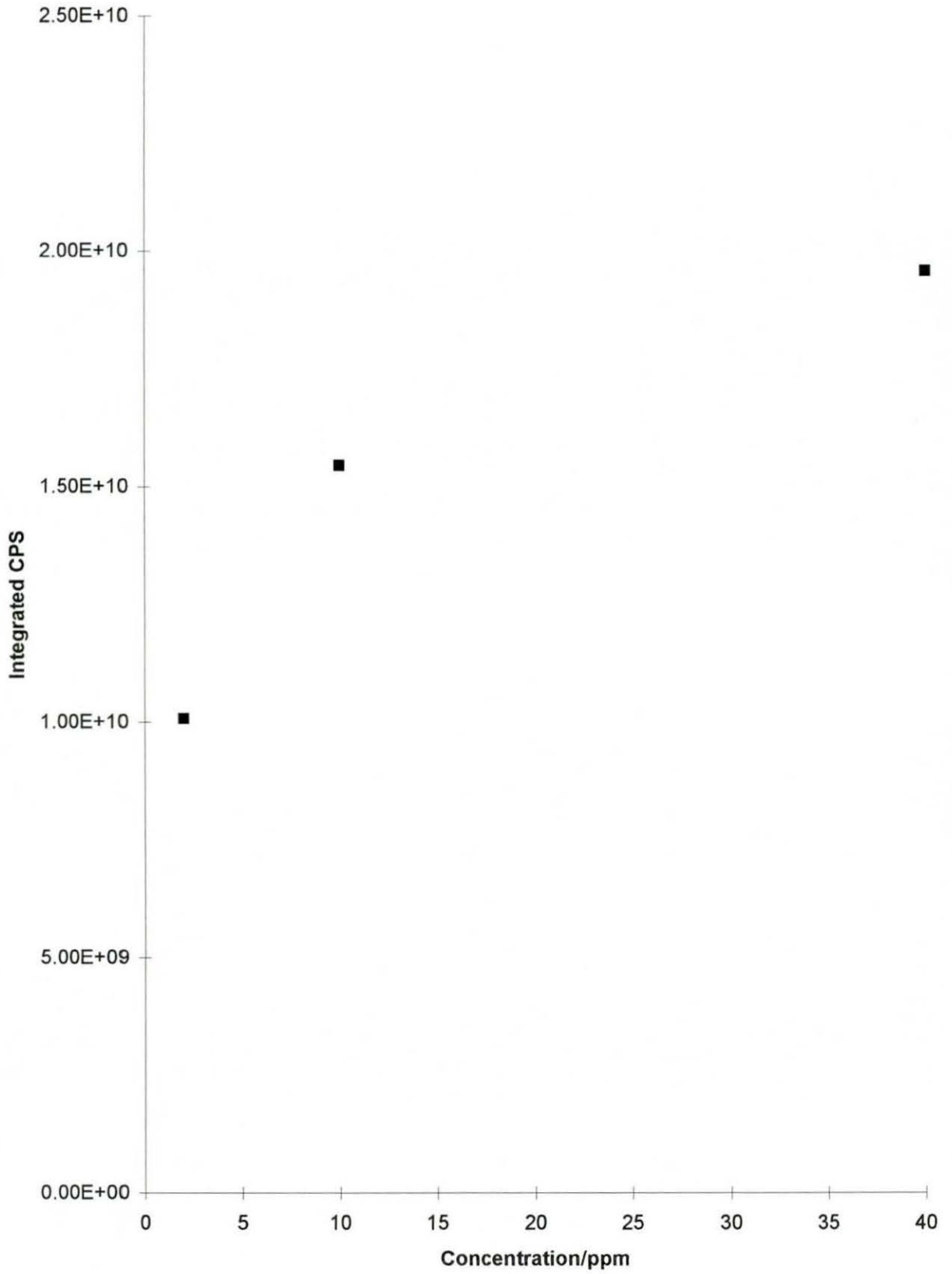


Fig.31

K (39) Calibration Curve



Samples were taken at 80  $\mu\text{m}$  intervals at the edge of the bone and at 500  $\mu\text{m}$  intervals towards the centre of the bone over a range of 18.5 mm. Figs 33 a,b,c show the concentration profiles for Mg, P, Ca, Na, Al, K, Fe, Zn, Sr and Pb across the bone sample (a,b,c are profiles for different elements at the same bone site).

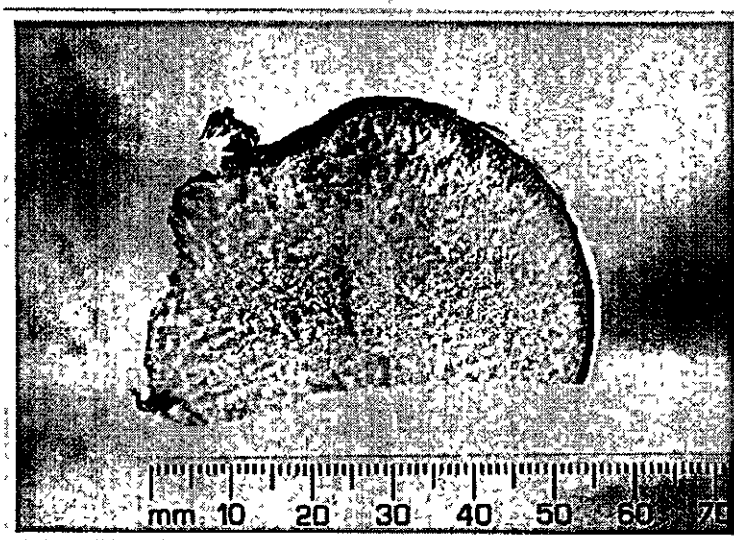
Analysis of the bone samples showed similar trends to those observed with the Loughborough system. Ca and P correlation was evident which is expected as the major inorganic component of bone is calcium phosphate. Na concentration also correlated with the Ca and P concentrations which was similarly observed on the Loughborough instrument.

The elemental concentrations showed good agreement with the Loughborough instrument, but did deviate from the expected bulk analysis results. These results were surface profiles which may account for the differences. It must also be noted that the internal standard concentration had to be assumed to be correct for the particular bone sample.

Using the smaller spots sizes and closer spacing intervals did allow a more detailed profile of the bone surface to be built up. It did appear that actual concentration gradients occur across the bone surface.

Of the minor components present, Al and Cu are interesting. The Cu concentration fell as the Al concentration steadily rose. There appeared to be a localised area of high Cu concentration, but this could have been surface contamination.

Fig. 32 Photograph of Typical Bone Sample



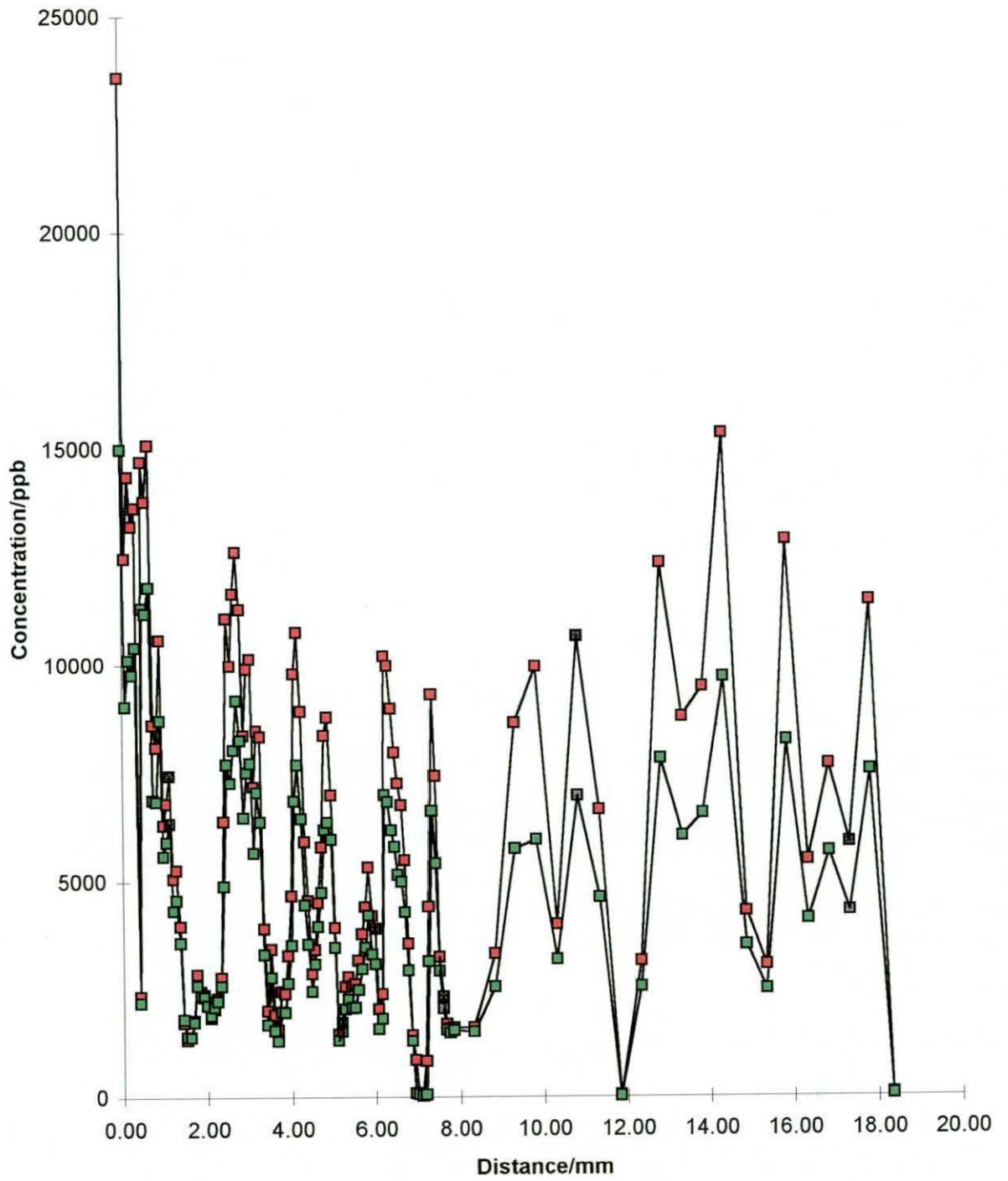
### 7.7.6 Analysis of Liver Samples

Liver samples were prepared and analysed by the same method described previously. A profile was produced with craters at 150  $\mu\text{m}$  intervals. The results are shown in Figs 34 a,b,c. Photographs of sampled craters on the liver surface can be seen in Figs 35a (500x) and 35b (1500x) magnification.

Poor calibration was achieved for analysis of the liver samples. Concentration units were therefore not given. This may have been caused by loss of focus or instrumental drift. Due to the limited period of time available on the instrument, the data was not interpreted until after the end of the experimental period. It was therefore not possible to repeat the calibration. The integrated count rates obtained for the liver samples are given to allow general trends to be identified. The significance of these results must therefore be

Fig.33a

### Ca and P Profile Of Bone 323/91



—■— Ca 45 —■— P 31



Fig.33b

Na K and Zn Profile Of Bone 323/91

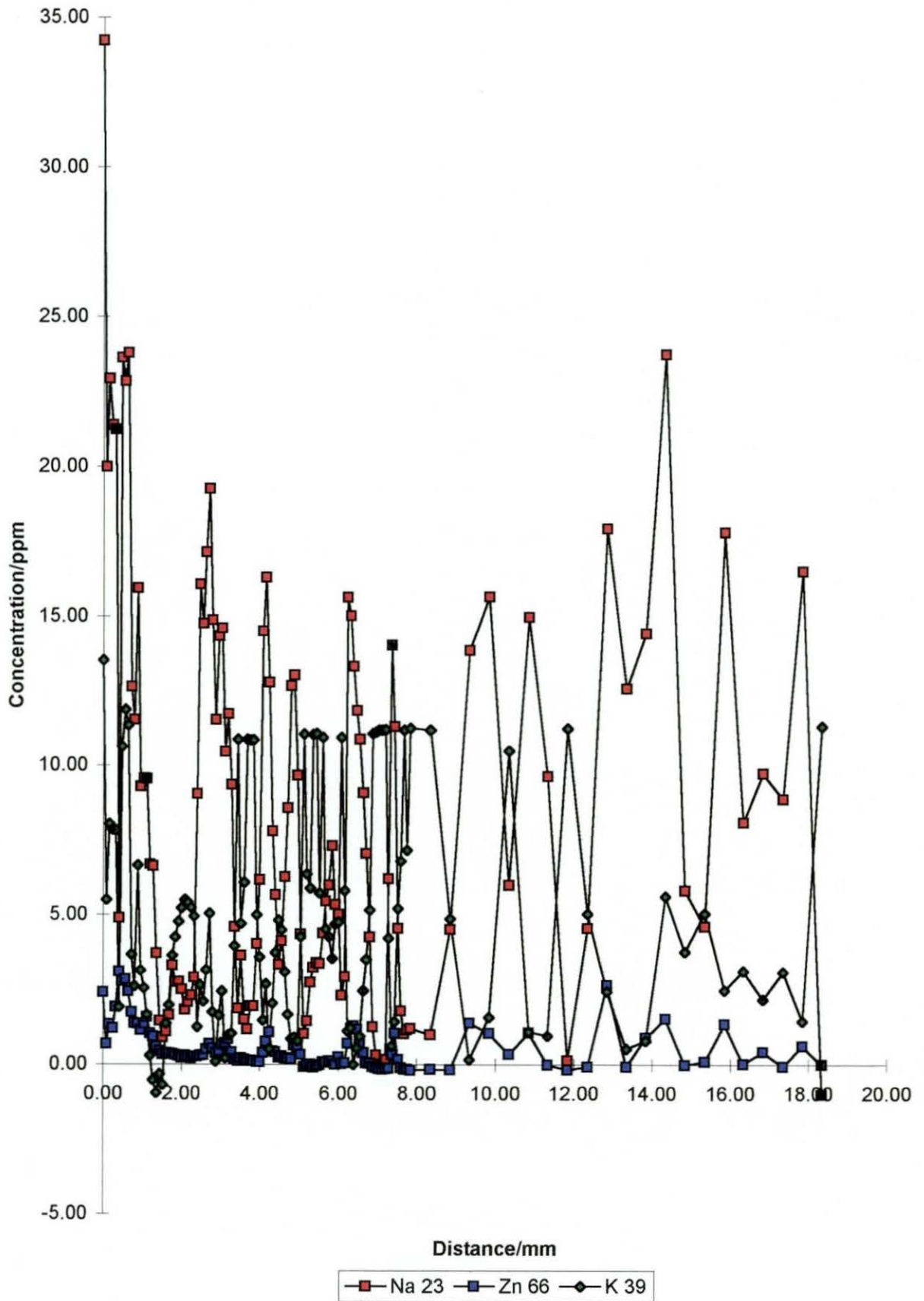
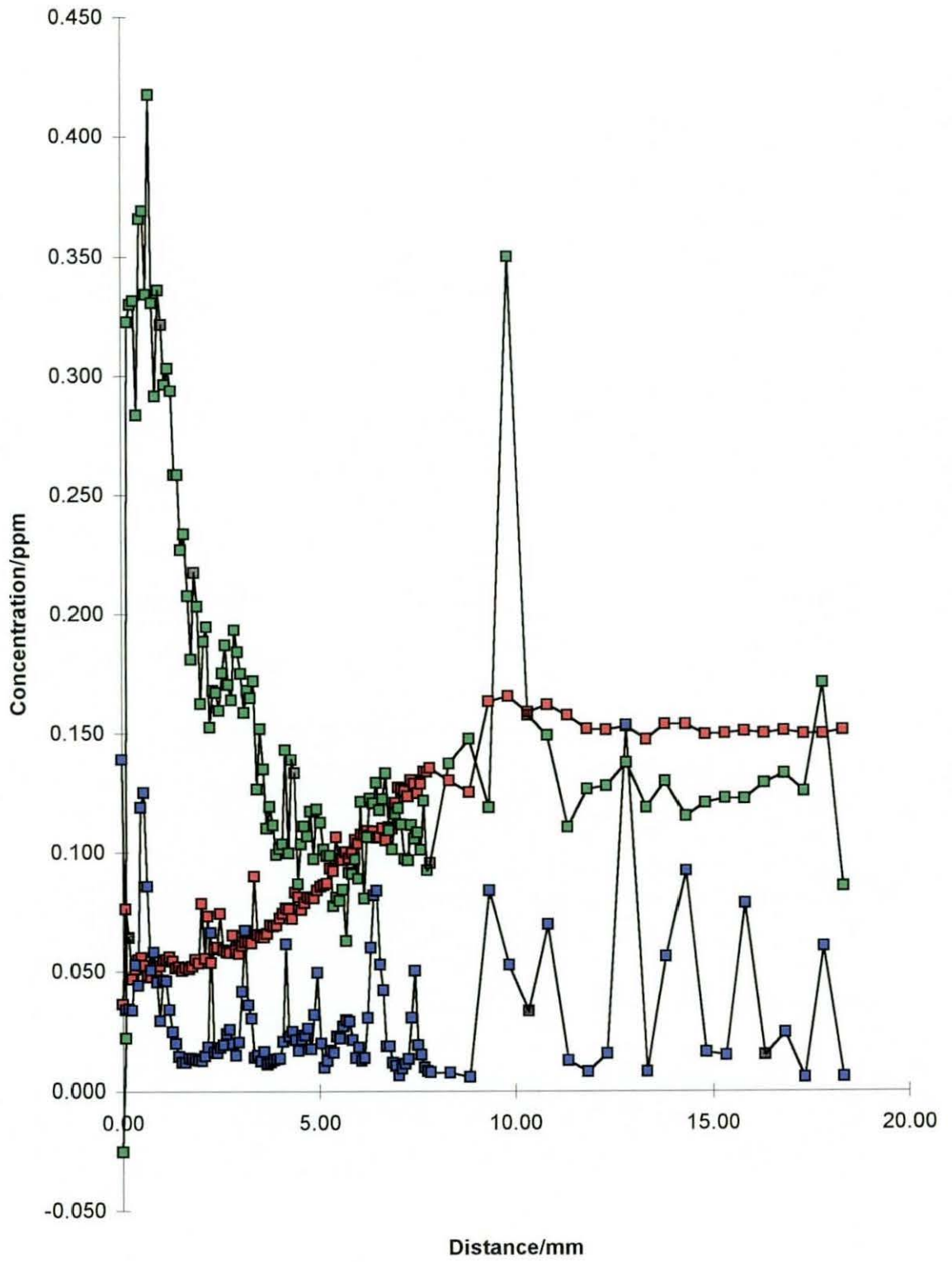


Fig.33c

### Al, Cu and Pb Profile Of Bone 323/91



—■— Al 27 —■— Cu 65 —■— Pb 208

Fig.34a

### Liver Profile

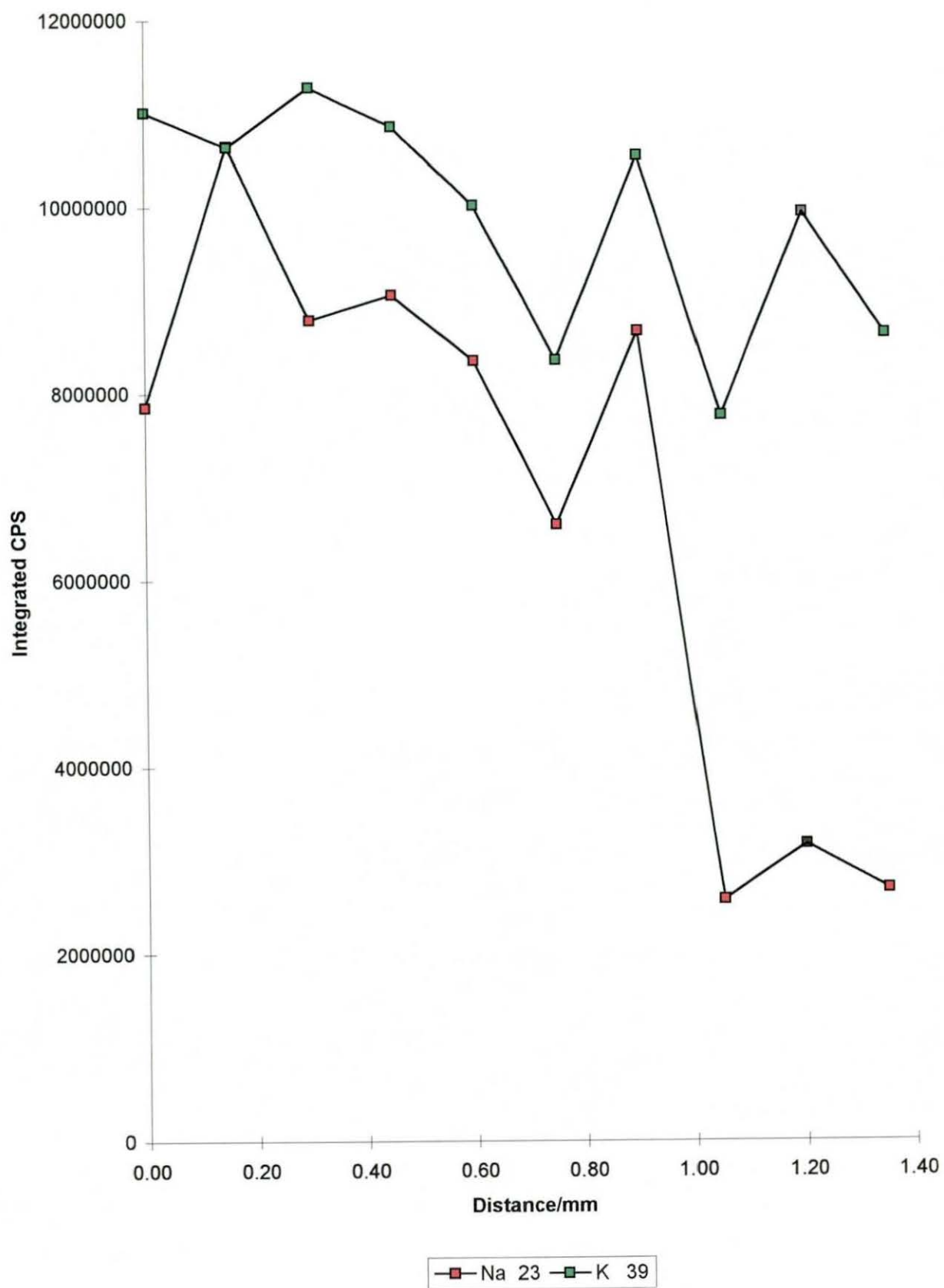


Fig.34b

### Liver Profile

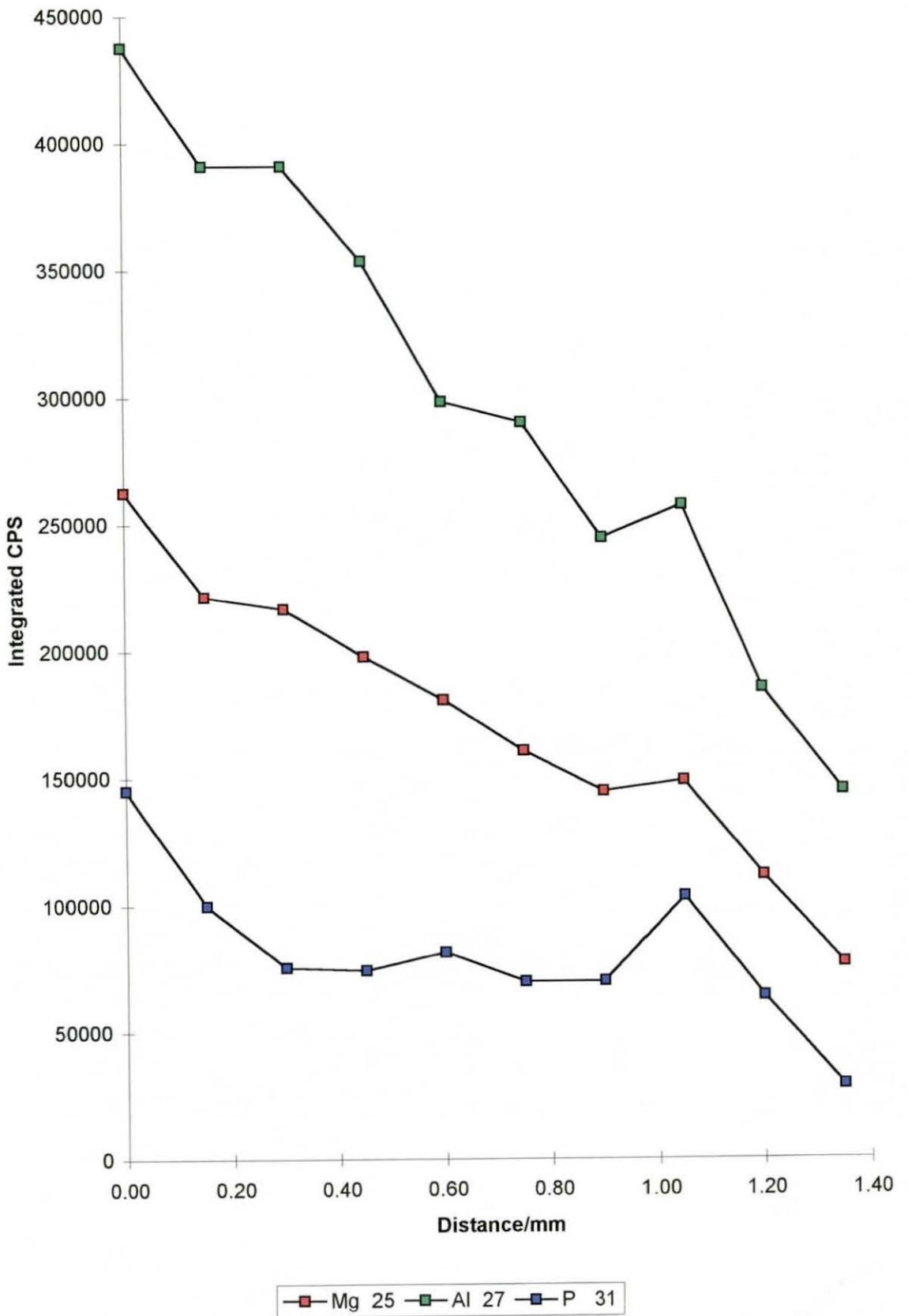
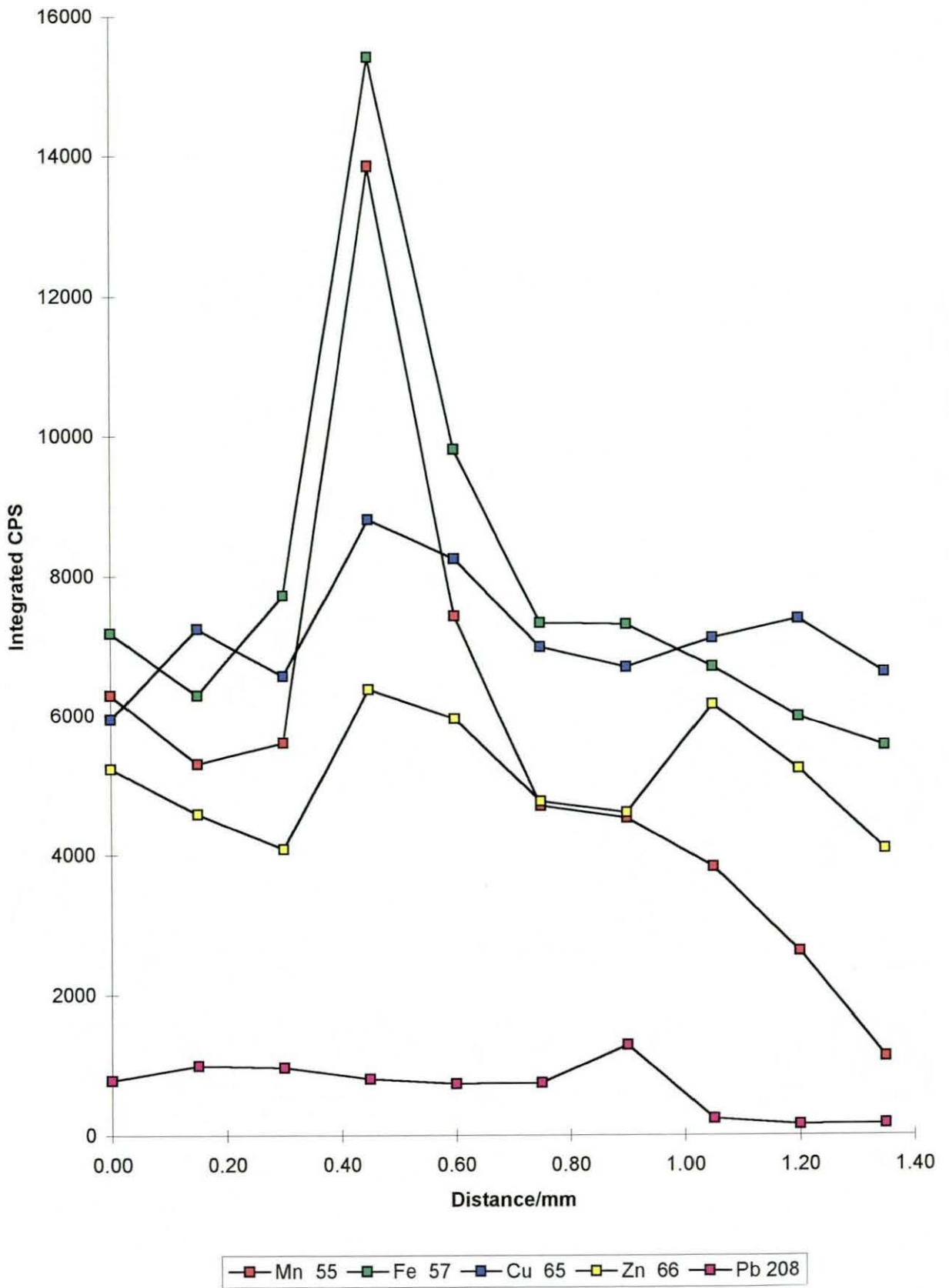


Fig.34c

### Liver Profile



questioned. Fe and Mn show correlation across the sample. Fe and Mn are chemically similar and may be co-stored within the liver. The liver showed high concentration levels of Na and K which is in agreement with the certified analysis of Bovine liver. The other minor components also showed similar trends to the certified values.

Fig. 35a Craters on the Surface of the Liver Samples (500x magnification)

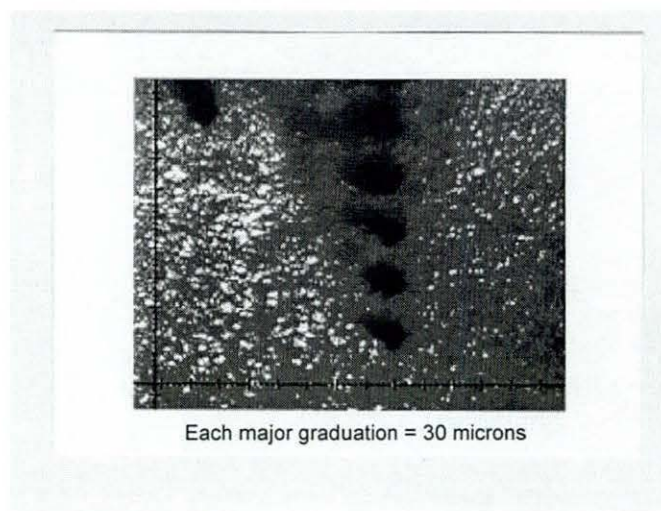
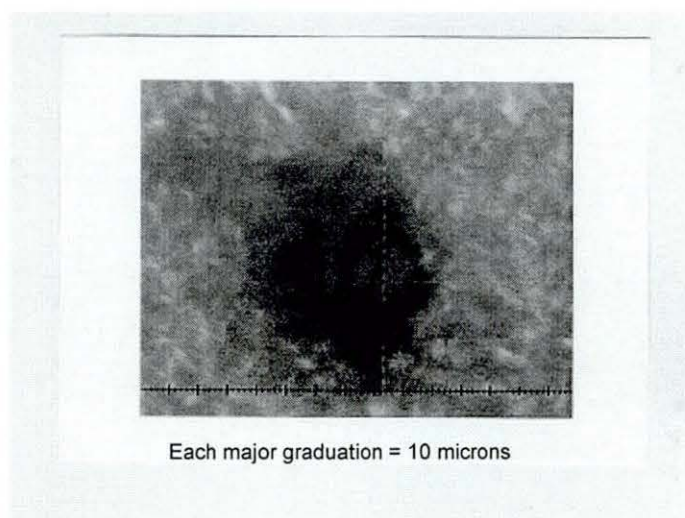


Fig. 35b Craters on the Surface of the Liver Samples (1500x magnification)



## **Chapter 8:**

# **Conclusions and Future Work**

### **8.1 Initial Studies**

From the initial fundamental studies it was evident that changing the laser energy and repetition rate varied the rate at which ablation took place. The precision of results was found to be affected by these parameters. At higher fluence the precision tended to be poorer, possibly caused by ejection of large droplets from the sample surface and evidence of the shockwave nebulisation effect described by Dyer<sup>92</sup>.

It is evident from the results presented, that it is possible to modify the absorption characteristics of an aqueous standard solution. The standards were simple and easy to prepare. Full elemental control of the make up of the standard was possible. Solution standards also offer the additional advantage of an infinitely renewable surface which is not seen for solid samples. The need for expensive certified materials is reduced, only being required for validation.

Poly(sodium 4-styrene-sulphonate) proved to be a suitable polymer for modification of the standard solutions. The stability of the polymer was good and did not appear to degrade when exposed to laser radiation at 248 nm over a fifteen minute period, this allowed adequate time for data collection. The apparent stability can be attributed to the reduction and broadening of the absorption maxima on exposure to UV radiation. Using this feature it was possible to produce aqueous standard solutions suitable for calibration.

Further work could involve investigations of other modifiers for the standard solutions. The main criteria for the modifier would be to be strongly absorbing at the laser wavelengths of interest and stable for long enough to allow data to be collected. Naphthalene sulphonic acid was investigated as an alternative modifier, but was not found to dissolve to the extent required for matching with the NIST standard.

## 8.2 Validation

Experiments carried out to match the absorption coefficient of an aqueous standard to that of NIST glass have shown that accuracy close to the certified value can be obtained. It must be noted, however, that an internal standard is required whose concentration is established in both materials to determine a conversion factor for use with all further calculations. This is necessary as the standard and sample do not give the same count rate for the same concentration of element present. It was hoped that the same count rates would be achieved, the fact that they were not could be attributed to various reasons. The first is that the sample is a solid whilst the standard is a solution, therefore the coupling and interaction of the laser with the surface could be different. The mechanism of ablation could vary between the solid and the solution. It has been postulated by Dyer<sup>92</sup> that for a solution, a shock wave is transmitted through the sample which additionally contributes to the ablation process. The formation of a plasma above the surface of the sample, attenuating the incoming laser radiation, may also vary between solid and solution.

From the TRA results shown in Fig.22, the NIST glass and the matched polymer solution do give a similar count rate at the start of the analysis. The count rate for the NIST glass falls rapidly after this period. This was thought to be due to loss of focus as the laser channelled deeper into the solid sample. The solution, however, presents what could be described as a constantly renewable surface and therefore focus will not be lost. Use of an



active focus system, particularly for solid samples may remove the need for an internal standard.

One possible advantage of the higher count rates achieved from the ablation of solutions is that it was possible to produce accurate calibration curves at lower concentrations than had been achieved previously. Detection limits of a few  $\mu\text{g l}^{-1}$  were achievable with a polymer additive concentration of a  $9.2 \text{ g dm}^{-3}$ . It would be possible to improve these limits by optimising the stability of the system, improvement of the blank level and producing a standard with a higher concentration of polymer additive. The blank level was higher when sampling the polymer additive, but gives a better estimate of the true blank.

It was possible to produce calibration curves for some of the traditionally more difficult elements such as Fe and K. This is thought to be due to the fact that dry plasma conditions were used, reducing the potential for the formation of interfering polyatomic species. It would be very interesting to repeat this work on either a high resolution ICP-MS or a quadrupole ICP-MS with a shielded torch and cool plasma to allow analysis of Na, Ca, K and Fe. This would give better detection limits and correlation coefficients for these traditionally difficult elements. This would also allow small concentration gradients to be more accurately monitored.

### **8.3 Analysis of Biological Samples**

Despite the differing signal intensities for solids and solutions, it has been shown that modified solution standards as calibrants can be used to produce mapped profiles of trace element concentrations across biological materials. The significance of the results obtained for the bone and liver samples requires further investigation and may become clear with time. The important point to note is that calibration has been shown to be successful and holds potential for profiling work in the future.

### **8.4 Future Work**

It would be of benefit to obtain bone samples from patients who were not osteoarthritic. This would allow elemental profiles to be compared, highlighting any differences which may allow conclusions to be drawn as to elements that contribute to the onset of osteoporosis.

The experiments carried out on the Loughborough instrument show the need for an improved optical system. This would allow production of smaller spot sizes giving smaller well defined craters. An optical system to allow the sample to be viewed would also be of benefit. This would help to establish which part of the sample is being ablated for future reference and cross correlation with other results obtained.

A computer controlled motorised translation stage would also be of benefit. Accurate repositioning of the sample could then be achieved. It would also be possible to accurately ablate more sample sites per cm allowing a more detailed profile map to be built up.

The system would also benefit from the design and construction of an ablation stage that could accommodate laser cells of varying sizes. Some of the bone samples were too large to fit in the current laser cell. A laser cell that would hold bone samples up to 100 mm in diameter would be useful. A laser cell capable of holding multiple standards and samples would also be of benefit, reducing the need to remove the cell and minimising disturbance of the plasma.

All of the experiments were carried out with laser radiation at 248 and 266 nm. It has now been widely accepted that UV radiation is more suited to this type of work than infrared radiation. The benefits are: better coupling, an aerosol largely comprised of vapour phase and micro-particulate particles which are more compatible with the ICP source, improved crater definition and less peripheral damage caused by a larger contribution from thermal ablation.

The Loughborough laser system has the capability of changing from the KrF transition at 248 nm to the ArF transition at 193 nm. The energy outputs achievable and the stability of the transition at 193 nm are not as good as at 248 nm. It would still, however, be interesting to compare results obtained in the far UV to those obtained at 248 nm. To carry out this investigation would require an enclosed system to be built with a constant purge of nitrogen. This would be necessary as at 193 nm the laser photons have such a high energy that a plasma could be formed in the air. This would attenuate the beam in a similar fashion to the plasma formed above the sample surface during ablation.

At 193 nm, one would expect that ablation would be almost entirely photochemical in nature with a minimal contribution from the thermal mechanism. This, with improved coupling, would produce well defined reproducible craters and a uniform aerosol that would be ideal for processing by an ICP source.

Results obtained for laser transitions at 266 and 248 nm showed that there appeared to be better coupling at 248 nm for the standards and the solutions. A larger count rate was obtained for the same elemental concentration at 248 nm and it was also noted that the ablation threshold was lower at 248 nm. Ablation threshold is given as the power density at which ablation begins. These differences may be more pronounced at 193nm.

## References

1. Reed, T., *J. Appl. Phys.*, 1961, **32**, 821.
2. Reed, T., *J. Appl. Phys.*, 1963, **34**, 2266.
3. Greenfield, S., Jones, I. and Berry, C., *Analyst*, 1964, **89**, 713.
4. Wendt, R. and Fassel, V., *Anal. Chem.*, 1965, **37**, 920.
5. Handbook of Inductively Coupled Plasma Spectrometry, Thompson, M. and Walsh, J.N., *Blackie*, Glasgow, 1983.
6. Houk, R.S., *Anal. Chem.*, 1985, **58**, 97.
7. Winge, R.K., Eckebe, D.E., Dekalb, E.L. and Fassel, V.A., *J. Anal. Atom. Spectrom*, 1988, **3**, 849.
8. Applications of Inductively Coupled Plasma Mass Spectrometry, Date, A.R. and Gray, A.L., *Blackie*, 1989.
9. Handbook of ICP-MS, Jarvis, K.E., Gray, A.L. and Houk, R.S., *Blackie*, 1992.
10. Jeffery, G.H., Bassett, J., Mendham, J. and Denney, R.C., Quantitative Chemical Analysis, Vogel 5<sup>th</sup> edition, 1989.
11. Baumann, H., *Fresenius J. Anal. Chem.*, 1992, **342**, 907.
12. Darke, S. and Tyson, J., *J. Microchem.*, 1994, **50**, 310.
13. Nixon, D., Fassel, V.A. and Knisley, R.N., *Anal. Chem.*, 1974, **46**, 210.
14. Park, C.J., Van Loon, J.C., Arrowsmith, P. and French, J.B., *Anal. Chem.*, 1987, **59**, 2191.
15. Date, A.R. and Cheung, Y.Y., *Analyst*, 1987, **112**, 1531.
16. Gunn, A.M., Millard, D.L. and Kirkbright, G.F., *Analyst*, 1978, **103**, 1066.
17. Park, C.J. and Hall G.E.M., *J. Anal. Atom. Spectrom*, 1987, **2**, 473.
18. Park, C.J. and Hall G.E.M., *J. Anal. Atom. Spectrom*, 1988, **3**, 355.
19. Park, C.J., PhD Thesis, University of Toronto.
20. Salin, E.D. and Horlick, G., *Anal. Chem.*, 1979, **51**, 2284.
21. Salin, E.D. and Horlick, G., *Anal. Chem.*, 1984, **56**, 2596.
22. Jiang, S.J. and Houk, R.S., *Anal. Chem.*, 1986, **58**, 1739.

23. Williams, J.G., Gray, A.L., Norman, P. and Ebdon, L., *J Anal Atom Spectrom* , 1987, 2, 469.
24. Gray, A. L., *Analyst*, 1985, 110, 551.
25. Arrowsmith, P., *Anal. Chem.*, 1987, 59, 1437.
26. Dinger, R., Rohr, K., and Weber, H., *J. Phys. D*, 1980, 13, 2301.
27. Darke, S.A., Long, S.E., Pickford, C.J. and Tyson, J.F., *J. Anal. At Spectrom.*, 1989, 4, 715.
28. Richner, P., Borer, M.W., Brushwyler, K.R. and Hieftje G.M., *Appl. Spectrosc*, 1990, 44, 1290.
29. Iida, Y., Tsuege, A., Uwamino, Y., Morikawa, H. and Ishizuka, T., *J. Anal. At Spectrom.*, 1981, 6, 541.
30. Marshall, J., Franks, J., Abell, I. and Tye, C., *J. Anal. At. Spectrom.*, 1991, 6, 145.
31. Perkins, W. T., Fuge, R. and Pearce, N.J.G., *J. Anal. At. Spectrom* , 1991, 6, 445.
32. Perkins, W. T., Fuge, R. and Pearce, N.J.G., *J Anal. At. Spectrom* , 1991, 7, 595.
33. Moenke-Blankenburg, L., *Laser Micro-Analysis*, Wiley, New York, 1989.
34. Hwang, Z.W., Teng, Y.Y., Li, K.P. and Sneddon, J., *Appl Spectrosc*, 1991, 45, 435.
35. Denoyer, E. R., Fredeen, K.J. and Hager, J.W., *Anal. Chem.*, 1991, 63, 445A.
36. Darke, S.A. and Tyson, J.F., *J. Anal. At. Spectrom.*, 1993, 8, 145.
37. Thiem, T. L., Lee, Y. and Sneddon, J. *Trends Anal. Chem* , 1993, 12, 18.
38. Lee, Y. I., Sawan, S. P., Thiem, T. L., Teng, Y. Y. and Sneddon J., *J. Appl. Spectrosc* , 1992, 46, 436.
39. Huang, T., Shibata, Y. and Morita, M., *Anal. Chem.*, 1993, 65, 2999.
40. Russo, R.E., Fernandez, A.J., Mao, X.L. and Shannon, M.A., Paper presented at the Federation Analytical Chemistry and Spectroscopy Society meeting, Cincinnati, July 1994.

41. Russo, R.E., Fernandez, A.J., Mao, X.L. and Shannon, M.A., Poster presented at the Federation Analytical Chemistry and Spectroscopy Society meeting, Cincinnati, July 1994.
42. Koppelaar, D.W., Alexander, M.L., Barinaga, C.J., Smith, M.R. and Mendoza, A., Paper presented at the Federation Analytical Chemistry and Spectroscopy Society meeting, Cincinnati, July 1994.
43. Srinivasan, R. and Mayne-Banton, V., *Appl. Phys. Lett.*, 1982, **41**, 576.
44. Garrison, B. J. and Srinivasan, R., *J. Appl. Phys*, 1985, **57**, 2909.
45. Sutcliffe, E. and Srinivasan, R., *J. Appl. Phys*, 1986, **60**, 3315.
46. Simon, P., *Appl. Phys.*, 1989, **48B**, 253.
47. Kuper, S. and Stuke, M., *Appl. Phys.*, 1987, **44B**, 199.
48. Geersten C., Briand, A., Chartier, Lacour, J.L., Mauchien, P., Sjostrom, S. and Mermet, J M, *J. Anal. At. Spectrom.*, 1994, **9**, 17.
49. Dyer, P.E., Jenkins S.D. and Sidhu, J., *Appl. Phys. Lett*, 1988, **52**, 1880.
50. Phillip, H.R., Cole, H.S., Liu, Y.S. and Sitnik, T.A., *Appl. Phys. Lett.*, 1986, **48**, 192.
51. Brannon, J.H., Lankard, J.R., *Appl Phys Lett.*, 1986, **48**, 1226.
52. Kawamura, T., Toyoda, K. and Namba, S., *Appl Phys. Lett*, 1984, **40**, 374.
53. Srinivasan, R. and Braren, B., *Appl. Phys. A*, 1988, **45**, 289.
54. Prabhu, R. K., Vijayalakshmi, S., Mahalingham, T. R., Viswanathan, K. S. and Matthews, C.K., *J. Anal. At. Spectrom.*, 1993, **8**, 565.
55. Pang, H., Wiederin, D.R., Houk, R.S. and Yeung, E.S., *Anal. Chem.*, 1991, **63**, 390
56. Richner, P., Borer, M.W., Brushwiler, K.R., Hieftje, G.M., *Appl. Spectrosc.*, 1990, **44**, 1290.
57. Thompson, M., Goulter, J.E. and Sieper, F., *Analyst*, 1981, **106**, 32.
58. Hager, J.W., *Anal. Chem.*, 1989, **61**, 1243.
59. Thompson, M., Chenery, S. and Brett, L., *J. Anal. At. Spectrom.*, 1989, **4**, 11.
60. Van Heuzen, A. A., *Spectrochim Acta*, 1991, **46B**, 1803.

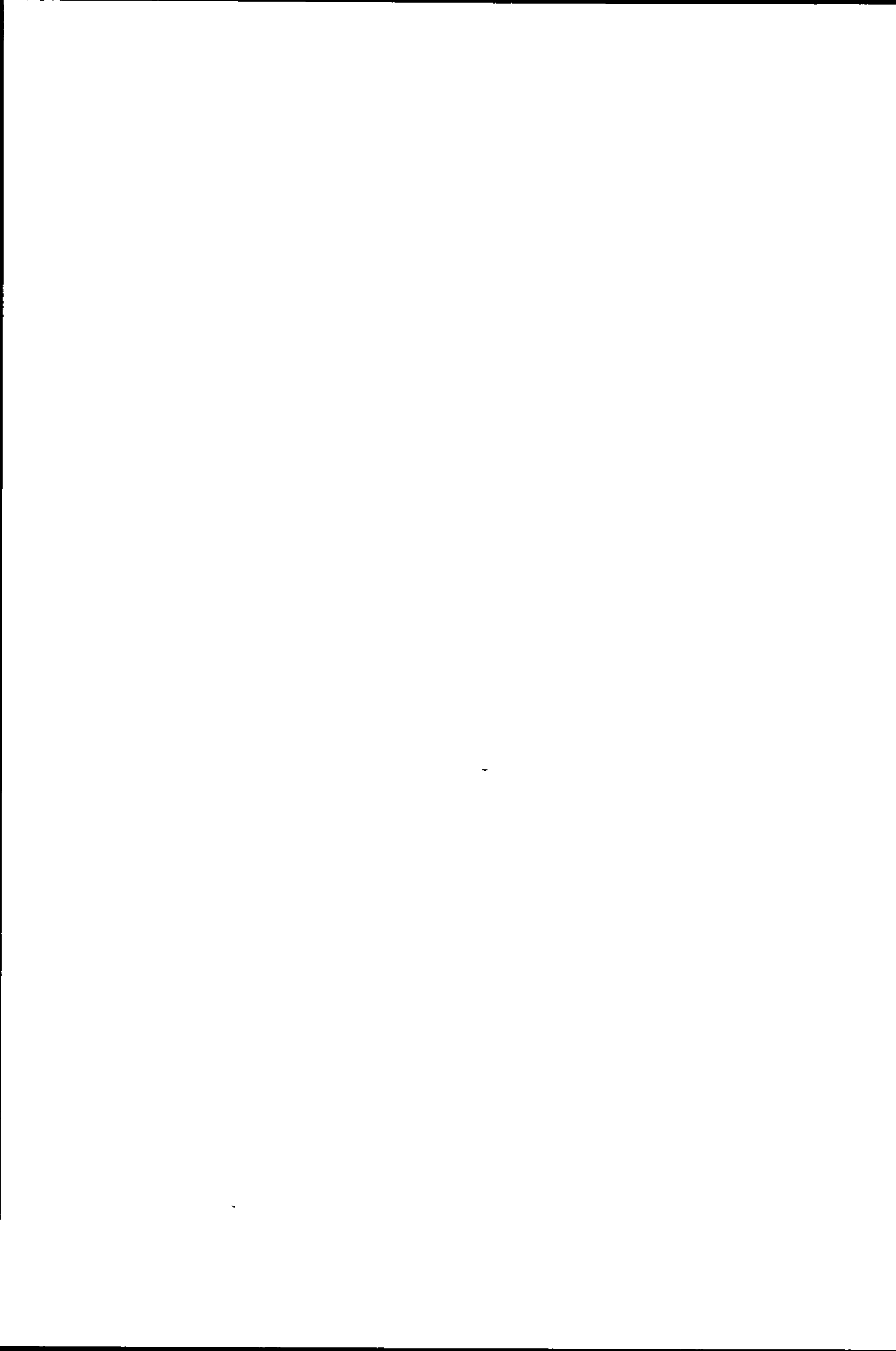
61. Van Heuzen, A. A., *Spectrochim. Acta*, 1991, **46B**, 1819.
62. Wiejer, P., Baeten, W. L. M., Bekkers, M. H. J. and Vullings, P. J. M. G.,  
*J. Anal. At. Spectrom.*, 1992, **7**, 599.
63. Williams, J.G. and Jarvis, K.E., *J. Anal. At. Spectrom* , 1993, **8**, 25.
64. Chenery, S. and Cook, J.M., *J. Anal. At. Spectrom.*, 1993, **8**, 299.
65. Moenke-Blankenburg, L., Schumann, T. and Nolte, J., *J Anal At. Spectrom* ,  
1994, **9**, 1059.
66. Russo, R.E., Mao, X.L., Chan, W. T., Bryant, M. F. and Kinard, W.F., *J. Anal.  
At. Spectrom.*, 1995, **10**, 295.
67. Fordham, P.J., Gramshaw, J.W., Castle, L., Crews, H.M., Thompson, D., Parry,  
S.J. and McCurdy, E. *J. Anal. At. Spectrom.*, 1995, **10**, 303.
68. Stix, J., Gauthier, G. and Ludden, J.N., *Can. Mineral*, 1995, **33**, 435.
69. Moissette, A., Shepherd, T.J. and Chenery, S.R , *J. Anal. At. Spectrom.*, 1996,  
**11**, 177
70. Pearce et al, Goldschmidt, V.M., *Conference Abstracts*, 1995, May 24-26.
71. Hamilton, D.L. and Hopkins, T.C., *Analyst*, 1995, **120**, 1373.
72. Durrant, S.F., *Analyst*, 1992, **117**, 1585.
73. Ward, N.I., Durrant, S.F. and Gray, A.L., *J. Anal At. Spectrom* , 1992, **7**, 1139.
74. Denoyer, E.R., *J. Anal. At. Spectrom.*, 1992, **7**, 1187.
75. Fuge, R., Palmer, T.J., Pearce, N.J.G. and Perkins, W.T., *Applied Geochem.*,  
1993, **2**, 111.
76. Chenery, S., Hunt, A. and Thompson, M., *J Anal. At. Spectrom.*, 1992, **7**, 647.
77. Ulens, K., Moens, Luc, Dams, R., Winckel, S.V. and Vandevolve, L., *J. Anal.  
At Spectrom.*, 1994, **9**, 187.
78. Watling R.J., Herbet, H.K., Delev, D. and Abell, I.D., *Spectrochim Acta*, 1994,  
**49B**, 205.
79. Evans, R.D., Outridge, P.M. and Richner, P., *J. Anal. At. Spectrom* , 1994, **9**,  
985.
80. Wagemann, R., *Can. Bull. Fish. Aquat. Sci.*, 1990, **224**, 191.



81. Evans, R.D. and Outridge, P.M., *J. Anal. At. Spectrom.*, 1995, **10**, 595.
82. Raith, A., Jeffries, T., Perkins, W.T. and Pearce, N.J.G., *Geoscientist*, 1995, **5**, 6.
83. Wang, S., Brown, R. and Gray, A L., *Applied Spectroscopy*, 1994, **48**, 1321.
84. Guo, X. and Lichte, F.E., *Analyst*, 1995, **120**, 2707.
85. Jeffries, T.E., Perkins, W.T. and Pearce, N.J.G., *Analyst*, 1995, **120**, 1365.
86. Albagli, D., Dark, M., Perelman, L.T., Rosenberg, C., Itzkan, I. and Feld, M.S., *Optics Letters*, 1994, **19**, 1684.
87. Gunn, J.S., Harrowfield, I.R. and Thresher, R.E., *J. Exp. Mar. Biol. Ecol.*, 1992, **158**, 1.
88. Abou-Shakra, F.R., Ward, N.I. and Everard, D.M., *Fertil. Steril*, 1989, **52**, 307.
89. Gunther, D., Jackson, S.E., Forsythe, L. and Longerich, H.P., Poster presented at 1995 FACSS meeting Cincinnati.
90. Raith, A., V.G. Elemental, Ion Path, Road Three, Winsford, Cheshire CW7 3BX.
91. Cousin, H., Weber, A., Magyar, B., Abell, I. and Gunther, D., *Spectrochim. Acta*, 1995, **50B**, 63.
92. Dyer, P., Private Communication 20<sup>th</sup> June 1995 Department of Applied Physics, University of Hull,
93. Riggs, B.L., and Melton, L.J. III. 1986. Involutional osteoporosis. *N. Engl. J. Med.*, 314:1676-1686.
94. Preventing and Reversing Osteoporosis. 1994, Alan R. Gaby, Prima Publishing.
95. Strouse, L. and Saltman, P. 1985, Biochemical changes in rat skeleton following long term dietary manganese and copper deficiencies. *Fed. Proc.*, 44-752.
96. Leach, R.M., Muenster A-M and Wein, E.M. 1969. Studies on the role of manganese in bone formation, 133:22-28
97. Cohen, L. and Kitzes, R. 1981, Infrared spectroscopy and magnesium content of bone mineral in osteoporitic women. *Isr. J. Med. Sci.*, 17:1123-1125.

98. Calhoun, N.R., Smith, J.C. and Becker, K.L. 1975, The effects of zinc on ectopic bone formation. *Oral. Surg.*, 39:698-706.
99. Yamaguchi, M. and Sakashita, T. 1986, Enhancement of vitamin D3 effect on bone metabolism in weanling rats orally administered zinc sulphate. *Acta Endocrinol*, 111:285-288.
100. Atik, O.S. 1983. Zinc and senile osteoporosis. *J. Am. Geriatr. Soc.*, 31:790-791.
101. Marie, P.J. and Hott, M. 1986. Short term effects of flouride and strontium on bone formation and resorption in the mouse. *Metabolism*, 35:547-551.
102. Kaehny, W. 1985. Newer understanding of aluminium metabolism, *IM* 6(6):131-140.
103. Anonymous. 1982. Food, pots, processing agents and antacids - all are sources. *Med. Tribune*, 28 April, 12.
104. Mongelli, N.S. 1972. Radiologic observations on the skeletal apparatus of young persons affected by chronic lead poisoning. Washington D.C.: US Environmental Protection Agency Abstract, 1355 (May): 260.
105. Roberts, N.R., Walsh, H.P.J., Klemmerman, L., Kelly, S.A. and Helliwell, T.R. *J. Anal. At. Spectrom.* 1997, in press.
106. Weijer, P., Baeten, W.L.M., Bekkers, M.H.J. and Vullings, P.J.M.G., *J. Anal. At. Spectrom.* 1991, 6, 609.
107. Perkins, W. T., Fuge, R., Pearce, N.J.G., Abell I.D. and Duller G.A.T., *J. Anal. At. Spectrom.*, 1992, 7, 53.
108. Perkins, W. T., Fuge, R. and Pearce, N.J.G., *J. Anal. At. Spectrom* , 1992, 7, 611.
109. Westgate, J.A., Perkins, W.T., Fuge, R., Pearce, N.J.G. and Wintle, A.G., *Appl. Geochemistry*, 1994, 9, 323.
110. Chenery, S., Cook, J., Styles, M. and Cameron, E. M., *Chem. Geol.*, 1995, 124, 55.
111. Jarvis, K.E. and Williams, J.G., *Chem. Geol.*, 1993, 106, 251
112. Hirata, F. and Nesbitt, R.W., *Geochim. Cosmochim. Acta*, 1995, 59, 2491.

113. Guo, X. and Lichete, F.E., *Analyst*, 1995, **120**, 2707.
114. *The Liver and its Diseases*. Schaffner, Sherlock and Leevy. Intercontinental Medical Book Corporation. 1974.
115. Roberts, N., Royal Liverpool University Hospital, Liverpool, L7 8XP, various communications throughout 1994-1995.



differing polymer additive concentrations from 0 to 40 g dm<sup>-3</sup> were prepared. Each solution contained 50 ppm of Mg, Cu, Zn, In, Ce and Pb. Fig 26 shows the effect of varying the polymer additive concentration on the observed count rate. Comparison of the results presented in Fig. 20 identifies the fact that there was less coupling between the laser and the standards at 266nm than at 248 nm, i.e. the count rates are lower at 266 nm for the same elemental concentration and polymer additive concentration. This was in agreement with the initial results shown in Fig. 14 which indicated that the polymer solution was less absorbing at 266 nm than at 248 nm.

It is apparent from Fig.26 that the addition of the polymer to a standard solution caused a similar effect at 266 nm with a Nd:YAG laser as at 248 nm with an excimer laser. Although it was difficult to compare the two sets of results accurately as laser energy, spot size, laser frequency, wavelength and concentration were all different. It is evident that in both cases an increase in polymer concentration caused an exponential increase in the observed count rate of a particular element. It can also be concluded that the polymer additive was still effective at modifying the absorption coefficient of the standard solution at 266 nm, but to a lesser degree than at 248 nm.

### **7.7.3 Detection Limits**

Determination of the detection limits for various elements was carried out as a comparison with those achieved on the Loughborough LA-ICP-MS system. Factors such as laser coupling, energy, spot size, instrument sensitivity and background level all have an effect on the detection limit. A 40 ppm standard solution with 30 g dm<sup>-3</sup> of polymer was used for this study. A higher polymer concentration was used to give a higher count rate and compensate for the lower absorbance at 266 nm. Five replicate data sets were acquired. The detection limit was calculated as the concentration of analyte giving a

signal equal to three times the standard deviation of the blank. The blank was acquired with the laser off, but the argon sweep gas through the laser cell on. These results are therefore acquired under similar conditions to the 'best estimate' described in section 6.13. Table 19 shows the detection limits achieved for a selection of elements.

Table 19: Detection Limits Achieved for Aqueous Standards Containing  $30 \text{ g dm}^{-3}$  of Polymer

Isotope	Detection Limit $\text{ng ml}^{-1}$	Isotope	Detection Limit $\text{ng ml}^{-1}$
Na <sup>23</sup>	3770	Mn <sup>55</sup>	25
Mg <sup>24</sup>	541	Fe <sup>56</sup>	2280
Al <sup>27</sup>	39	Cu <sup>65</sup>	144
P <sup>31</sup>	5568	Zn <sup>66</sup>	146
K <sup>39</sup>	52807	Cd <sup>114</sup>	204
Ca <sup>44</sup>	6820	Pb <sup>208</sup>	42

It can be seen that the detection limits achieved were generally worse than those achieved for the Loughborough system, see Table 12. The instrument blank was particularly high due to the fact that the instrument was being used for the analysis of a variety of geological and biological samples, giving the potential for increased contamination of the system. The sensitivity achieved for the standard solution was not as high as the Loughborough machine, this may be due to the fact that the actual energy coupled with the sample was estimated to be  $0.26 \text{ GW cm}^{-2}$  compared to  $0.35 \text{ GW cm}^{-2}$ . A final reason was that, even at higher polymer concentrations, the coupling is not as efficient at 266 nm as at 248 nm.